IL-4 downregulates BCL6 to promote memory B cell selection in germinal centers

Laila Shehata

A dissertation

submitted in partial fulfillment of the

requirements for the degree of

Doctor of Philosophy

University of Washington

2023

Reading Committee:

Marion Pepper, Chair

Elia Tait Wojno

Meghan Koch

Program Authorized to Offer Degree:

Immunology

University of Washington

Abstract

IL-4 downregulates BCL6 to promote memory B cell formation in germinal centers

Laila Shehata

Chair of the Supervisory Committee:

Marion Pepper

Department of Immunology

Germinal center (GC)-derived memory B cells (MBCs) play a pivotal role in humoral immunity by differentiating into protective antibody-secreting cells upon re-infection. Despite extensive research focused on GC formation and the cellular interactions occurring within the GC microenvironment, the precise signals which regulate MBC selection and exit remain incompletely understood. In these studies, we focus on the role of interleukin-4 (IL-4) in the GC using murine blood-stage *Plasmodium* infections as a model of for a type 1 immune response. Our findings demonstrate that IL-4 signaling can trigger the selection and exit of GC B cells by modulating the expression of BCL6, the primary transcription factor within the GC. Specifically, we show that IL-4 induces negative autoregulation of BCL6, leading to a loss in expression of this anti-apoptotic factor within GC B cells. Consequently, in the presence of excess IL-4, there is increased GC B cell death and a loss of selection stringency.

Furthermore, we demonstrate that in the absence of IL-4-mediated downregulation of BCL6, B cells with lower affinity can persist within the GC and contribute to the MBC pool. This observation highlights the critical role of IL-4-mediated downregulation of BCL6 in maintaining selection stringency and affinity maturation within the MBC population. By elucidating the role of IL-4 in modulating the fate of GC B cells, we have demonstrated the significance of IL-4 signaling in shaping the dynamics of the GC selection and subsequent memory formation.

The importance of both GCs and memory formation are further underscored in chapter 3, in which we analyze the B cell response generated by both protein nanoparticle vaccines and by natural infection with SARS-CoV-2. As the formation of class-switched MBCs and LLPCs are the primary correlate of protection for vaccination, our finding that a nanoparticle displaying the receptor binding domain of SARS-CoV-2 can elicit the formation of a robust GC with class-switched B cells was very promising for the future of nanoparticle vaccines.

Collectively, these findings offer novel insights into the mechanisms underlying MBC selection and affinity maturation within the GC. Through the identification of IL-4 as a negative regulator of BCL6 expression and its impact of GC B cell survival, our study advances the current understanding of how the immune system maintains an optimal balance between selection stringency and the generation of diverse MBC populations. Further research in this area will likely explore additional signaling pathways and molecular players involved in the complex network of interactions governing GC-derived MBC selection, and ultimately will contribute to the development of strategies aimed at enhancing immune responses and vaccine efficacy.

Acknowledgements

First and foremost, I would like to thank my mentors who have been so supportive of me throughout this process. To Dr. Laura Walker: thank you for encouraging me to plan my own experiments even when you knew I would fail, for forcing me to present at company-wide meetings even though it made me so nervous, and for teaching me why science is fun. You prepared me so well for grad school, and I still look back at your list of advice for how to succeed at it when I need a boost. To Dr. Marion Pepper: thank you for valuing me as a person first and a scientist second. It meant the world to me that you texted me every day when I had COVID, that you invited my roommates and I over for dinner to talk to us about why being a woman in academia is worth it, and that you understood why I needed to stay home from lab to focus on getting Taylor Swift tickets. I have learned so much from you over the past 5 years about how to think about scientific problems and how to get things done while still treating people with kindness and respect. I truly could not have asked for a better grad school mentor, and I only wish everyone else was as lucky as I have been to have had you as my PI for this stage of my career. Most importantly, both you and Laura have become people I am as comfortable with asking career or science advice as I am sending a silly article, and I am so grateful for that.

Major thanks to everyone in the Pepper lab; I am so happy to have overlapped with so many wonderful, intelligent, ridiculous people. Thank you to Mary, Lauren, and Gretchen for being B cell wizards and guiding me through the intricacies of this field. Huge thank you to Brian for having the best ideas and also always challenging me to defend mine, as well as for making my time in the mouse room more enjoyable with the most random conversations. Jason, Courtney, and Derek, you're all so fun to talk to and I'm so glad we're friends and semi-

neighbors. And lastly, I don't think I would have had nearly as good of a time if not for my fellow children at play, Kennidy, Kurt and Mikel. Kennidy, thank you for being my gossip pal and making me feel at home in the lab. Mikel, thank you for being the most inclusive friend and for your advice and science wisdom throughout the years. Kurt, thank you for being my twin on this journey – I still think you're the only person I could have dealt with for this long and you made me laugh basically every day of it.

Thank you to my friends, both in Seattle and afar, for being such lovely supportive humans. Zoo Squad, your friendship made Seattle feel like home, and I'm so thankful to have all of you around for darts, dinner, True American, and everything in between. Special shoutout to Molly and Hannah for being the best roommates for 4 years and keeping me sane (or at least jointly insane) during the pandemic. For my Adimab friends and grad school cohort, I love that we all went down this road together and have had each other for complaints and support throughout the years. To all of my MIT friends, but especially Bella and Mira, thank you for being not only incredibly smart and successful but also insanely kind, caring, and weird. You inspire me constantly and I am so grateful to have you in my life. Can't wait for our commune.

Finally, the biggest thank you to my family. To my fiancé Elya: your love and support and all-around silliness and joy for life have kept me going throughout the toughest years of this Ph.D. To my parents, Patricia and Ibrahim: thank you for your unending encouragement and for always making me feel like things will be okay. I so appreciate that you always asked to hear how my project is going, but also reminded me how little that mattered when my answer was 'bad'. And to my sister, Soraya, thank you for being my best friend and the best double doctor to be. I love that we did this together.

Lastly, thank you to the mice whose lives were sacrificed for this work.

TABLE OF CONTENTS

List of Figures.....ix

List of Tables.....xi

1. Introduction.....12

    1.1 Generation of the adaptive immune response.....12

    1.2 T-dependent B cell activation.....13

    1.3 Germinal center initiation and process.....15

    1.4 Memory B cell selection.....17

    1.5 Role of cytokines in the germinal center.....19

    1.6 Questions to address.....21

2. IL-4 downregulates BCL6 to guide memory B cell selection in the germinal center.....23

    2.1 Introduction.....23

    2.2 Results.....24

        2.2.1 IL-4 can be produced by GC Tfh cells and perceived by GC B cells during *Plasmodium* infection.....24

        2.2.2 IL-4 has opposing effects on the B cell response over the course of infection.....27

        2.2.3 IL-4 downregulates BCL6 and enhances expression of CD80.....33

        2.2.4 IL-4 directly downregulates BCL6 on GC B cells via negative autoregulation.....40

        2.2.5 IL-4-mediated cell death limits the formation of GC-derived MBCs.....46

        2.2.6 IL-4 signaling regulates MBC selection stringency.....53

2.2.7 A lack of IL-4 signaling in B cells promotes longer-lasting GCs and lower affinity MBCs.....60
2.3 Discussion.....63
3. Characterization of protein nanoparticles as a vaccine tool.....66
3.1 Introduction.....66
3.2 Results.....68
3.2.1 Displayed antigen is immunodominant to nanoparticle scaffolds.....68
3.2.2 Mild COVID-19 induces persistent, neutralizing anti-SARS-CoV-2 IgG antibody.....71
3.2.3 RBD nanoparticle vaccines elicit a robust B cell response.....74
3.3 Discussion.....77
4. Concluding Remarks.....78
5. Materials and Methods.....84
6. References.....95

List of Figures

Figure 2.1. Kinetics of IL-4 production and IL4Rα expression throughout acute *Plasmodium* infection.....26

Figure 2.2. The effect of IL-4 on the antigen-specific B cell response varies over the course of infection.....30

Figure 2.3. IL4C treatment does not impact plasma cell differentiation.....32

Figure 2.4. IL-4 administered after GC formation limits GC size and output.....37

Figure 2.5. IL-4 downregulates BCL6 during an ongoing GC.....38

Figure 2.6. IL-4 does not downregulate BCL6 in T cells.....40

Figure 2.7. IL-4 signaling in GC B cells triggers BCL6 negative autoregulation.....44

Figure 2.8. IL-4-mediated acts directly on B cells in a STAT6-dependent manner to downregulate BCL6.....46

Figure 2.9. IL-4 increases pre-memory GC B cell death.....50

Figure 2.10. Excess IL-4 leads to increased GC B cell death and loss of MBCs.....52

Figure 2.11. IL-4 signaling regulates MBC selection stringency.....57

Figure 2.12. Characterization of the memory response in IL4RαKO **mice**.....59

Figure 2.13. Lower affinity B cells persist into the memory pool in the absence of B cell-intrinsic IL-4 signaling.....62

Figure 3.1. B cell responses to nanoparticle scaffolds and displayed antigens.....70

Figure 3.2. Healthy controls do not have SARS-CoV-2 RBD or spike-specific antibodies.....71

Figure 3.3. Mild COVID-19 induces persistent, neutralizing IgG antibodies.....73

Figure 3.4. Anti-spike antibodies highly correlate with anti-RBD antibodies.....74

Figure 3.5. RBD nanoparticles elicit robust B cell responses in mice.....76

Figure 4.1. IL-4 downregulates BCL6 in type 1 immune responses.....79

Figure 4.2. CD40:CD40L signaling may promote BCL2 expression.....82

List of Tables

Table 5.1. Antibodies used for flow cytometry.....93

Table 5.2. UMI adapters for BCR sequencing.....94

1. Introduction

1.1 Generation of the adaptive immune response

The immune system is a highly intricate network composed of molecules, cells, and tissues designed to safeguard organisms from detrimental microbes (termed "pathogens"). It functions to distinguish self from non-self and harmless from harmful, and it undertakes a coordinated campaign to clear foreign pathogens. This is accomplished through two tiers of immunity: innate and adaptive. The innate immune system encompasses sentinel cells at barrier tissues as well as circulating molecules and cells that possess receptors specialized in identifying invariant motifs that are commonly found on pathogens, also known as pathogen-associated molecular patterns (PAMPs)[1]. Following recognition of a PAMP, innate cells are activated and can begin to produce inflammatory signals such as cytokines and chemokines to both directly harm the invading pathogen as well as to recruit additional immune cells to the site of infection. While this response is often highly effective, it is also limited by its inflexibility. Therefore, a key feature of the innate response is its ability to activate the adaptive immune response, which allows for the generation of highly specific and long-lasting memory against pathogen-derived antigens.

The adaptive immune response primarily involves white blood cells, specifically T and B lymphocytes. These cells possess the remarkable capacity to rearrange their antigen-recognizing cell surface receptors, known as T cell receptors (TCRs) and B cell receptors (BCRs), respectively. This process of somatic gene rearrangement grants T and B cells the potential to recognize an almost infinitely diverse array of pathogens[2]. Upon recognition of an antigen by a TCR or BCR, the corresponding lymphocyte undergoes both proliferation and differentiation, leading to the development of a large pool of antigen-specific effector cells. These effector cells

have the ability to target infected cells via cytotoxic activity (T cells) or the invading pathogen itself via antibody secretion (B cells)[3]. Consequently, the adaptive immune response achieves a high degree of specificity and effectiveness in targeting pathogens.

An essential attribute of the adaptive immune system is its capacity to form long-lived memory cells, which reside in tissues and lymphoid organs. These memory cells can be quickly reactivated upon re-exposure to a pathogen, enabling rapid clearance of the infectious agent. Thus, while the innate immune system plays a critical role in pathogen recognition and initiation of the overall immune response, the activation of the adaptive immune response is indispensable for acquiring antigen-specific defenses that can be recalled over extended periods, sometimes as long as the lifespan of the host organism.

1.2 T-dependent B cell activation

An anchor of this lifelong protective immunity is the presence of B cells and the antibodies they generate. Antibodies, also known as immunoglobulins, represent the secreted form of the BCR. They are soluble, highly specific proteins capable of both directly binding to pathogens to neutralize them as well as activating other immune cells to phagocytose the pathogen via the complement cascade or Fc-mediated opsonization. However, the production of antibodies is contingent upon proper B cell development, activation, and subsequent differentiation into antibody-secreting cells (ASCs), also called plasma cells[4].

B cells originate from hematopoietic stem cells residing in the bone marrow. They undergo a series of sequential development stages involving gene shuffling and testing of the variable (V), diversity (D), and joining (J) genes that comprise their BCRs. This process, known as VDJ rearrangement, ensures the generation of a diverse repertoire of BCRs capable of recognizing a

wide range of antigens[2]. B cells that successfully complete this receptor editing and survive tolerance checkpoints, which prevent strong reactions to self-antigens, are permitted to migrate from the bone marrow to peripheral tissues. These naive B cells co-express IgM and IgD BCRs and circulate through secondary lymphoid organs such as the lymph nodes and the spleen, where they await activation through antigen recognition.

When a naive B cell encounters an antigen capable of binding to its BCR, this event initiates antigen internalization through receptor-mediated endocytosis. Within the B cell, the internalized antigen undergoes processing, leading to the generation of antigenic peptides that subsequently associate with major histocompatibility complex class II (MHC II) molecules. These peptide-MHC II complexes are then presented on the surface of the B cell. B cells also undergo a series of migratory changes, relocating from the B cell follicles to the boundary region between the B cell and T cell zones, known as the T-B border, such that they can present antigens to naive $CD4^+$ helper T cells (Tfh).

Upon recognition by a naive Tfh, a signaling synapse is formed between the B and T cells, characterized by MHC II:TCR interactions, as well as costimulatory signals through CD40:CD40 ligand (CD40L) and ICOS ligand (ICOSL):ICOS interactions[5]. These receptor-ligand interactions play a crucial role in activating both B and T cells. Moreover, cytokines released by activated Tfh cells or neighboring natural killer T lymphocytes (NKTs) provide additional stimulation for proliferation and differentiation of B and Tfh cells[6,7]. Following these interactions, a subset of B cells differentiates into short-lived ASCs, or plasmablasts, that secrete primarily low affinity IgM^+ antibodies[8]. This extrafollicular B cell response is critical for early control of infection, as it supplies a wave of serum antibody while other B cells begin the lengthier process of affinity maturation in the germinal center.

1.3 Germinal center initiation and process

Germinal centers (GCs) are specialized structures that form within the B cell follicles of secondary lymphoid organs and play a critical role in the development of the adaptive immune response[9–11]. These dynamic microenvironments are crucial for generating high affinity antibodies and selecting of B cells with improved antigen-binding properties. Upon activation of B and Tfh cells as described above, both lymphocytes undergo epigenetic and transcriptional changes that promote their migration into the B cell follicles and subsequent formation of GCs. Specifically, both cell types upregulate the chemokine receptor CXCR5, enabling responsiveness to the chemokine CXCL13, which is abundantly produced by follicular dendritic cells (FDCs) within the B cell follicles.

Concomitantly, B and Tfh cells upregulate the transcription factor BCL6, which serves as the central regulator of the GC response. BCL6 functions as a transcriptional repressor, inhibiting the expression of genes involved in terminal differentiation, such as BLIMP1 and GATA3. Additionally, BCL6 controls B cell positioning within the GC by repressing the expression of S1PR1 and EBI2 while inducing the expression of S1PR2, thereby maintaining B cells tethered within the GC. Importantly, BCL6 also promotes the expression of activation-induced cytidine deaminase (AID), a key enzyme responsible for BCR class-switching and somatic hypermutation (SHM)[12]. Moreover, BCL6 also acts as an anti-apoptotic signal by repressing the expression of the pro-apoptotic factor BIM and the DNA damage sensor ATR, allowing B cells to undergo multiple rounds of damage prone SHM without triggering apoptosis[13].

The GC is comprised of two distinct regions: the dark zone (DZ) and the light zone (LZ). The DZ is characterized by intense B cell proliferation and SHM, leading to the generation of B cells with diverse antigen receptor specificities. Within the LZ, B cells receive pro-survival signals

through interactions with their BCR and antigens presented by FDC immune complexes. Additionally, receptor-ligand interactions between B and T cells initiated by MHC II-TCR recognition, contribute to B cell survival signals[14]. B cells that fail to receive adequate help are destined for apoptosis, while those that do receive survival signals have two possible fates: migration back into the DZ for further clonal expansion or differentiation into memory B cell (MBC) or long-lived plasma cell (LLPCs).

Both MBCs and LLPCs play distinct roles in providing future protection against pathogens, albeit through different mechanisms. MBCs retain the expression of membrane bound BCRs and are distributed across secondary lymphoid organs, peripheral tissues, the bone marrow, and in circulation[15]. They ensure a rapid response upon re-exposure to the antigen by either reseeding secondary germinal centers or undergoing rapid differentiation into high-affinity ASCs. Their presence in secondary GCs allows for the initiation of an accelerated and focused immune response, while their capacity to differentiate into ASCs enables the production of specific antibodies against the re-encountered pathogen.

In contrast, LLPCs significantly downregulate their BCR expression and instead serve as dedicated antibody-secreting factories[15]. They predominately reside in the bone marrow, although recent studies have identified them in certain mucosal tissues as well. LLPCs maintain low levels of circulating serum antibodies, providing a first line of defense upon re-exposure to the pathogen. Their sustained antibody production helps to prevent reinfection or limit the severity of the subsequent infection, as demonstrated by the emphasis on generating robust LLPC populations in vaccination strategies. Although the mechanisms underlying LLPC formation are relatively well understood, there remain significant gaps in our understanding of the processes that govern the successful selection of high affinity MBCs.

1.4 Memory B cell selection

The GC-derived memory B cell pool consists of B cells with high affinity to the specific antigen, however it still encompasses a wide range of affinities. Lower affinity MBCs still play a crucial role in recall responses by recognizing heterologous antigens that higher affinity clones may not bind effectively. The mechanisms governing selection within the GC that support both the expansion of higher affinity clones while remaining permissive to some lower affinity clones remain an area of active investigation.

Two prevailing models of positive selection in the GC are the death- and birth-limited models of positive selection, nicely summarized by Victora and Nussenzweig[10]. The death-limited model proposes that higher affinity B cells receive signals that enable their migration to the DZ to undergo proliferation, while lower affinity clones are eliminated by apoptosis. In the birth-limited model, all B cells can enter the DZ, but the extent of proliferation corresponds to affinity, resulting in a considerable expansion of higher affinity clones compared to lower affinity clones. Both models are supported by experimental observations, including the finding that a significant proportion of LZ B cells do not reenter the DZ, supporting the death-limited model[16,17], and the observation of clonal bursts dominating the GC response supporting the birth-limited model[18,19]. It is likely that a combination of both models is involved: lower affinity B cells are more prone to apoptosis, and high affinity clones receive greater proliferative signals.

Both models agree that BCR affinity is a critical determinant of selection. The exact mechanisms by which BCR affinity influences selection are still debated. It is unclear whether survival signals are initiated by BCR binding to antigen, or if they are attributed to T cell help following antigen internalization, processing, and presentation. Studies using antigen delivery via DEC-205, which decouples BCR and T cell help, have shown that B cell proliferation can

occur independently of BCR signaling[16,20,21]. However, the addition of BCR signal in conjunction with DEC-205 does enhance positive selection, suggesting a likely synergy between BCR and T cell help in promoting B cell survival and proliferation[16,22,23].

On a molecular scale, the regulation of GC selection is still being investigated. Several groups have demonstrated that the transcription factor c-myc is transiently upregulated as B cells receive T cell help in the LZ, promoting GC cycling[24,25]. These c-myc$^+$ cells migrate to the DZ, where the transcription factor AP4 maintains the transcriptional programs initiated by c-myc, facilitating entry into the cell cycle and subsequent proliferation[26]. Notably, c-myc and BCL6 have been shown to be antagonistic, but c-myc appears to act as an anti-apoptotic factor to promote B cell survival during its transient upregulation and corresponding transient downregulation of BCL6[26]. CD40-CD40L interactions have also been shown to transiently disrupt the BCL6 repressor complex, allowing for the temporary alleviation of repression of the DNA damage sensor ATR[27]. This disruption may serve as a checkpoint to eliminate B cells with ongoing DNA damage via apoptosis, ensuring the maintenance of genomic integrity.

Throughout the GC reaction, a subset of LZ GC B cells exits the GC instead of cycling back into the DZ. Studies have consistently shown that early GC emigrants predominantly consist of MBCs and are generally of lower affinity compared to late GC emigrants, which are primarily LLPCs[25,28]. Distinct transcriptional and cell surface protein profiles have been identified in pre-memory and pre-plasma cell GC B cells. Recent RNASeq and imaging experiments have contributed to the identification of memory precursors, and have shown that these cells are found in the LZ, particularly near the GC border, and have high transcriptional similarity to MBCs[29–31]. Various groups have characterized memory precursors as CCR6$^+$ or Ephrin-B1$^+$S1PR2$^-$ [20,29,32,33]. The transcription factor BACH2 has been implicated in predisposing GC B cells towards MBC

differentiation, though it is not sufficient to do so[25,34]. The transcription factors HHEX and TLE3 were demonstrated to be required for MBC differentiation[35].

Notably, the downregulation of BCL6 and the release of its repression of pro-migratory cues is a necessary step for a memory precursor to successfully migrate out of the GC and complete its differentiation into a long-lived MBC. Also critical is the upregulation of various signals to promote MBC survival and maintenance. Bhattacharya et al. identified several such signals, including KLF2, SKI, NFKB, and BCL2[33]. Through retroviral transductions, they confirmed that BCL2, SKI, and NFKB promote B cell division, while BCL2, NFKB, and KLF2 reduce the frequency of apoptotic B cells. The importance of BCL2 for proper MBC survival has been corroborated by multiple independent studies[29–32,36]. Critically, the precise signals that initiate the downregulation of BCL6, upregulation of the pre-memory transcription factor HHEX, or upregulation of BCL2 and other MBC survival signals, as well as the temporal order of these steps, remain unknown.

1.5 Role of cytokines in the germinal center

The GC process involves intricate interactions between GC B cells and Tfh cells, mediated by cognate and receptor-ligand interactions. Several studies have highlighted the significance of these interactions, including not only MHC II:TCR, but also CD40:CD40L, ICOSL:ICOS, PD-L1/PD-L2:PD-1, SAP:SLAM and others, in guiding B cell proliferation and differentiation[37–40]. However, cytokines also play a critical role in B cell fate determination. Interferon gamma, interleukin (IL)-4, and IL-13 promote class-switching to specific antibody isotypes associated with different types of infections[7,41,42]. Other cytokines such as IL-2, IL-6, and IL-10, are involved in B cell activation and the differentiation of Tfh or T follicular regulatory (Tfr) cells[43–

[45]. Recently, IL-9 has been identified as a key cytokine in promoting MBC development[31,46]. However, the primary cytokines produced within the GC are IL-21 and IL-4.

IL-21, predominately produced by Tfh cells in both the extrafollicular region and the GC, is one of the most extensively studied and pleiotropic cytokines involved in the GC process. Tfh cells begin producing IL-21 as early as 2-3 days after immunization[47]. IL-21 acts through the STAT3 pathway to promote expression of BCL6 and thereby promote GC formation[48,49]. In the absence of the IL-21 receptor, GCs are significantly smaller and there is an imbalance of organization that favors the LZ[47]. This observation is consistent with other studies showing that IL-21-producing Tfh cells are primarily located near the DZ-LZ border and that IL-21 upregulates the transcription factor AP4, promoting B cell proliferation in the DZ[50,51]. Interestingly, IL-21 also upregulates BLIMP1, which antagonizes BCL6, allowing for the exit of LLPCs from the GC[52–56]. However, since BLIMP1 is a key transcription factor in LLPC development but is not required for MBC formation, this dual role of IL-21 in regulating BCL6 does not contribute to MBC exit.

The role of IL-4 in the GC has not been as extensively characterized as IL-21, although it has been established to be essential to proper type 2 immune responses[57,59]. Nevertheless, several studies have demonstrated that IL-4, acting through STAT6, promotes BCL6 expression in B cells and synergistically enhances GC formation alongside IL-21[47,48,58]. However, studies using STAT6 knockout mice have shown that normal, properly organized GCs can still form, albeit with a slight delay compared to wild-type mice, suggesting compensatory effects of IL-21 in the absence of IL-4[47]. Despite this known role for IL-4 in supporting GC formation, several groups observed that Tfh cells do not begin to produce IL-4 until after they have entered the B cell follicles and GC formation is already underway[47,50,60]. These findings were reconciled by recent

work from Facundo Batista's lab, which demonstrated that NKT cells near the T-B border are responsible for an early wave of IL-4 over the first 3-5 days of influenza infection, and that Tfh cells start producing IL-4 as the early NKT-derived IL-4 recedes, around 6-9 days post-infection[6]. Notably, they also show that the early NKT-derived IL-4 does promote faster GC formation.

Although Tfh cells within the GC produce IL-4 and activated B cells upregulate the IL-4 receptor alpha (IL4Rα), the role of IL-4 within the GC itself has only recently begun to be elucidated[60,61]. Work from Jason Cyster's lab in 2021 demonstrated that FDCs in the GC can bind IL-4, which limits excessive IL-4 signaling in B cells[62]. Conditional knockout of IL4Rα on FDCs increased the bioavailability of IL-4 within the GC, resulting in a reduced memory B cell formation and decreased MBC affinity. The authors hypothesized Tfh production of IL-4 triggered by interactions with high affinity GC B cells could restrain memory cell formation and promote the continued participation of lower affinity clones within the GC, thereby diversifying the memory B cell response. However, further evidence is required to support this hypothesis, as it implies an inefficient production of IL-4 if FDCs are constantly required to limit the reach of the cytokine.

1.6 Questions to address

The GC process is incredibly intricate and encompasses numerous complex signaling pathways. The successful generation of high affinity GC-derived MBCs and LLPCs is critical for the establishment of robust humoral immunity, and plays a pivotal role in the efficacy of many successful vaccines. Furthering our understanding of the mechanisms governing selection and exit of high affinity MBCs from the GC would therefore contribute to the development of more

effective vaccination strategies. Despite recent advancements in the field, including the identification of memory precursors within the GC and the characterization of key transcription factors involved in MBC differentiation, the specific signals and molecular mechanisms responsible for the selection of MBCs for GC exit are still unknown.

In the studies presented here, we employed tetramer enrichment strategies to study the development of antigen-specific B cell responses in several infection and immunization models. In chapter 2, we focus on elucidating the role of IL-4 in the GC using murine models of blood-stage *Plasmodium* infection. Our findings revealed that, similar to IL-21, IL-4 exerts a dual influence on GC dynamics. It facilitates the upregulation of BCL6 expression in naive B cells, while subsequently triggering negative autoregulation of BCL6 within the GC, priming memory precursors for exit. We explored the impact of both excessive IL-4 levels and restricted IL-4 signaling on the magnitude and quality of the memory B cell pool. In chapter 3, in collaboration with several other research groups, we investigated the potential of protein nanoparticle vaccines. This research was conducted during the ongoing SARS-CoV-2 pandemic, and we characterized the longevity of the antibody elicited following infection. Furthermore, we evaluated the effectiveness of several protein nanoparticles displaying the SARS-CoV-2 receptor binding domain in inducing a GC B cell response and the generation of class-switched MBCs. Notably, one of these nanoparticles has now obtained approval as a vaccine in South Korea. Overall, our studies contribute to the broader understanding of the GC response and the factors which influence selection and generation of high affinity MBCs. The insights gained from our work hold promise for the development of novel vaccination strategies.

2. IL-4 downregulates BCL6 to promote memory B cell selection in germinal centers

2.1 Introduction

Germinal centers (GCs) are highly organized structures found within B cell follicles. In the GC, activated B cells proliferate, diversify their B cell receptors, and are selected to mature into memory cells that provide humoral protection from disease[5]. Temporally and spatially distinct and complex interactions between B cells and other cells in the GC including $CD4^+$ T follicular helper (Tfh) cells and follicular dendritic cells (FDCs) influence the initiation, maintenance, and dissolution of GCs. While many of these interactions have been well-characterized, many others, including how affinity-matured memory B cells (MBCs) are selected to exit the GC, remain poorly defined[25,32,37,63–67]. Specifically, the mechanisms underlying the $CD4^+$ T cell-mediated selection process that leads to the downregulation of GC B cell-defining transcriptional programs and concomitant upregulation of transcriptional programs associated with long-lived memory B cell formation are unknown[26,35,68]. It is well accepted that BCL6, a repressive transcription factor, actively maintains the GC and must be downregulated for MBCs to form, but the signals that initiate the downregulation of BCL6 have not been identified[69,70]. Understanding how this process takes place is critical for generating high affinity memory B cell formation for optimal vaccine development or for targeting this process therapeutically during autoimmunity.

Interleukin-4 (IL-4) is a key T cell-derived molecule that has been attributed with conflicting roles in the regulation of the GC[47,62]. Early after the initiation of an anti-viral response, IL-4 produced by natural killer T cells is able to stimulate GC formation by promoting B cell expression of BCL6[6,47,48]. BCL6 acts via repressor-of-repressor circuits to modulate transcriptional programs that keep B and Tfh cells tethered in the GC and prevent them from terminally differentiating[70–72]. BCL6 also suppresses the DNA damage sensor ATR, thereby

acting as an anti-apoptotic factor to keep GC B cells alive as they undergo rounds of DNA damage-prone somatic hypermutation[13,73]. Yet how subsequent IL-4 production by $CD4^+$ Tfh and GC Tfh cells impacts BCL6 expression, GC maintenance, and memory formation is unclear. Recent work from Duan and colleagues demonstrated that excess availability of IL-4 could reduce memory B cell formation and reduce selection stringency, although the underlying mechanisms were not defined[62]. Herein we have sought to define how IL-4 functions in the GC and to determine if it could influence the selection or exit of MBCs through its regulation of BCL6. We demonstrate that while IL-4 promotes BCL6 in naive and activated B cells to encourage GC formation, it can also induce the negative autoregulation of BCL6 in a GC B cell-intrinsic manner. This IL-4-mediated downregulation of BCL6 initiates a selection event, allowing pre-memory GC B cells that can obtain additional survival signals to exit the GC, whereas those that cannot undergo cell death.

2.2 Results

2.2.1 IL-4 can be produced by GC Tfh cells and perceived by GC B cells during Plasmodium infection

To better understand how $CD4^+$ T cell-derived IL-4 can impact B cell differentiation during infection, we first characterized the identity and kinetics of IL-4-producing $CD4^+$ T cells specific for *Plasmodium*-derived antigens during a GC response. To accomplish this, KN2 (knock-in huCD2) mice that express cell surface-associated huCD2 protein under control of the IL-4 promoter were infected with 10^6 *Plasmodium yoelii*-GP66 (*P.y*-GP66)-infected red blood cells (iRBCs). We examined IL-4 production from days 6-18 after *Plasmodium* infection as our previous work demonstrated that this is a critical window for *Plasmodium*-specific B cell

differentiation, encompassing the initiation and propagation of the GC as well as early memory formation[74]. IL-4 producing GP66-specific $CD4^+$ T cells were identified using previously published tetramer enrichment and flow cytometric techniques[75]. In response to *Plasmodium*, the number of IL-4-producing T cells increased throughout the acute stage of infection, as previously shown in influenza and helminth infections[6,50,76] (**Figure 2.1A and 2.1B**). Of interest, although Tfh cells contributed to early IL-4 production, the majority of IL-4-producing $CD4^+$ T cells identified were GC Tfh (**Figure 2.1B**). This indicates that in a Type 1 immune response to infection, the bulk of $CD4^+$ T cell-derived IL-4 is produced by GC Tfh cells after the GC has formed, suggesting contributions beyond solely early GC formation.

We generated B cell tetramers containing the *Plasmodium* blood-stage antigen Merozoite Surface Protein-1 (MSP1) to characterize IL-4 receptor alpha chain (IL4Rα; CD124) expression on responding B cells over the course of infection[74]. There was a large population of $IL4R\alpha^+$ MSP1-specific $CD38^+GL7^-$ B cells in uninfected mice (day 0), suggesting naive B cells can receive IL-4 signals early in infection (**Figure 2.1C and 2.1D**). IL4Rα expression remained high on MSP1-specific $CD38^+GL7^-$ as well as $GL7^+$ B cells throughout acute *P.y*-GP66 infection (**Figure 2.1D**). Overall, this demonstrates that B cells are capable of perceiving Tfh- and GC Tfh-derived IL-4 both prior to and within an ongoing GC.

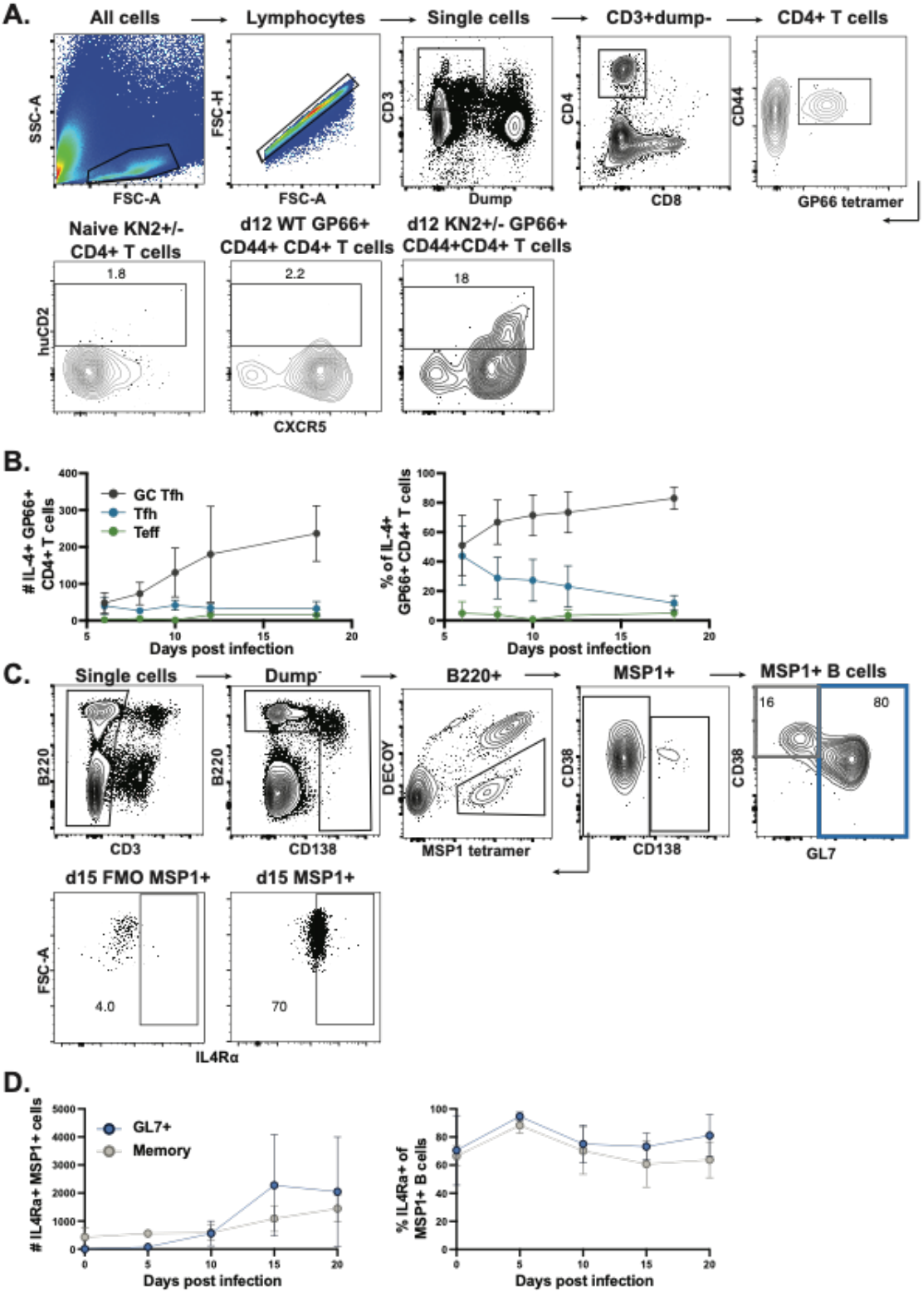
A.
All cells
Lymphocytes
Single cells
CD3+dump-
CD4+ T cells
SSC-A
FSC-A
FSC-H
FSC-A
CD3
Dump
CD4
CD8
CD44
GP66 tetramer
Naive KN2+/- CD4+ T cells
d12 WT GP66+ CD44+ CD4+ T cells
d12 KN2+/- GP66+ CD44+CD4+ T cells
1.8
2.2
18
huCD2
CXCR5
B.
GC Tfh
Tfh
Teff
IL-4+ GP66+ CD4+ T cells
% of IL-4+ GP66+ CD4+ T cells
Days post infection
Days post infection
C.
Single cells
Dump-
B220+
MSP1+
MSP1+ B cells
B220
CD3
B220
CD138
DECOY
MSP1 tetramer
CD38
CD138
16
80
CD38
GL7
d15 FMO MSP1+
d15 MSP1+
FSC-A
4.0
70
IL4Rα
D.
GL7+
Memory
IL4Ra+ MSP1+ cells
% IL4Ra+ of MSP1+ B cells
Days post infection
Days post infection

Figure 2.1. Kinetics of IL-4 production and IL4Rα expression throughout acute *Plasmodium* infection. KN2$^{+/-}$ mice were infected with blood-stage *P.y*-GP66, and GP66-specific CD4$^+$ T cells and MSP1-specific B cells were assessed for IL-4 production or IL4Ra expression, respectively, at the time points indicated. (**A**) Representative gating strategy for evaluating GP66-specific CD4$^+$ T cells. Non-doublet lymphocytes were gated on CD3$^+$B220$^-$CD11b$^-$CD11c$^-$CD4$^+$CD8$^-$, then further gated as CD44$^+$GP66$^+$. Gating on huCD2 expression on naive KN2$^{+/-}$ CD4$^+$ T cells (left), and WT (middle) and KN2$^{+/-}$ (right) gp66$^+$CD44$^+$CD4$^+$ T cells 12 days post-*P.y*-GP66 infection. (**B**) Number (left) and frequency (right) of IL-4-producing (huCD2$^+$) GP66-specific CD4$^+$ T cells by subset, with GC Tfh identified as PD-1$^+$CXCR5$^-$ (grey), Tfh as PD-1$^-$CXCR5$^+$ (blue), and Teff as PD-1$^-$CXCR5$^-$ (green). Data are combined from three independent experiments with 6-8 mice per time point. (**C**) Representative gating strategy for evaluating MSP1-specific B cells and plasmablasts. Non-doublet lymphocytes (A) were further gated on CD3$^-$B220$^+$decoy$^-$MSP1$^+$ cells. Memory B cells (grey) were defined as CD138$^-$CD38$^+$GL7$^-$ and GL7$^+$ B cells (blue) as CD138$^-$CD38$^{+/-}$GL7$^+$. Representative gating for IL4Rα on MSP1-specific B cells from WT mice infected with *P.y*-GP66 using a staining panel excluding (left; fluorescence minus one or FMO) or including (right) IL4Rα. (**D**) Number and frequency of IL4Rα-expressing MSP1$^+$ memory and GL7$^+$ B cells. Data are combined from three independent experiments with 6 mice per time point.

2.2.2 IL-4 has opposing effects on the B cell response over the course of infection

The kinetics of CD4$^+$ GC Tfh production of IL-4 in conjunction with GC B cell expression of IL4Rα suggested a role for IL-4 in the GC that perhaps went beyond solely GC entry. We therefore asked how *in vivo* administration of exogenous IL-4 at various time points affects B cell development after *Plasmodium* infection. In an effort to maximize IL-4 bioavailability, we utilized

complexed IL-4 (IL4C; recombinant IL-4 complexed to anti-IL-4 antibody) to prolong the half-life of the cytokine *in vivo*[77], a strategy commonly used to assess *in vivo* exogenous IL-4 signaling[6,62]. We infected C57BL/6 (WT) mice with 10^6 *Plasmodium chabaudi* (*P.ch*)-iRBCs and administered IL4C or phosphate buffered saline (PBS) intravenously on the first 3 days of infection to determine if early IL-4 enhances $CD38^-GL7^+$ GC B cell differentiation as seen in influenza and other infections[6,77] (**Figure 2.2A**). We observed a significant increase in the number and frequency of MSP1-specific GC B cells by day 8 post-infection in mice treated with IL4C compared to untreated controls, suggesting that this role for early IL-4 in promoting GCs is common to multiple infections[6] (**Figure 2.2B and 2.2C**).

We next asked if IL4C administration to *P.ch*-infected WT mice during an ongoing GC had a similar effect. Mice were administered PBS or IL4C in staggered three-day windows following GC formation (day 10) and the MSP1-specific B cell response was analyzed one day following the last treatment (**Figure 2.2D**). Although there was no significant impact on the B cell response when mice received IL4C on days 10 and 12, there was a surprising loss of MSP1-specific B cells when IL4C was administered on days 12 and 14 (**Figure 2.2E**). A similar trend was observed for the later IL4C treatment windows as well. Importantly, MSP1-specific cells in IL4C-treated mice did not have higher plasmablast numbers, BLIMP1 expression, or anti-MSP1 serum IgG, indicating that IL-4 is not diverting MSP1-specific B cells to a plasmablast fate (**Figure 2.3A-2.3C**). Thus, although early IL-4 encourages GC formation and the ensuing antigen-specific GC B cell expansion, IL-4 restrains the B cell response once GCs have developed. Of interest, in mice treated with IL4C on days 12 and 14 that experienced the greatest loss of MSP1-specific B cells, there were no significant changes in the frequencies of any one specific B cell subset examined

(**Figure 2.2F**), suggesting that IL-4 may be impacting and restricting the GC process, which could affect multiple subsets equally.

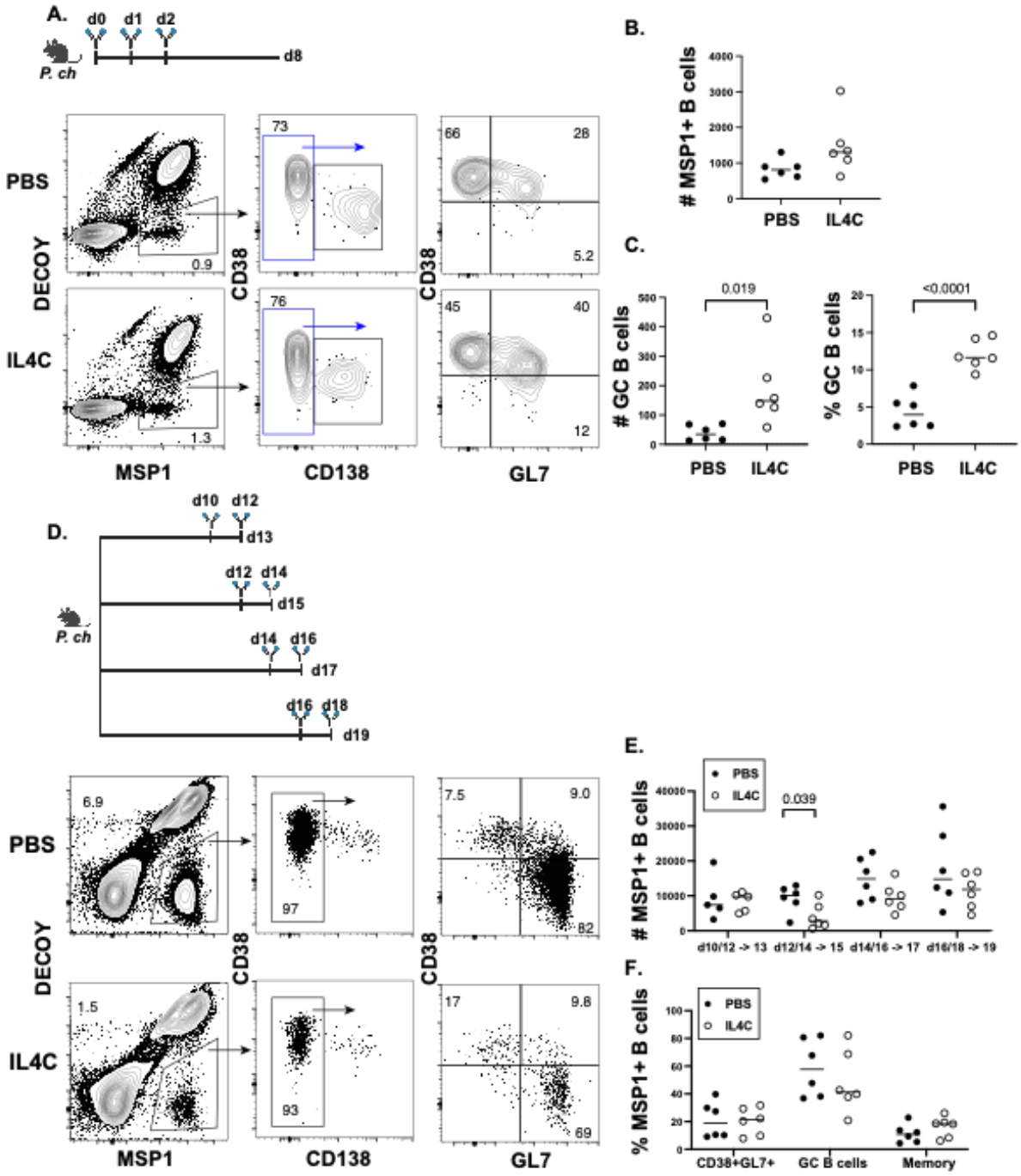

Figure 2.2. The effect of IL-4 on the antigen-specific B cell response varies over the course of infection. (**A**) WT mice were infected with *P.ch* and treated with PBS or IL4C on days 0, 1, and 2 post-infection. Representative flow cytometry plots of MSP1-specific cells at 8 days post-infection from mice treated with PBS (top) or IL4C (bottom), with further gating on non-plasma

cells ($CD138^-$) and GC B cells ($CD38^-GL7^+$) as defined in Figure 2.1. (**B**) Total MSP1-specific B cells in each treatment group at day 8. (**C**) Number (left) and frequency (right) of MSP1-specific GC B cells in each treatment group at day 8. Data are combined from two independent experiments with 6 mice per group. (**D**) WT mice were infected with *P.ch* and treated with IL4C or PBS over two-day windows and MSP1-specific B cell responses were analyzed the following day, as indicated. Representative flow cytometry plots from mice treated with PBS (top) or IL4C (bottom) on days 12 and 14 and analyzed on day 15. (**E**) Number of MSP1-specific B cells at each time point analyzed. (**F**) Frequency of $CD38^+GL7^+$, GC B cells, and MBCs ($CD38^+GL7^-$ $CD73^{and/or}CD80^+$) in each treatment group at day 15, following PBS or IL4C treatment on days 12 and 14. Data are combined from two independent experiments with 5-6 mice per group.

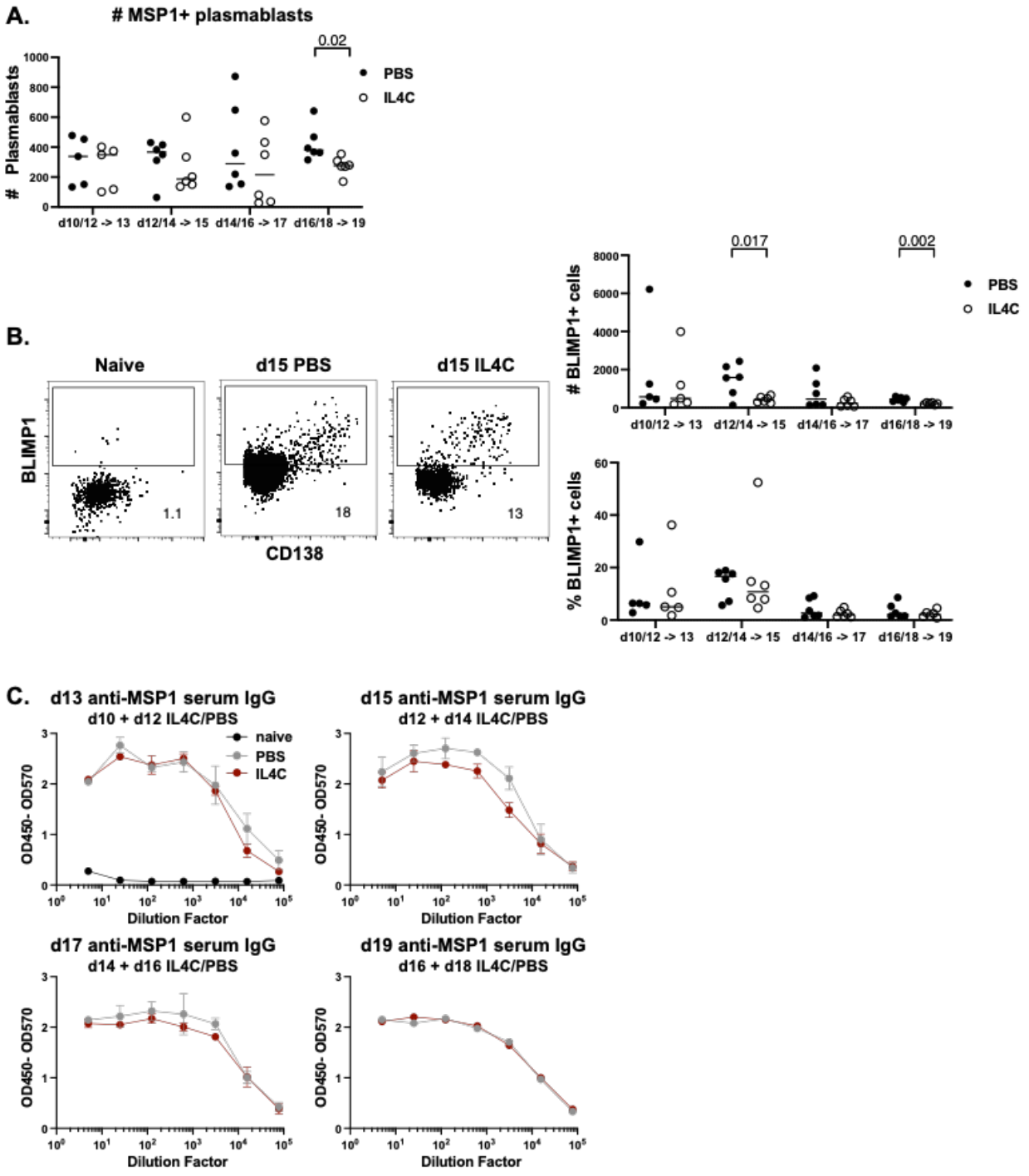

Figure 2.3. IL4C treatment does not impact plasma cell differentiation. WT mice were infected with *P.ch* and treated with PBS or IL4C for two-day treatment windows as shown in Fig 1D. (**A**) Number of MSP1^{+} plasmablasts (gating as in Figure 2.1 at each endpoint. (**B**)

Representative flow plots and quantification of BLIMP1 expression in total $MSP1^{+}B220^{+}CD3^{-}$ lymphocytes in naive mice, or mice treated with PBS or IL4C on days 12 and 14 and analyzed on day 15. (**C**) Serum was collected at each endpoint and anti-MSP1 IgG levels were measured by ELISA. Anti-MSP1 IgG ELISA dilution curves from serum collected at each endpoint. Data are combined from two independent experiments with 5-6 mice per group.

2.2.3 IL-4 downregulates BCL6 and enhances expression of CD80

To test if IL-4 was restricting the GC, we next imaged spleens to visualize GCs in mice treated with IL4C on days 12 and 14. Interestingly, we found that GCs in IL4C-treated mice were smaller in size, supporting our hypothesis that IL-4 can constrain an ongoing GC response (**Figure 2.4A and 2.4B**). This could reflect an effect of IL-4 on GC precursors, GC B cells, exiting GC B cells, or all three B cell populations. Cells transitioning through a $CD38^{+}GL7^{+}$ state (see model in **Figure 2.5A**) include both GC precursors and pre-memory, exiting GC B cells as shown in analyses of B cell populations in UBP-2A-Fucci mice (which report distinct phases of cell cycle) as well as B cells responding to infection with lymphocytic choriomeningitis virus (Armstrong strain; $LCMV_{arm}$)[29,31,78]. However, the markers used to identify these pre-memory cells thus far are proteins that are either also expressed on GC precursors (CCR7, CD62L) or are also expressed prior to and within the GC (Ephrin B1)[29,31]. This makes it difficult to accurately define B cells exiting the GC by flow cytometry. We therefore sought to identify a marker of GC-exiting pre-memory B cells that is not expressed on GC precursors or GC B cells but is upregulated on MBCs. We hypothesized that within the $CD38^{+}GL7^{+}$ "GC transit" B cell population, differing expression of BCL6 and the co-stimulatory molecule CD80 could be used to distinguish pre-GC B cells from post-GC B cells. Activated B cells upregulate BCL6 very

early after immunization, and GC transit B cells show increasing BCL6 expression as the GC develops[79] (**Figure 2.5B and 2.5C**). In order to form memory B cells, GC B cells must downregulate BCL6[34,70,80]. This releases the repression of numerous migratory and functional programs, including allowing the expression of CD80[81]. Indeed, we did not observe $CD80^+$ cells in the GC when BCL6 is most highly expressed, yet a distinct population of $CD80^+BCL6^-$ GC transit B cells emerges after cells begin to downregulate BCL6 and form MBCs 10 days after *Plasmodium* infection[82,83] (**Figure 2.5B and 2.5C**). We can therefore identify "entering" GC transit cells as $BCL6^+CD80^-CD38^+GL7^+$ B cells and "exiting" GC transit cells as $BCL6^-CD80^+CD38^+GL7^+$ GC B cells.

To test if and how IL-4 could be impacting these populations, we analyzed BCL6 and CD80 expression on $MSP1^+$ B cells by flow cytometry after IL4C treatment. In opposition to the current paradigm that IL-4 promotes BCL6, we observed an insignificant decrease in BCL6 expression in GC B cells as well as a significant loss of BCL6 in GC transit B cells in mice treated with IL4C on days 12 and 14 compared to controls (**Figure 2.5D**). To confirm that this was not unique to an IL4C signal as opposed to non-complexed IL-4, we also treated mice with non-complexed IL-4 on days 12-14. Both the loss of MSP1-specific cells noted in Figure 2.2 as well as the loss of BCL6 expression were recapitulated with IL-4 alone, demonstrating that this phenotype is IL-4-mediated and not dependent upon signaling alterations due to complexing IL-4 with antibody (**Figure 2.4C; Figure 2.5E**).

Our data suggested that IL-4 signaling may differentially impact B cells at different stages of differentiation during an immune response. To test this hypothesis directly, we isolated naive splenic B cells from naive mice or $GL7^+$ splenic B cells from mice at least 12 days post-*Plasmodium* infection and cultured them with an agonistic anti-CD40 antibody (1 ug/mL) to

promote *in vitro* GC B cell survival[84,85]. Both cell types were cultured in the presence or absence of non-complexed recombinant IL-4 (10 ng/mL) for 24 hours. Naive B cells analyzed after 24h culture with anti-CD40 and IL-4 had significantly higher BCL6 expression than those cultured with anti-CD40 alone, consistent with previous literature[48] (**Figure 2.5F**). However, $GL7^+$ B cells cultured in the presence of anti-CD40 and IL-4 lost BCL6 expression (**Figure 2.5F**), mirroring the *in vivo* phenotype observed in mice treated with IL4C or IL-4 **(Figure 2.5D and 2.5E)**. This indicates that IL-4 can have opposing effects on BCL6 expression in B cells at various stages of differentiation, perhaps contingent on the level of BCL6 already present in the cell.

While the reduction in $BCL6^+$ GC transit B cells could be indicative of a loss of GC precursors, it corresponded to an increase in the frequency of $CD80^+$ GC transit B cells, suggesting that IL-4 may be downregulating BCL6 in GC B cells, resulting in increased GC exit (**Figure 2.5G and 2.5H**). We further analyzed expression of the ectonucleotidase CD73, used to identify functional memory B cells that have received $CD4^+$ T cell help[74,82,83,86]. Nearly all of the $CD80^+$ GC transit B cells in both PBS- and IL4C-treated mice co-expressed CD73, further supporting the idea that these are indeed exiting pre-memory B cells (**Figure 2.5G and 2.5H**). Surprisingly however, despite the proportional increase in exiting $CD73^+CD80^+$ GC transit B cells, IL4C-treated mice exhibited a specific loss of GC-derived class-switched (IgM^-IgD^-; $swIg^+$) $CD73^+CD80^+CD38^+GL7^-$ MBCs (**Figure 2.4D; Figure 2.5I**). Thus, although IL-4 appears to be increasing GC exit into the GC transit pool, the overall loss of MSP1-specific B cells and of GC-derived MBCs suggests that the IL-4-mediated downregulation of BCL6 may not be the only signal required for long-lived MBC formation.

As Tfh cells are also a critical part of GCs, we characterized the effect of IL-4 on the antigen-specific T cell response. We infected mice with *Py*-gp66, treated them with IL4C on days 12 and 14, and analyzed the gp66-specific CD4+ T cell response on day 15. Interestingly, although there was a marked loss of GC Tfh and Tfh cells with IL4C treatment, there was no decrease in BCL6 expression in either subset (**Figure 2.6A and 2.6B**). This was true of splenic T cells isolated from *Plasmodium*-infected mice and cultured with IL-4 (10 ng/mL) for 24h as well (**Figure 2.6C**). The lack of IL-4-mediated downregulation of BCL6 in Tfh cells is perhaps not surprising given that activated T cells have been shown to downregulate IL4Rα, and thus are not poised to respond to IL-4[89]. As GC B cells are known to maintain Tfh cells, it is possible that the downregulation of BCL6 and resulting loss of GC B cells is responsible for the corresponding reduction in Tfh numbers[87].

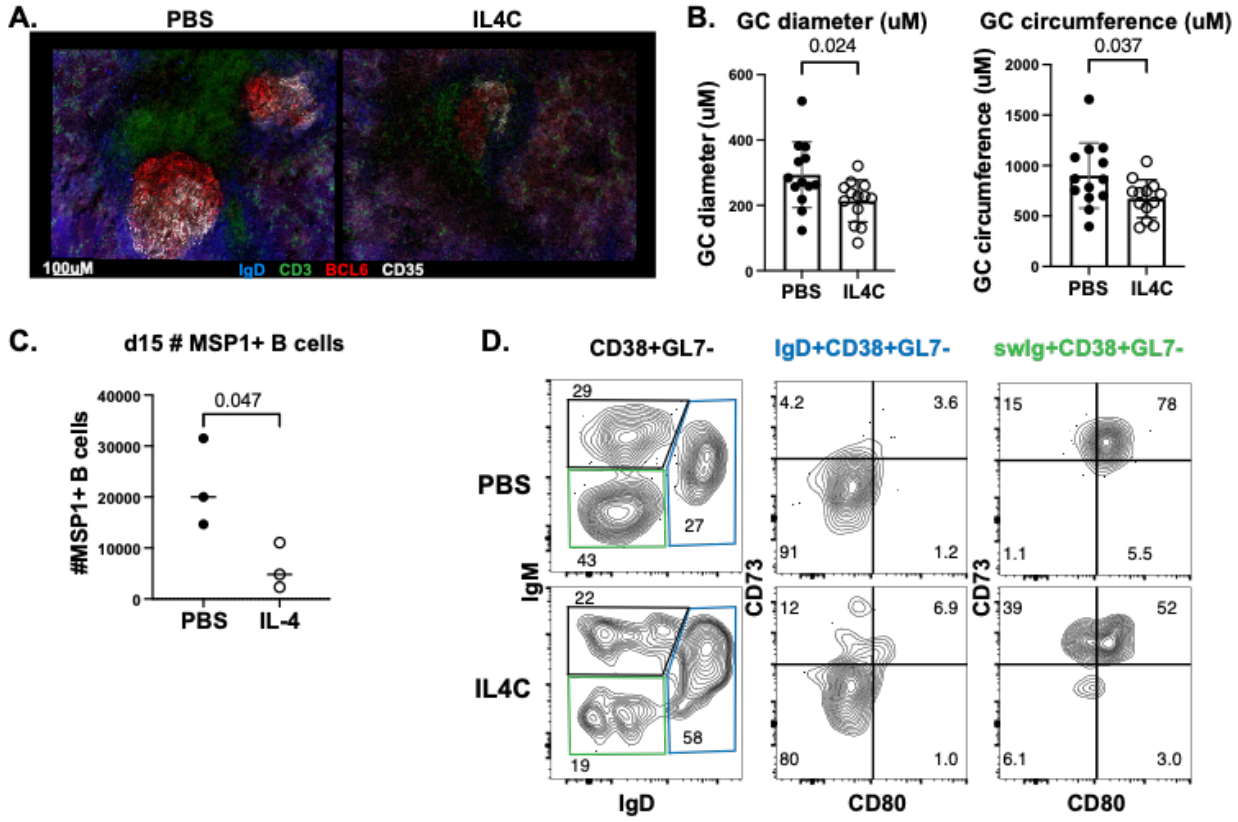

Figure 2.4. IL-4 administered after GC formation limits GC size and output. WT mice were infected with *P.ch* and treated with IL4C or PBS on days 12 and 14, and analyzed on day 15. **(A)** Representative images of GCs from spleen sections stained with anti-IgD, anti-CD3, anti-BCL6, and anti-CD35; PBS-treated (left) and IL4C-treated (right). (**B**) Diameter (left) and circumference (right) of GCs in mice treated with PBS or IL4C; each dot represents one GC. Spleens were collected from two independent experiments and 3 spleens per group were sectioned and stained, with 4-5 GCs analyzed per section. (**C**) Number of $MSP1^+$ B cells at day 15 in mice treated with PBS or non-complexed IL-4 on days 12, 13, and 14 post-*P.ch* infection. Data are representative of one experiment with 3 mice per group. (**D**) Representative flow cytometry plots indicating gating of CD73 and CD80 on MSP1-specific IgD^+ (blue) and $swIg^+$ (green) $CD38^+GL7^-$ B cells on day 15 in PBS- or IL4C-treated mice.

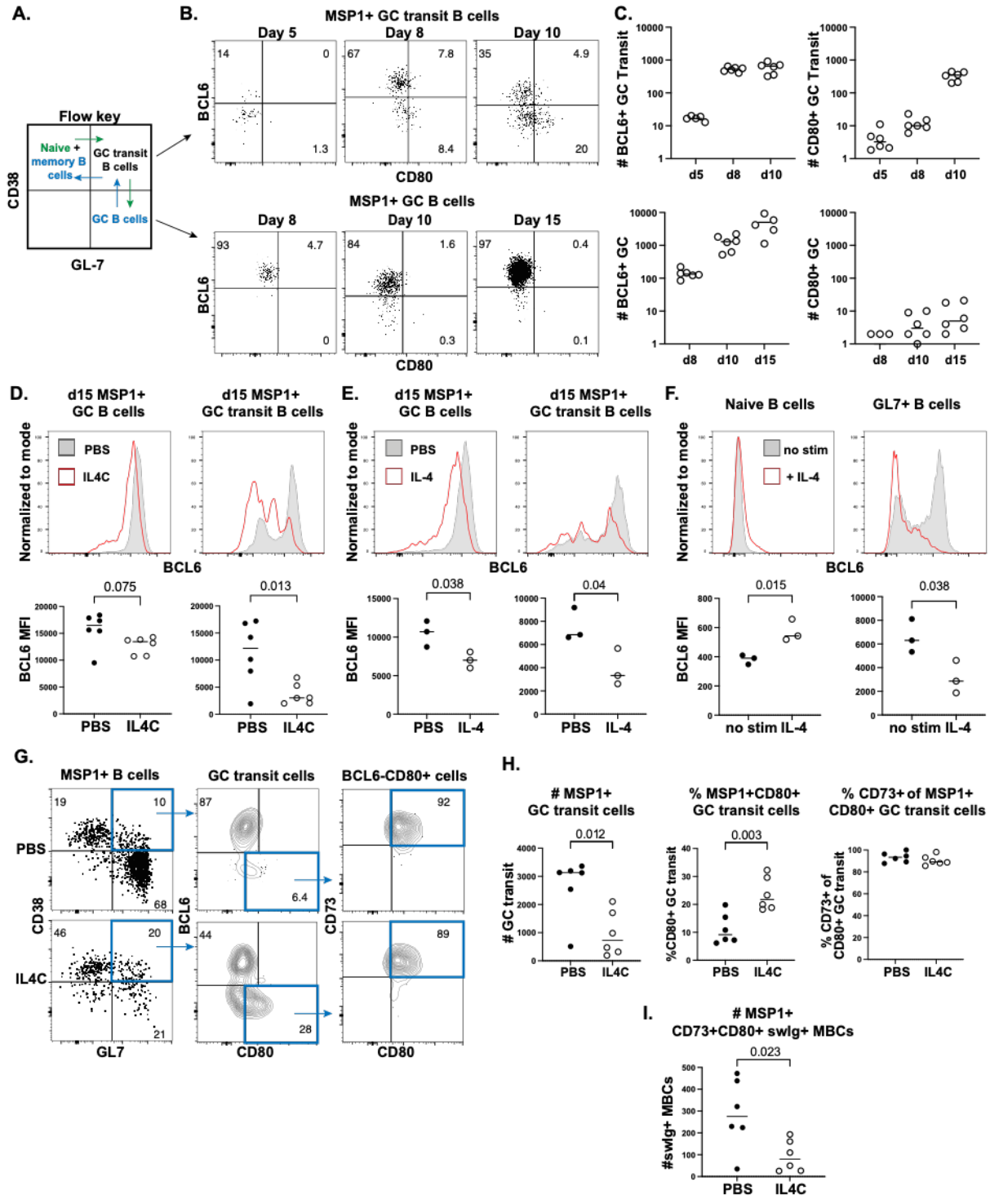

Figure 2.5. IL-4 downregulates BCL6 during an ongoing GC. (**A**) Flow key indicating the identification of naive and memory B cells, GC transit B cells, and GC B cells by CD38 and GL7 expression. (**B**) Representative flow plots and (**C**) quantification of BCL6 and CD80 expression

in MSP1$^+$ GC transit B cells (bottom) and GC B cells (top) from *P.ch*-infected WT mice on the indicated days post-infection. Data are combined from two independent experiments with 6 mice per group. Representative histograms (top) and quantified mean fluorescent intensity (MFI) of BCL6 expression (bottom) in GC B cells and GC transit B cells at day 15 in mice treated with (**D**) PBS (grey) or IL4C (red) on days 12 and 14 post-*P.ch* infection or (**E**) PBS or non-complexed IL-4 on days 12, 13, and 14 post-*P.ch* infection. Data in (D) are combined from two independent experiments with 6 mice per group, and data in (E) are from one experiment with 3 mice per group. (**F**) Naive or GL7$^+$ B cells were isolated from naive or *P.ch*-infected murine spleens, respectively, and cultured with agonistic anti-CD40 antibody with or without non-complexed IL-4. Representative histograms and quantified MFI of BCL6 expression after 24h. Data are combined from three independent experiments, with each symbol representing the average of three technical replicates from each experiment. (**G**) Representative flow plots and (**H**) quantification of GC transit B cell expression of CD80 and CD73 in mice treated with PBS or IL4C. (**I**) Number of MSP1$^+$swIg$^+$CD73$^+$CD80$^+$ MBCs. Data are combined from two independent experiments with 6 mice per group.

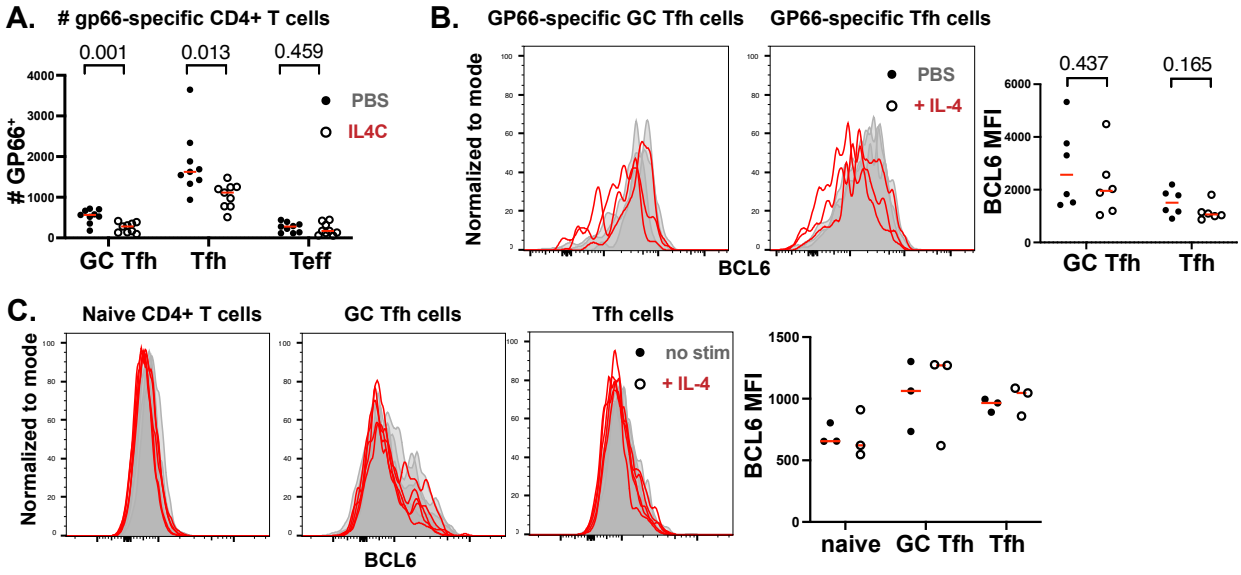

Figure 2.6. IL-4 does not downregulate BCL6 in T cells. WT mice were infected with *Py*-gp66 and treated with IL4C or PBS on days 12 and 14, and the gp66-specific CD4+ T cell response was analyzed on day 15. **(A)** Number of gp66-specific GC Tfh, Tfh, and Teff cells. **(B)** BCL6 expression on GC Tfh and Tfh cells. T cells were negatively selected from murine splenocytes and cultured with or without 10 ng/mL of recombinant IL-4 for 24h, then stained for flow cytometry. **(C)** BCL6 expression on naive CD4+ T cells ($CD44^{-}CD62L^{+}CXCR5^{-}PD\text{-}1^{-}$), GC Tfh cells ($CD44^{+}CD62L^{-}CXCR5^{+}PD\text{-}1^{+}$), and Tfh cells ($CD44^{+}CD62L^{-}CXCR5^{+}PD\text{-}1^{-}$).

2.2.4 IL-4 directly downregulates BCL6 on GC B cells via negative autoregulation

We sought to understand both how IL-4 was regulating BCL6 expression in GC B cells and why this may not be enough to generate long-lived MBCs. Although our primary B cell culture data suggested that IL-4 is acting directly on B cells to downregulate BCL6, we aimed to confirm this *in vivo* using mice in which IL4Rα is conditionally deleted from GC B cells. S1PR2 is upregulated as B cells enter the GC and acts as a tethering protein to maintain B cell positioning within the GC[88]. S1PR2creERT2$^{+/-}$TdTomato^{flox} mice have been shown to accurately

label GC B cells and fate map GC-derived MBCs[25]. We therefore crossed S1PR2creERT2$^{+/-}$ Tdtomato^{flox} mice to IL4Rα^{flox} mice to allow for the conditional deletion of IL4Rα from GC B cells after the GC has formed. We infected S1PR2creERT2$^{+/-}$Tdtomato^{flox} IL4Rα^{flox} and their S1PR2creERT2$^{-/-}$ littermates with *P.ch* and fed them tamoxifen chow beginning on day ten[25]. We then analyzed the MSP1-specific B cell response on day 20 to determine if IL4Rα-expressing GC-experienced cells were more likely to have downregulated BCL6 and exited the GC compared to IL4Rα-deficient cells, which cannot respond to IL-4 (**Figure 2.7A**). Using TdTomato as a fate reporter for S1PR2 expression, we observed that while >90% of MSP1-specific B cells were TdTomato^{+}, only ~50-70% of the cells within each B cell subset had successfully deleted IL4Rα (as seen by flow cytometric analysis of anti-IL4Rα staining) (**Figure 2.7A**). This has been previously described with these mice, and suggests that the IL4Rα locus may be less accessible than the Rosa26 locus for the cre recombinase[62]. Interestingly, within the TdTomato^{+} cells from the S1PR2creERT2$^{+/-}$ mice, the frequency of BCL6^{+} GC transit B cells was significantly higher in the IL4Rα^{-} population compared to the IL4Rα^{+} population (**Figure 2.7B**). This loss of BCL6 in IL4Rα^{+} GC transit B cells additionally corresponded to an increase in CD80^{+} GC transit B cells, further supporting that these CD80^{+} cells GC transit cells are GC-experienced, as they were fate-mapped with S1PR2 (**Figure 2.7B**). Together, these findings demonstrate that IL-4 is directly acting on GC B cells to downregulate BCL6.

As it was now evident that expression of IL4Rα on GC B cells was required for the IL-4-mediated loss of BCL6 expression in GL7^{+} B cells, we next sought to understand how IL-4 was differentially affecting BCL6 in B cells. Important work in the oncology field and more recently in CD4^{+} T cells has demonstrated that BCL6 is able to negatively autoregulate its own expression, a process that is often disrupted in B cell lymphomas[71,90,91]. It was formally possible

that while early IL-4 enhances BCL6 expression and GC entry early in an immune response, administration of IL-4 to GC B cells that express a high enough threshold of BCL6 may promote BCL6 to bind its own promoter and negatively autoregulate its own expression. We therefore sought to elucidate the specific signaling components that may be involved in this regulatory cascade. IL-4 can signal through both STAT6 and IRS-2, although its ability to promote BCL6 expression has been shown to depend upon the STAT6 binding site in the BCL6 promoter region[48,92,93]. To demonstrate a role for STAT6 signaling in the IL-4-mediated repression of BCL6, we treated *P.ch*-infected WT and STAT6-deficient (STAT6KO) mice with IL4C and analyzed BCL6 and CD80 expression in MSP1-specific GC transit B cells as above. Of interest, both GC B cells and GC transit B cells in both WT and STAT6KO mice were able to express equivalent amounts of BCL6, consistent with prior literature demonstrating that IL-21 and other molecules contribute to B cell expression of BCL6[47,53,94] (**Figure 2.8A**). However, while IL4C treatment of WT cells led to BCL6 downregulation and CD80 upregulation as shown above, GC transit B cells that lack STAT6 did not alter their expression of BCL6 or CD80 in response to IL4C, demonstrating that this IL-4 driven process is STAT6-dependent (**Figure 2.8A and 2.8B**).

We next directly tested if the IL-4-STAT6 pathway was promoting BCL6 to engage its negative autoregulation by using ΔBPS1 mice, which have an 8-nucleotide deletion in the BCL6 promoter binding site 1 (BPS1) that prohibits BCL6 from binding to its own promoter[71]. We adoptively transferred splenic B cells isolated from CD45.2$^+$ ΔBPS1 mice into CD45.1$^+$ WT hosts, infected the hosts with *P.ch* and treated the mice with IL4C on days 12 and 14, prior to analysis of the MSP1-specific B cell response on day 15 (**Figure 2.7C; Figure 2.8C**). In both GC B cells and GC transit B cells, BCL6 expression remained significantly higher in the ΔBPS1 cells than in WT cells (**Figure 2.7C**). Additionally, the IL-4-mediated downregulation of BCL6

in WT GC transit B cells corresponded to an increase in CD80 expression, whereas CD80 was not upregulated in ΔBPS1 GC transit B cells after IL4C treatment (**Figure 2.7D**). We additionally used the same primary murine B cell culture setup as above to determine how non-complexed IL-4 affects both ΔBPS1 naive and GC B cells. We isolated naive or $GL7^+$ B cells from WT or ΔBPS1 naive mice or mice 10 days post-$LCMV_{arm}$ infection, respectively, and cultured them with an agonistic anti-CD40 antibody (1 ug/mL) in the presence or absence of IL-4 (10 ng/mL) for 24h. IL-4 similarly increased BCL6 expression in WT and ΔBPS1 naive B cells (**Figure 2.7E**). However, while WT $GL7^+$ B cells downregulated BCL6 in response to IL-4, consistent with our findings in Figure 2, ΔBPS1 $GL7^+$ B cells showed no significant change in BCL6 expression following culture with IL-4 (**Figure 2.7E**). In fact, BCL6 expression was significantly higher in ΔBPS1 $GL7^+$ B cells cultured with IL-4 compared to WT $GL7^+$ B cells. Together, these data show that IL-4 signaling via STAT6 leads to BCL6 negative autoregulation in $GL7^+BCL6^+$ B cells, enhancing GC exit via a $CD38^+GL7^+CD80^+$ transition stage, yet these cells do not survive to become MBCs.

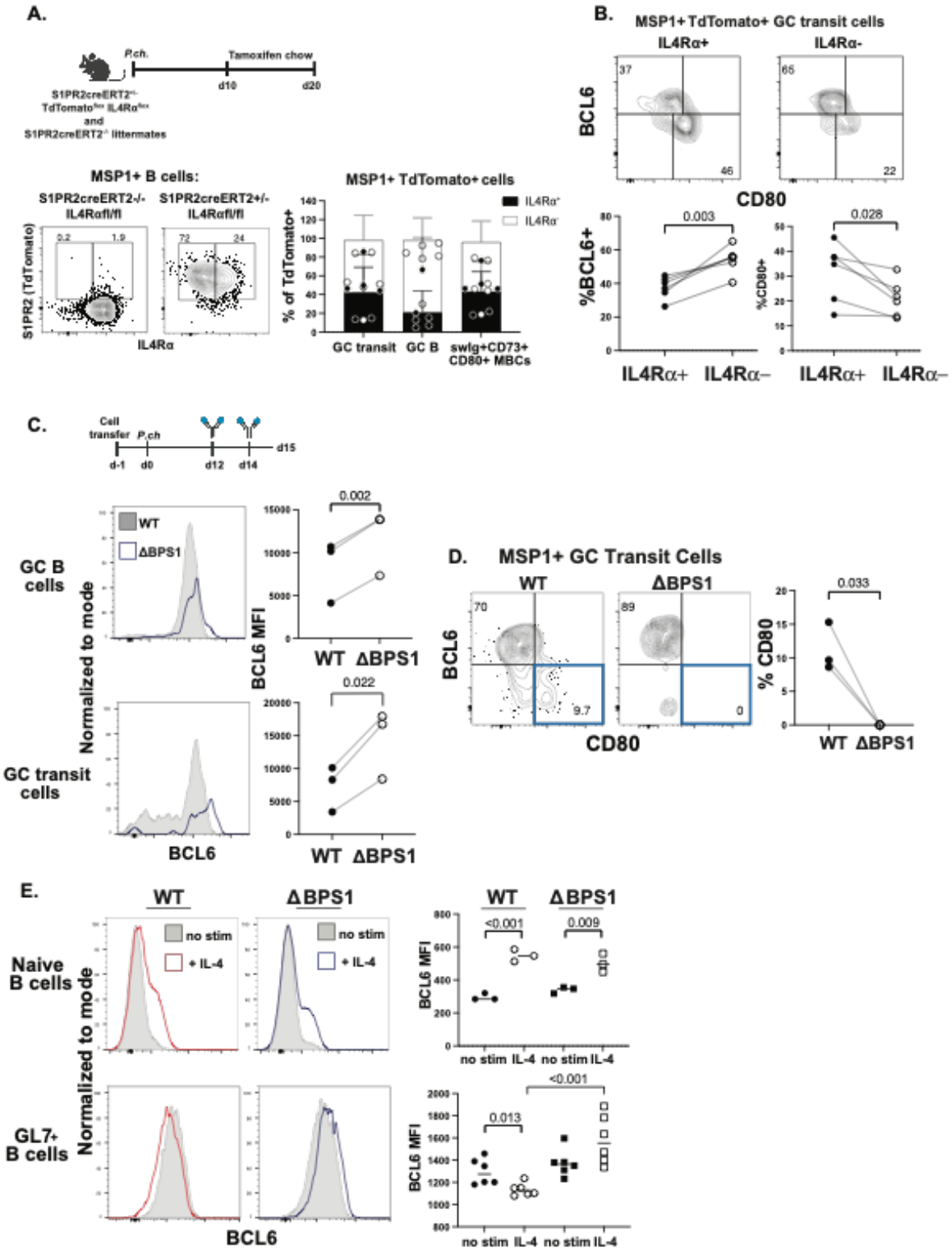
A.
P.ch.
Tamoxifen chow
d10
d20
S1PR2creERT2-/- TdTomatolox IL4Rαlox and S1PR2creERT2+/- littermates
MSP1+ B cells:
S1PR2creERT2-/- IL4Rαfl/fl
S1PR2creERT2+/- IL4Rαfl/fl
S1PR2 (TdTomato)
IL4Rα
0.2
1.9
72
24
MSP1+ TdTomato+ cells
% of TdTomato+
IL4Rα+
IL4Rα-
GC transit
GC B
swIg+CD73+ CD80+ MBCs
B.
MSP1+ TdTomato+ GC transit cells
IL4Rα+
IL4Rα-
BCL6
37
46
65
22
CD80
%BCL6+
%CD80+
0.003
0.028
IL4Rα+
IL4Rα–
IL4Rα+
IL4Rα–
C.
Cell transfer
P.ch
d-1
d0
d12
d14
d15
GC B cells
GC transit cells
WT
ΔBPS1
Normalized to mode
BCL6
BCL6 MFI
0.002
0.022
WT
ΔBPS1
D.
MSP1+ GC Transit Cells
WT
ΔBPS1
BCL6
CD80
70
9.7
89
0
% CD80
0.033
WT
ΔBPS1
E.
WT
ΔBPS1
Naive B cells
GL7+ B cells
no stim
+ IL-4
Normalized to mode
BCL6
BCL6 MFI
<0.001
0.009
0.013
<0.001
no stim
IL-4
no stim
IL-4

Figure 2.7. IL-4 signaling in GC B cells triggers BCL6 negative autoregulation. (**A**) S1PR2creERT2$^{+/-}$-TdTomato^{flox}IL4Rα^{flox} mice and S1PR2creERT2$^{-/-}$ littermates were infected with *P.ch* and fed tamoxifen chow beginning 10 days post-infection and analyzed on day 20. Representative flow plots and quantification of TdTomato^{+} cells that retained or successfully deleted IL4Rα shown on the bottom. IL4Ra gating based on FMO control, as shown in Figure 2.1. (**B**) Representative flow plots (top) and quantification (bottom) of BCL6 and CD80 expression within IL4Rα^{+} or IL4Rα^{-} MSP1^{+}TdTomato^{+} GC transit B cells from S1PR2creERT2$^{+/-}$ TdTomato^{flox} IL4Rα^{flox} mice. Data are combined from three independent experiments with 6 mice per group. (**C**) Splenic B cells were isolated from ΔBPS1 mice and transferred into WT hosts. The mice were infected with *P.ch*, treated with IL4C on days 12 and 14, and the MSP1-specific B cell response was analyzed on day 15. Representative histograms and quantification of BCL6 expression in WT (grey) and ΔBPS1 (blue) GC B cells and GC transit B cells on day 15. (**D**) Representative flow plots depicting BCL6 by CD80 expression in MSP1^{+} GC transit B cells and quantified frequency of CD80^{+} GC transit B cells. Data are from two independent experiments with three mice. (**E**) BCL6 expression on naive or GL7^{+} B cells isolated from naive or LCMV-infected murine spleens, respectively, and cultured with agonistic anti-CD40 antibody with or without non-complexed IL-4 for 24h. Data are from one experiment, with each symbol representing replicates from one (naive) or two pooled (GL7^{+}) mice.

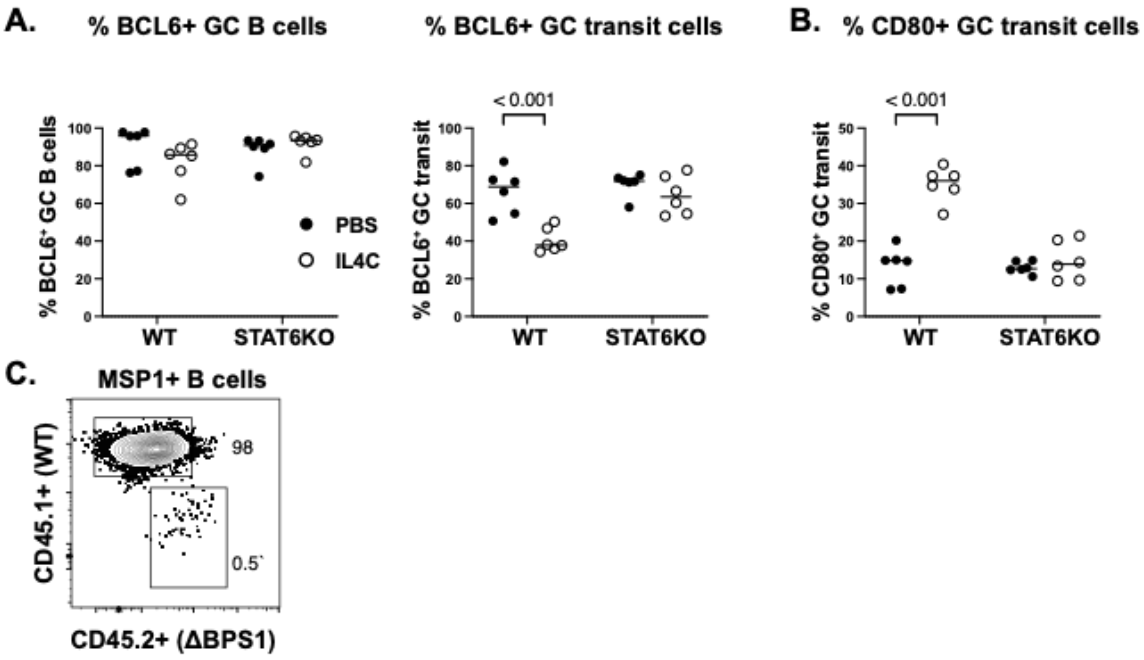

Figure 2.8. IL-4-mediated acts directly on B cells in a STAT6-dependent manner to downregulate BCL6. WT and STAT6KO mice were infected with *P.ch* and treated with IL4C or PBS on days 12 and 14, and the MSP1-specific B cell response was analyzed on day 15. (**A**) Frequency of MSP1$^+$ GC B cells and GC transit B cells expressing BCL6. (**B**) Frequency of MSP1$^+$ GC transit B cells expressing CD80. Data are combined from two independent experiments with 6 mice per group. (**C**) Splenic B cells were isolated from ΔBPS1 mice and transferred into WT hosts. The mice were infected with *P.ch*, treated with IL4C on days 12 and 14, and the MSP1-specific B cell response was analyzed on day 15. Representative flow plot indicating gating on MSP1$^+$CD45.1$^+$ WT and CD45.2$^+$ ΔBPS1 B cells.

2.2.5 IL-4-mediated cell death limits the formation of GC-derived MBCs

To better understand why the IL-4-mediated downregulation of BCL6 was not associated with enhanced MBC formation and survival, we began to dissect where along the path of MBC

formation these cells were lost. We first interrogated any changes in GC cycling, as a disruption of positive selection of light zone (LZ) GC B cells into the dark zone (DZ) could explain the lack of swIg$^+$ MBCs (**Figure 2.5I**). However, there were no changes in the proportion of GC B cells in the LZ or DZ, as measured by CXCR4 and CD86 expression, in response to IL4C treatment (**Figure 2.9A**). We confirmed this by examining the expression of c-myc, a transcription factor which is transiently upregulated as GC B cells migrate into the DZ[11,47]. We did not observe any changes in c-myc expression in GC B cells, BCL6$^-$CD80$^+$ GC transit B cells (exiting GC), or CD73$^+$CD80$^+$ memory B cells in WT mice infected with *P.ch* and treated with IL4C or PBS (**Figure 2.9B**).

To test if IL4C treatment was impacting the formation of memory precursors in the GC or their successful exit, we additionally analyzed expression of CD23 and BCL2 on the three populations described above. CD23 is upregulated on GC B cells that have recently received IL-4 and/or CD40L signals from T cells, and CD23$^+$ GC B cells have been identified as memory B cell precursors[24,62]. IL4C treatment led to a significant increase in CD23$^+$BCL6$^-$CD80$^+$ GC transit B cells, whereas GC B cells and MBCs had modest, but statistically insignificant increases in CD23 expression in response to IL4C (**Figure 2.10A**). This suggests that IL-4 is promoting memory B cell differentiation, and is consistent with our hypothesis that the CD80$^+$ GC transit B cells have recently left the GC in response to IL-4 signaling. We also stained for BCL2, an anti-apoptotic protein that is critical for MBC survival[33,34,36,68]. BCL2 is highly expressed by naive B cells, is downregulated upon GC entry, and is upregulated again as GC B cells form MBCs[36]. Importantly, it can repress BCL6, and it has been suggested that this antagonism is mutual[32,34]. Interestingly, GC B cells and MBCs from mice treated with IL4C had a striking loss of BCL2 compared to control-treated mice, while BCL2 expression in BCL6$^-$CD80$^+$ GC transit B cells was unchanged

between groups (**Figure 2.10B**). This suggests that B cells may be dying while exiting the GC due to a lack of BCL2 upregulation within the GC, which could explain the numerical loss of GC transit B cells and GC-derived MBCs following IL4C treatment (**Figure 2.2H and 2.2I**). Importantly, ~80% of MBCs were still $BCL2^+$, suggesting that the vast majority of these cells are still viable (**Figure 2.10B**). Together, these data suggest that IL-4 downregulates BCL6 in GC B cells to promote MBC formation, but is insufficient to upregulate BCL2, which could replace BCL6 as an anti-apoptotic signal. This results in an increase in GC exit, but may also lead to cell death, as exiting GC B cells that lack both BCL6 and BCL2 would not have the signals needed to survive as long-lived MBCs.

To test if the diminished expression of BCL2 in GC B cells following IL4C treatment is indicative of increased death of IL-4 "selected" pre-memory GC B cells and recently formed MBCs, we administered IL4C or PBS simultaneously with the pan-caspase inhibitor emricasan to WT mice infected with *P.ch* (**Figure 2.10C**). Emricasan treatment resulted in an increase in MSP1-specific B cells regardless of PBS or IL4C treatment, demonstrating that, as expected, blocking cell death increases MSP1-specific B cell numbers in the presence or absence of IL-4 treatment (**Figure 2.10D**). However, while mice treated with both PBS and emricasan had only modest increases in GC B cells and $swIg^+CD73^+CD80^+$ MBCs compared to PBS-treated mice (fold changes of 1.22 and 0.15, respectively), mice receiving IL4C and emricasan had a 5-fold increase in GC B cells and a 6-fold increase in $swIg^+CD73^+CD80^+$ MBCs compared to mice treated with IL4C alone, demonstrating that IL-4 is leading to increased GC B cell death (**Figure 2.10D**). Consistent with this finding, mice treated with IL4C and emricasan had a significantly higher number of $BCL6^-$ GC B cells compared to mice treated with PBS and emricasan, indicating that there is a large proportion of GC B cells dying due to IL-4-mediated downregulation of BCL6

(**Figure 2.10E**). IL4C and emricasan treatment also resulted in an increase in $CD80^+$ GC transit B cells compared to IL4C alone, suggesting that IL-4-mediated cell death is preventing pre-memory cells from surviving after exiting the GC (**Figure 2.10F**).

We additionally validated these results in BCL2 transgenic mice (BCL2-Tg), which have a functional human BCL2 transgene expressed only in the murine B cell lineage[68]. We infected WT and BCL2-Tg littermates with *P.ch* and treated them with IL4C or PBS on days 12 and 14 (**Figure 2.9C**). As with the use of emricasan, there was no loss in antigen-specific B cells between BCL2-Tg mice treated with PBS or IL-4 at day 15 (**Figure 2.9D**). Consistent with BCL2 acting antagonistically to the GC transcriptional program, BCL2-Tg mice did not form significantly larger GCs (**Figure 2.9D**). However, IL4C treatment in BCL2-Tg mice resulted in a significant increase in $swIg^+CD73^+CD80^+$ MBCs compared to littermate controls, whereas PBS treatment in BCL2-Tg mice did not specifically impact $swIg^+CD73^+CD80^+$ MBCs (**Figure 2.9D**). Together, these data demonstrate that the loss of B cells in response to IL4C treatment is due to the death of pre-memory $swIg^+$ GC B cells following the IL-4-mediated downregulation of BCL6. Preventing this cell death through either caspase inhibition or overexpression of an anti-apoptotic signal fully recovers both GC B cells and GC-derived MBCs.

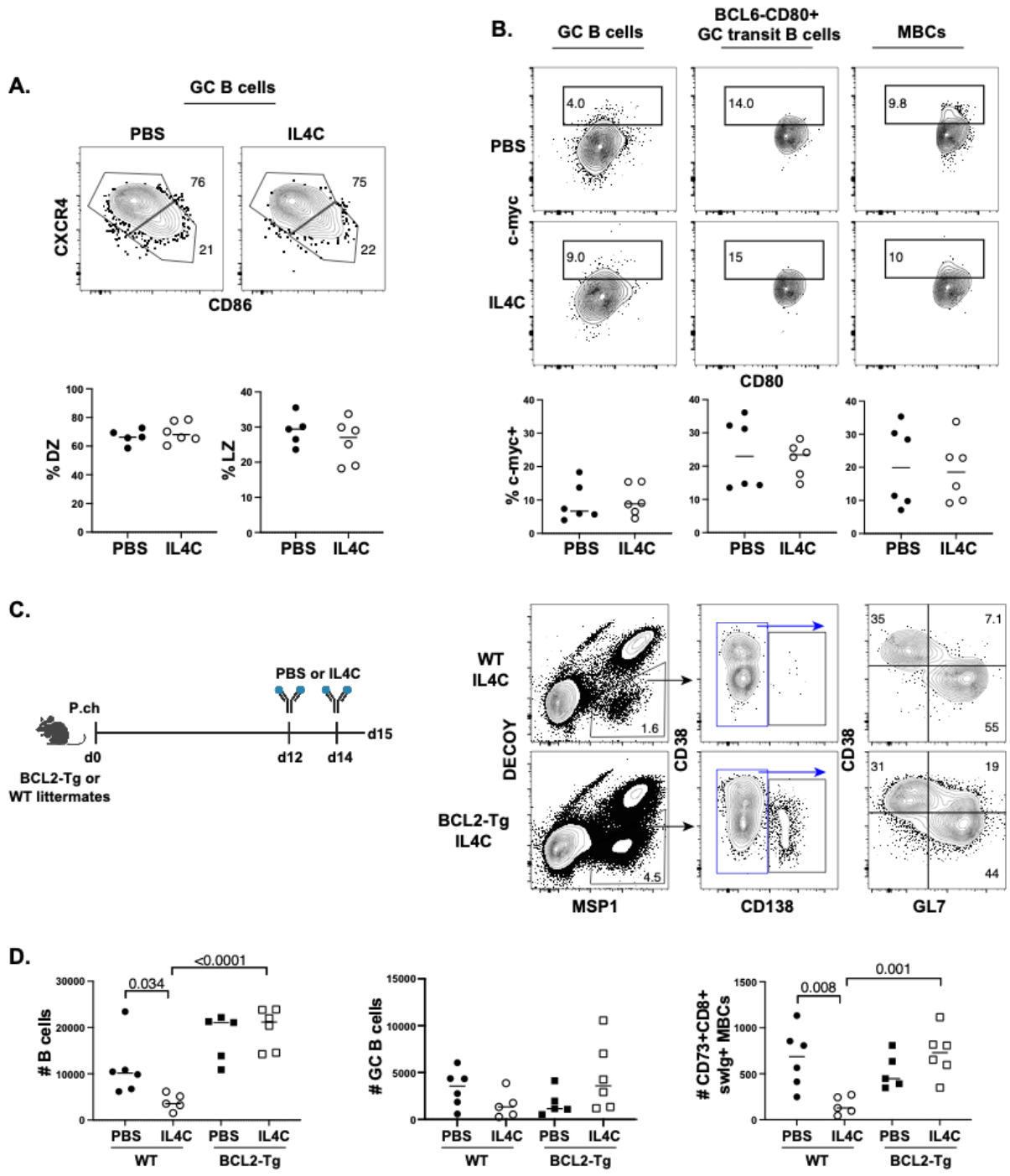

Figure 2.9. IL-4 increases pre-memory GC B cell death. WT mice were infected with *P.ch* and treated with PBS or IL4C on days 12 and 14. (**A**) Representative flow plots and quantification of MSP1^{+} GC B cells in the dark zone (CXCR4^{hi}CD86^{lo}) or light zone (CXCR4^{lo}CD86^{hi}). (**B**) Representative flow plots and quantification of MSP1^{+}c-myc^{+} GC B cells (left), BCL6^{-}CD80^{+} GC

transit B cells (middle), and MBCs (right). Data are combined from three independent experiments with 5-6 mice per group. (**C**) WT mice and BCL2-Tg littermates were infected with *P.ch* and treated with PBS or IL4C on days 12 and 14 and analyzed on day 15. Representative flow plots showing gating on $MSP1^+$ B cells from WT (top) and BCL2-Tg (bottom) mice treated with IL4C. (**D**) Number of $MSP1^+$ total B cells, GC B cells, and $swIg^+$ $CD73^+CD80^+$ MBCs in each group. Data are combined from three independent experiments with 5-6 mice per group.

.

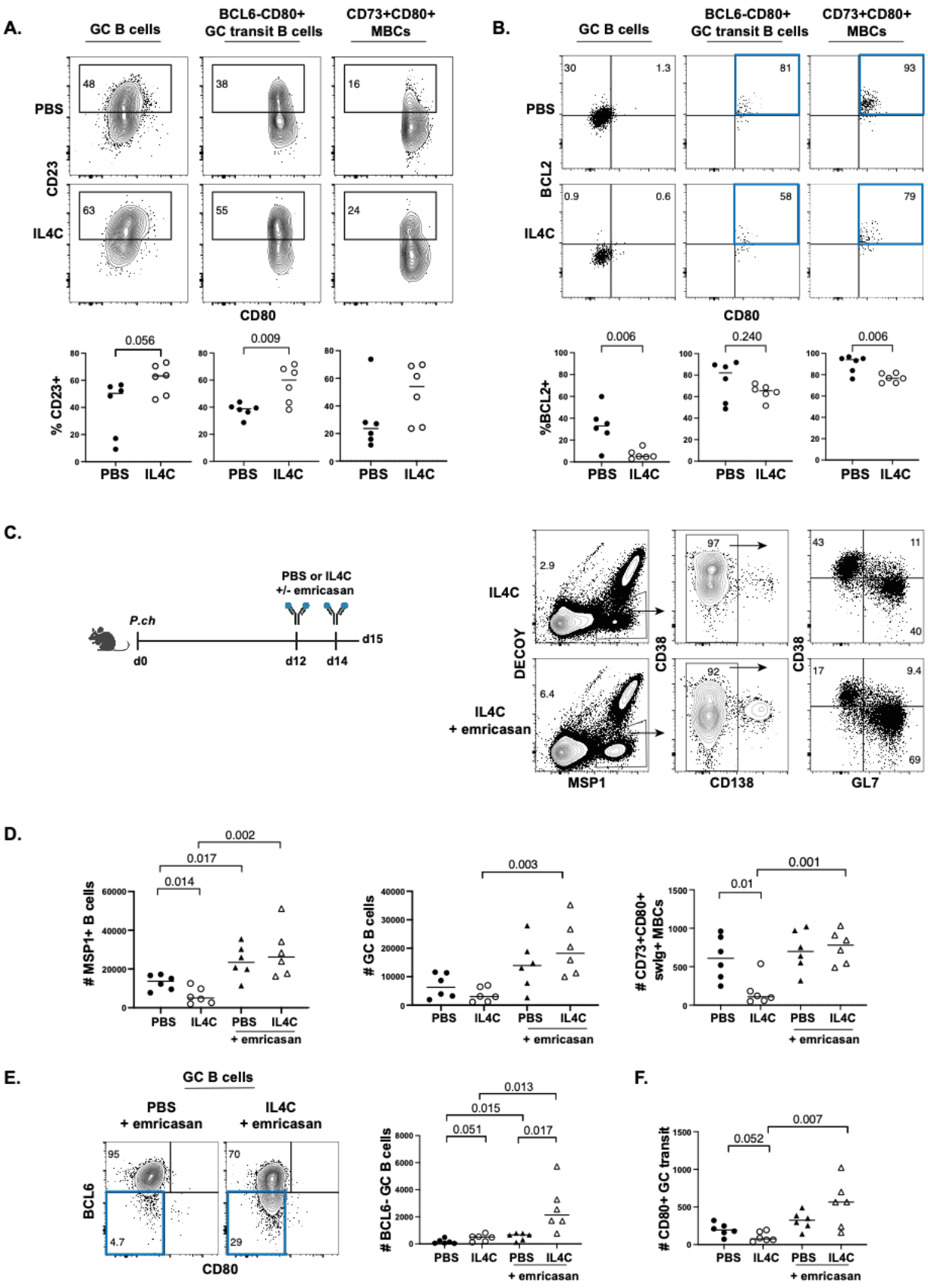
A.
GC B cells
BCL6-CD80+ GC transit B cells
CD73+CD80+ MBCs
PBS
IL4C
CD23
CD80
48
38
16
63
55
24
0.056
0.009
% CD23+
PBS
IL4C
B.
GC B cells
BCL6-CD80+ GC transit B cells
CD73+CD80+ MBCs
PBS
IL4C
BCL2
CD80
30
1.3
81
93
0.9
0.6
58
79
0.006
0.240
0.006
%BCL2+
C.
PBS or IL4C +/- emricasan
P.ch
d0
d12
d14
d15
IL4C
IL4C + emricasan
DECOY
MSP1
CD38
CD138
GL7
2.9
97
43
11
40
6.4
92
17
9.4
69
D.
MSP1+ B cells
0.002
0.017
0.014
GC B cells
0.003
CD73+CD80+ swIg+ MBCs
0.001
0.01
PBS
IL4C
+ emricasan
E.
GC B cells
PBS + emricasan
IL4C + emricasan
BCL6
CD80
95
4.7
70
29
BCL6- GC B cells
0.013
0.015
0.051
0.017
F.
CD80+ GC transit
0.052
0.007

Figure 2.10. Excess IL-4 leads to increased GC B cell death and loss of MBCs. WT mice were infected with *P.ch* and treated with IL4C or PBS on days 12 and 14, and the MSP1-specific B cell response was analyzed on day 15. Representative flow plots and quantification of $MSP1^+$ (**A**) $CD23^+$ and (**B**) $BCL2^+$ GC B cells (left), $BCL6^-CD80^+$ GC transit B cells (middle), and MBCs (right). Data are combined from three independent experiments with 5-6 mice per group. (**C**) WT mice were infected with *P.ch* and treated with PBS or IL4C both with or without emricasan on days 12 and 14. Representative flow plots showing gating on $MSP1^+$ B cells from mice treated with IL4C (top) or IL4C and emricasan (bottom) on day 15 post-infection. (**D**) Number of $MSP1^+$ total B cells, GC B cells, and $swIg^+CD73^+CD80^+$ MBCs in each group. (**E**) Flow plots and quantification of $BCL6^-$ GC B cells. (**F**) Number of $CD80^+$ GC transit B cells in each group. Data are combined from three independent experiments with 6 mice per group.

2.2.7 IL-4 signaling regulates MBC selection stringency

Together, our data suggested that GC B cell-intrinsic IL-4 signaling has the capacity to drive the exit of nascent, $CD23^+CD80^+$ memory precursor cells from the GC. This raises the possibility that IL-4 from GC Tfh cells could be a key cue involved in the selection of somatically hypermutated (SHM) GC B cells. Germinal center selection is necessary to ensure that a diverse population of B cells with mutated BCRs of sufficient affinity survive into the MBC pool, and this selection process occurs via interactions with GC Tfh cells and antigen-bearing follicular dendritic cells[10]. The specific cues that direct this selection process remain unknown. Based on our data, we hypothesized that IL-4 from a GC Tfh cell can select B cells to exit the GC via the downregulation of BCL6. Additional cues to the B cell would lead to the expression of anti-apoptotic molecules like BCL2, which would then promote long-lived MBC survival. We therefore aimed to assess if

modulating IL-4 signaling could alter GC B cell selection into the MBC pool. We hypothesized that the addition of exogenous IL4C would inappropriately "select" GC B cells that had not undergone sufficient cycles of somatic hypermutation and affinity maturation to have been selected under physiological conditions. To test this, we sorted MSP1-specific IgG^+CD80^+ GC transit B cells and $IgG^+CD73^+CD80^+$ MBCs on day 15 following PBS or IL4C treatment on days 12 and 14 and bulk-sequenced their B cell receptors (BCRs). Cells from the IL4C-treatment group in both populations had fewer somatic hypermutations than those from control-treated mice, which has been shown to correlate with affinity[28] (**Figure 2.11A**).

To verify that MBCs formed in the presence of excess IL-4 are in fact of lower affinity, we used a re-challenge model to induce memory B cell differentiation into plasmablasts, which allows for the analysis of MBC-derived serum antibodies by ELISA. We infected mice with *P.y.*-GP66 and administered PBS or IL4C every other day from day 12 through day 25, then re-challenged the mice with 10^7 *P.y.*-GP66-iRBCs. We analyzed anti-MSP1 IgG antibody titers in the serum by ELISA under normal and chaotropic or "stringent" conditions using a urea wash to disrupt weak bonds to get a measure of antibody affinity/avidity. Serum was collected at both 25 days post-infection and 5 days post-challenge when $swIg^+$ MBCs differentiate into plasmablasts[74] (**Figure 2.11B**). There were no significant differences in serum anti-MSP1 IgG levels prior to challenge at day 25 as measured by normal or stringent ELISA, suggesting that antibody quantity or quality present at this time point was not impacted by IL4C treatment [95] (**Figure 2.11B, Figure 2.12A**). After challenge, normal ELISAs revealed higher serum antibody titers in both challenged groups, although not significantly so for the IL4C-treated animals. Furthermore, although there are not significant differences in antibody titers seen in stringent ELISAs on serum from the two groups at day 25, after rechallenge, stringent ELISAs showed a significant drop in signal from the IL4C-

treated mice compared to the PBS-treated mice (**Figure 2.11B**). This indicates that while early antibody secreting cells are not impaired in the IL4C-treated mice after a primary infection, MBCs formed in the presence of excess IL-4 were of lower affinity than those formed in control-treated mice. Together, these results suggest that IL-4-mediated downregulation of BCL6 and the resulting increase in cell death underlies both the loss of MBCs and of high affinity MBCs.

These results led us to hypothesize that in an environment with physiological levels of IL-4 signaling, a lack of IL4-signaling may maintain longer GCs and produce lower affinity MBCs. To test this, we infected WT mice and global IL4Rα-deficient (IL4RαKO) mice with *P.y*-GP66 and analyzed the MSP1-specific B cell response at day 60 to determine if there were differences in GC maintenance or memory B cells (**Figure 2.11C**). Importantly, IL4RαKO mice have been shown to develop GCs at a similar rate to WT mice, likely due to the outsize role of IL-21 in promoting GC formation and in keeping with our data demonstrating equivalent BCL6 expression in STAT6KO B cells[47,96]. WT and IL4RαKO mice infected with *P.y*-GP66 had similar numbers of total MSP1-specific B cells and no differences in the number of $swIg^+CD73^+CD80^+$ MBCs, demonstrating that IL-4 is not the only cue that can promote MBC formation (**Figure 2.11D**). However, IL4RαKO mice had significantly larger GCs at day 60 by both number and frequency (**Figure 2.11D**). The larger GCs cannot be attributed to a lack of parasite clearance, as the IL4RαKO mice controlled parasitemia as well as the WT mice throughout infection (**Figure 2.12B and 2.12C**). Together, these data suggest that while MBCs can still form, there may be increased retention or survival of GC B cells in the absence of IL-4 signaling. Importantly, there were no significant differences in serum anti-MSP1 IgG levels as measured by ELISA or by stringent ELISA (**Figure 2.12D and 2.12E**). Thus, while IL-4 may impact MBC survival and selection within the GC, it may not affect plasma cell selection.

We next sought to determine whether the longer lasting GCs were due to enhanced survival of lower affinity GC B cells, which would then result in the formation of lower affinity MBCs. To test this, we re-challenged WT and IL4RαKO mice with 10^7 *P.y*-GP66-iRBCs at day 60 and analyzed the serum antibody response 5 days post-challenge, when MBCs have begun to differentiate into plasmablasts[74] (**Figure 2.11C**). Serum anti-MSP1 IgG levels were similar between the two re-challenged groups by normal ELISA, indicating that the lack of IL-4 signaling does not impact MBC differentiation into plasmablasts (**Figure 2.11E**). Stringent ELISAs, however, revealed a significant reduction in signal in serum from IL4RαKO mice compared to serum from WT mice at day 5 post-challenge, suggesting that the bulk of IL4RαKO MBC-derived antibodies were lower affinity than those from WT mice (**Figure 2.11F**). This indicates that in the absence of IL-4-mediated downregulation of the anti-apoptotic BCL6, lower affinity B cells can persist in the GC, thus leading to a lower affinity MBC pool. Together, these findings suggest that IL-4 tightly regulates MBC selection in the GC, and that both too little or too much IL-4 signaling can lead to a loss of MBC selection stringency.

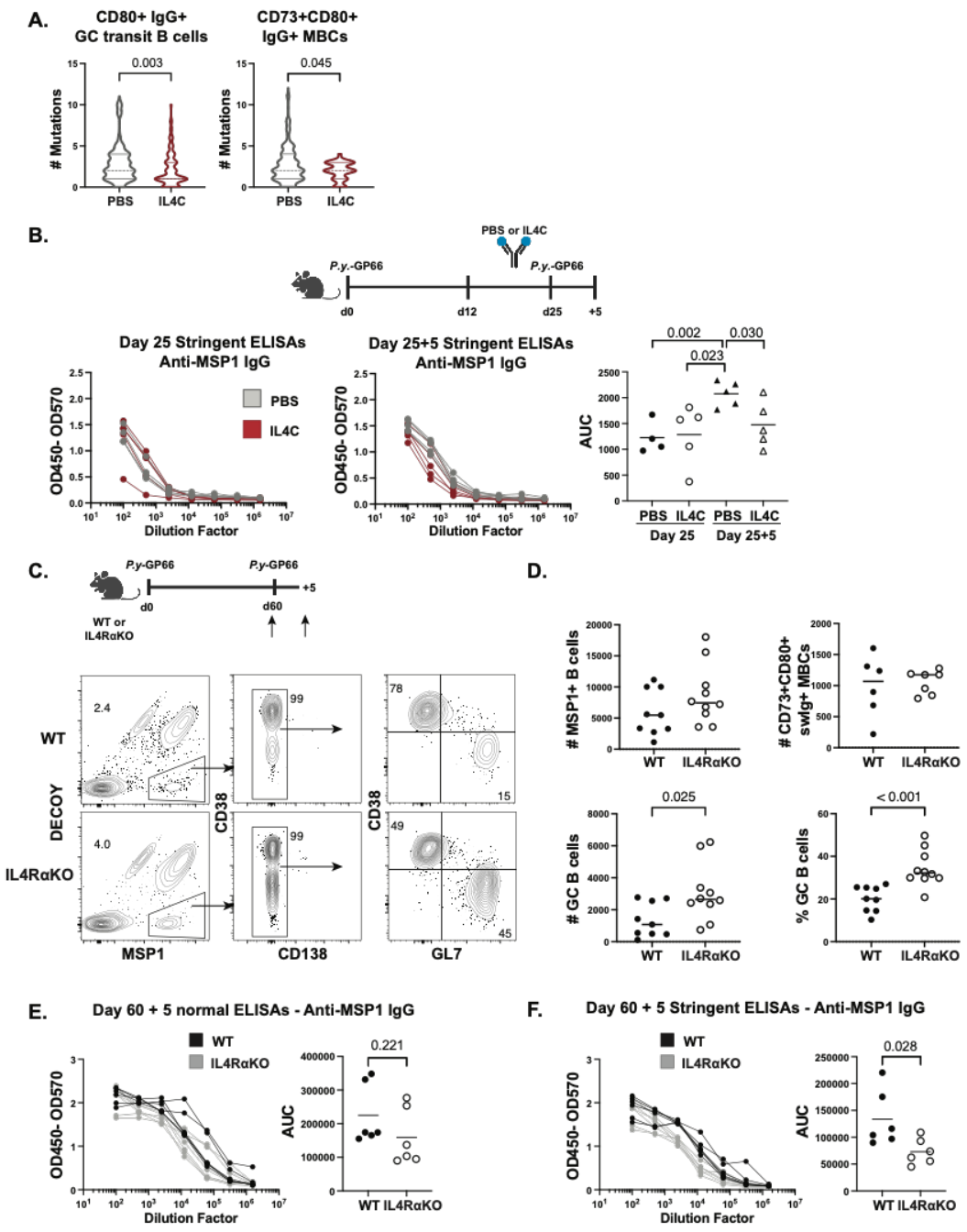

Figure 2.11. IL-4 signaling regulates MBC selection stringency. (**A**) Number of somatic hypermutations in MSP1^{+}IgG^{+} CD80^{+} GC transit and CD73^{+}CD80^{+} memory B cells sorted and sequenced on day 15 following PBS or IL4C treatments on days 12 and 14. Data are representative of two independent experiments with 6 mice per group. (**B**) WT mice were infected with *P.y.*-GP66 and treated with PBS or IL4C every other day between days 12-25, and re-challenged on

day 25. Stringent ELISA dilution curves and AUC for anti-MSP1 IgG in serum collected at day 25 and 5 days post-challenge. Data are combined from two independent experiments with 4-5 mice per group. (**C**) WT and IL4RαKO mice were infected with *P.y*-GP66 and the MSP1-specific B cell response was analyzed on day 60, or mice were re-challenged on day 60 and analyzed 5 days post-challenge. Representative flow plots showing gating on $MSP1^+$ B cells from each group. (**D**) Number of $MSP1^+$ B cells and $swIg^+CD73^+CD80^+$ MBCs (top) and number and frequency of GC B cells (bottom) at day 60. Data are combined from three independent experiments with 6-10 mice per group. (**E**) Normal and (**F**) stringent ELISA dilution curves and AUC for anti-MSP1 IgG in serum collected 5 days post-challenge. Data are combined from two independent experiments with 6 mice per group.

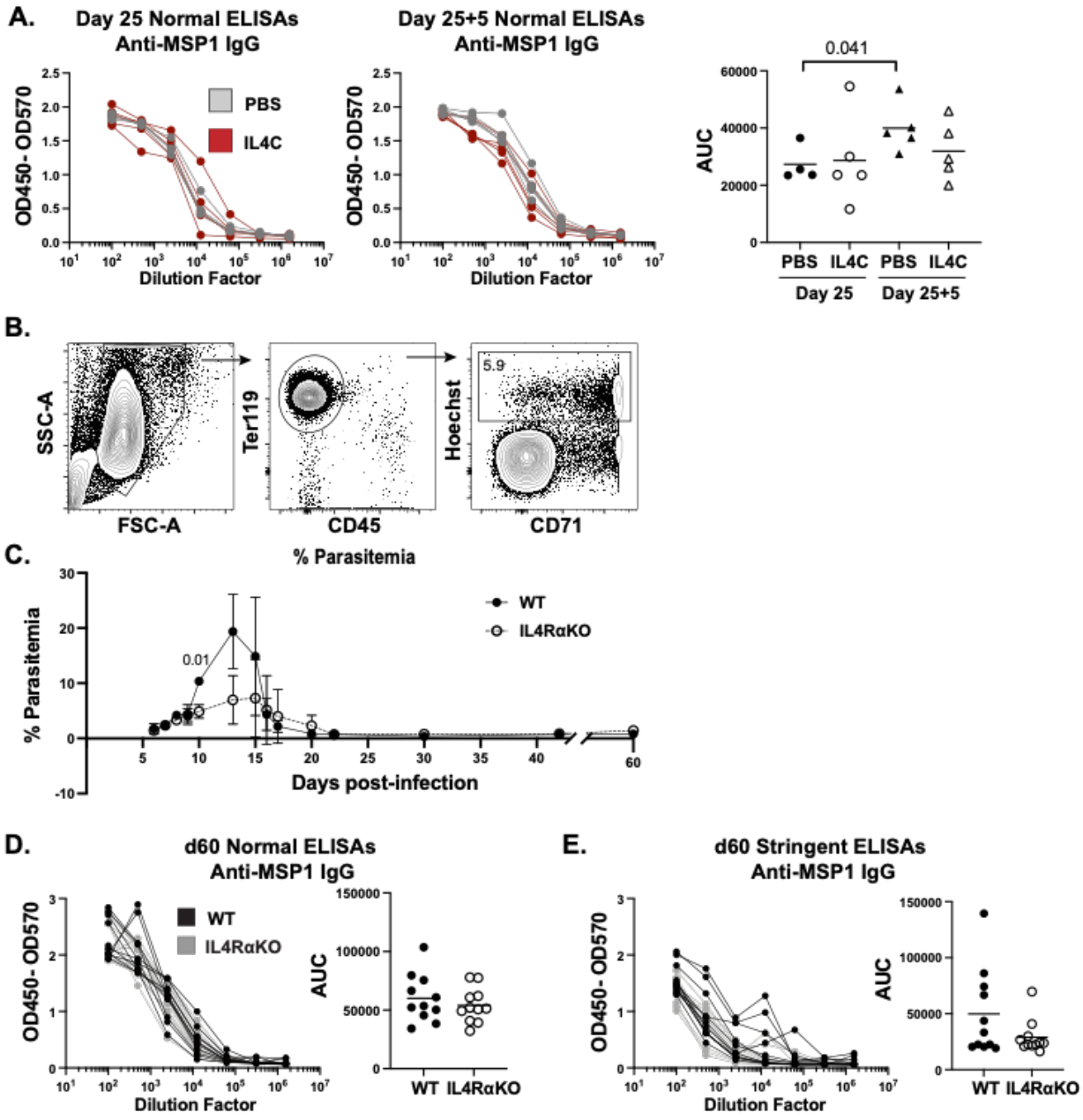

Figure 2.12. Characterization of the memory response in IL4RαKO mice. WT mice were infected with *P.y.*-GP66 and treated with PBS or IL4C every other day between days 12-25, and re-challenged on day 25. (**A**) Normal ELISA dilution curves and AUC for anti-MSP1 IgG in serum collected at day 25 and 5 days post-challenge. Data are combined from two independent

experiments with 4-5 mice per group. WT and IL4RαKO mice were infected with *P.y*-GP66 and analyzed 60 days post-infection. (**B**) Representative gating scheme to identify *Plasmodium*-infected iRBCs, gated as $Ter119^{+}CD45^{-}Hoechst^{+}$ in 1uL of blood from a WT mouse 9 days post-infection. (**C**) Parasitemia throughout the 60 days of infection in each group. Data are combined from three independent experiments with 6-7 mice per group. Dilution curves and AUC of (**E**) normal and (**F**) stringent ELISAs to assess anti-MSP1 IgG serum levels. Data are combined from four independent experiments with 11 mice per group.

2.2.8 A lack of IL-4 signaling in B cells promotes longer-lasting GCs and lower affinity MBCs

Although GC formation has shown to be largely normal in IL4RαKO mice, the lack of IL-4 signaling in other cell populations may be involved in the increased GC longevity and lower affinity MBCs observed above. To address this, we infected $S1PR2creERT2^{+/-}$ $Tdtomato^{flox}IL4R\alpha^{flox}$ mice and their $S1PR2creERT2^{-/-}$ littermates with *P.y.*-GP66 and fed them tamoxifen chow from day 10 through day 60 (**Figure 2.13A**). This model allows us to determine whether a specific lack of IL-4 signaling in GC B cells impacts GC persistence and MBC formation. As observed with these mice at day 20 (**Figure 2.7A**), there was an incomplete deletion of IL4Rα on $TdTomato^{+}$ B cells, limiting numerical analyses between groups. Within the MSP1-specific $TdTomato^{+}$ (S1PR2 fate-mapped) population from $S1PR2creERT^{+/-}$ mice, there is no difference in the frequency of $IL4R\alpha^{-}$ cells found within total B cells or $swIg^{+}CD73^{+}CD80^{+}$ MBCs, indicating that GC-derived MBCs can still form in the absence of IL-4 signaling, as shown above (**Figure 2.13B**). However, there was a significantly increased proportion of $IL4R\alpha^{-}$ B cells within the GC compared to other B cell subsets, suggesting these cells are more likely to be retained in the GC (**Figure 2.13B**). Similarly, there was a consistently higher frequency of GC B

cells within the IL4Rα^{-}TdTomato^{+} population compared to GC B cells within the IL4Rα^{+}TdTomato^{+} population (**Figure 2.13C**). This recapitulates the findings in the IL4RαKO mice, demonstrating that GCs can persist for longer in the absence of the IL-4-mediated downregulation of BCL6, potentially due to increased GC B cell survival. Importantly, we also noted that within the MSP1-specific TdTomato^{+} population from S1PR2creERT$^{+/-}$ mice, the tetramer mean fluorescence intensity (MFI) was significantly higher on IL4Rα^{+} TdTomato^{+}swIg^{+}CD73^{+}CD80^{+} MBCs compared to their IL4Rα^{-} counterparts within the same animal (**Figure 2.13D**). The MFI of antigen binding has been shown to correlate with BCR affinity, thus this indicates that the absence of IL-4 signaling in GC B cells may result in the formation of lower affinity GC-derived MBCs[97–100]. This agrees with our observations in the IL4RαKO mice that the IL-4-mediated downregulation of BCL6 in GC B cells is necessary to limit the persistence of lower affinity GC B cells in the memory B cell pool.

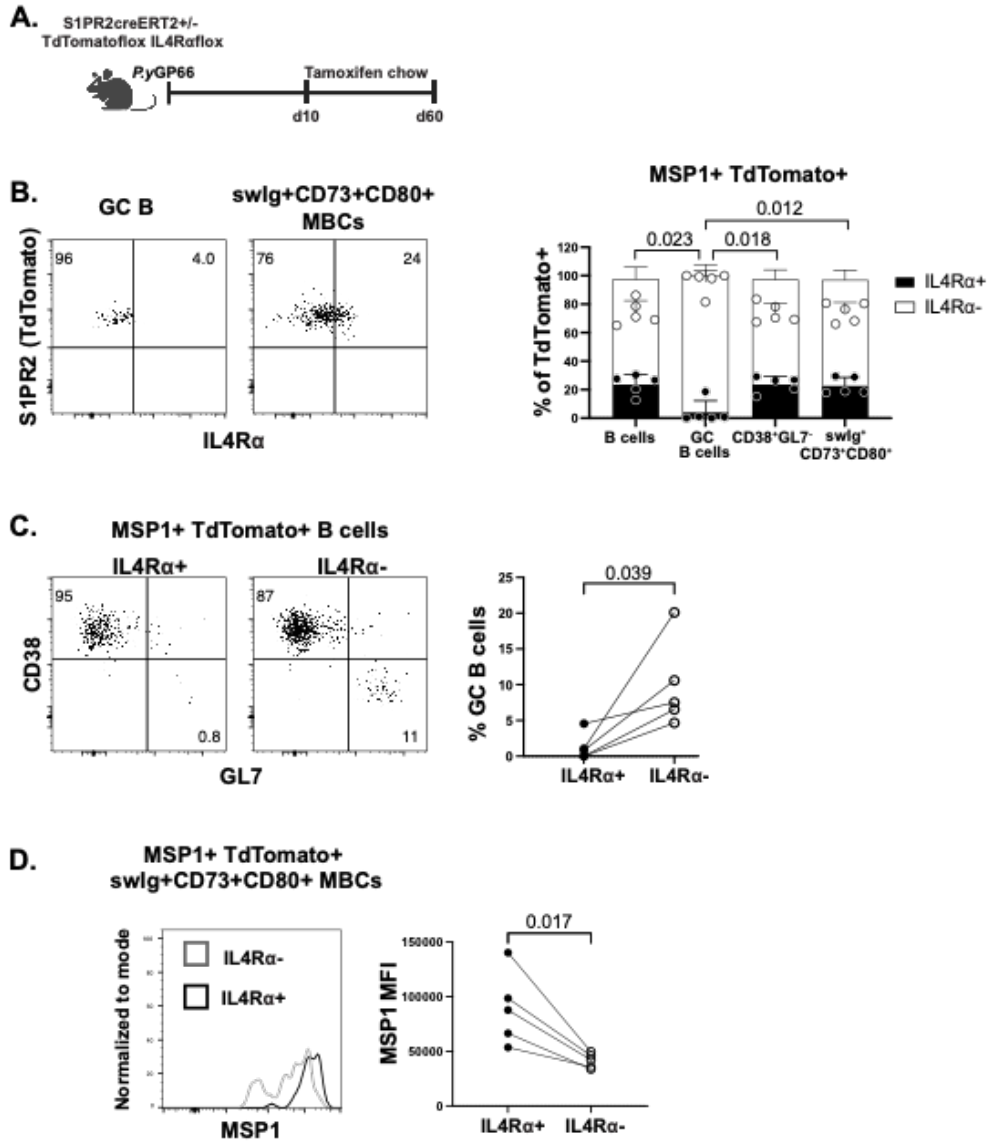

Figure 2.13. Lower affinity B cells persist into the memory pool in the absence of B cell-intrinsic IL-4 signaling. (A) S1PR2creERT2$^{+/-}$TdTomato^{flox}IL4Rα^{flox} mice and S1PR2creERT2$^{-/-}$ littermates were infected with *P.y*-GP66 and fed tamoxifen chow beginning 10 days post-infection and analyzed on day 60. (B) Representative flow plots and quantification of IL4Rα^{+} and IL4Rα^{-} TdTomato^{+} B cells. (C) Representative flow plots and quantification of GC B cells within IL4Rα^{+} or IL4Rα^{-} MSP1-specific TdTomato^{+} B cells. (D) Representative histograms and quantification of MSP1 tetramer MFI on IL4Rα^{+} and IL4Rα^{-}

MSP1$^+$TdTomato$^+$swIg$^+$CD73$^+$CD80$^+$ MBCs. Data are combined from three independent experiments with 5 mice per group.

2.3 Discussion

Our data support a model in which IL-4 can promote either GC B cell entry or exit depending on the amount of BCL6 expression in a given cell. Cells that express no to low levels of BCL6 enhance BCL6 expression in response to IL-4 signaling, while those that have high levels of BCL6, like GC B cells, downregulate BCL6 in response to IL-4. More specifically, as previously shown, IL-4 produced by NKT cells or Tfh cells early in an immune response acts upon naive and early activated B cells to promote BCL6 expression and thereby promote migration into GCs[6,48,58]. In multiple models, there continues to be a significant amount of IL-4 produced by CD4$^+$ T cells following GC formation within the GC itself[7,60,101], consistent with our own findings that GC Tfh are the predominant CD4$^+$ T cell source of IL-4 in response to *Plasmodium* infection. However, the role of IL-4 within the GC has only recently been examined through our work and very recently from the work of Duan and colleagues[62], which demonstrated that unrestricted IL-4 availability in the GC can constrain memory cell formation. In keeping with earlier reports that IL-4 is broadcast around a T cell instead of secreted directly at the synapse[102], their data suggested that IL4Rα expressed on FDCs serves as a sink for excess IL-4, thereby limiting its effects on bystander GC B cells that are not actively engaged with a GC Tfh cell. Importantly, these studies did not define the mechanism via which IL-4 was acting on GC B cells.

Herein, we demonstrate that IL-4 acts on GC B cells to downregulate BCL6, whether administered exogenously or perceived *in situ*, by enhancing BCL6 expression to a threshold level that triggers its own negative autoregulation[71,90,91]. This correlates with increased cell death, which

we found to be associated with a loss in selection stringency as measured by both a decrease in somatic hypermutation as well as in the affinity of antibodies from MBC-derived plasmablasts. We found that in the absence of IL4Rα signaling, B cells were preferentially able to remain in the GC, although they could still exit to form MBCs. This suggested a potential lack of the positive selection that would limit survival to high affinity clones over their lower affinity counterparts. Indeed, we determined that a global or GC B cell-intrinsic loss of IL-4 signaling resulted in the formation of lower affinity MBCs. Together, our findings indicate that BCL6 serves as a tunable switch responding to T cell IL-4 secretion, thereby releasing cells that have acquired adequate help and have therefore been selected.

We additionally identified a novel approach to distinguish memory precursors that have exited the GC through a combination of differing BCL6 and CD80 expression. This allowed us to determine that while IL-4 increased the proportion of exiting GC B cells, it also increased GC B cell death, as evidenced by the higher number of $BCL6^-$ GC B cells and $CD80^+$ GC transit B cells found when mice were treated with IL4C in conjunction with the pan-caspase inhibitor emricasan. One possible explanation for the IL-4-mediated cell death was the finding that GC B cells did not appropriately upregulate the anti-apoptotic protein BCL2 in response to IL4C treatment. It has previously been suggested that during a selection event, the downregulation of BCL6 should release repression of BCL2, as BCL2 is required for proper MBC survival[33,34]. Our findings therefore decouple these two events, and raise the possibility that two distinct signals from T cells are required for MBC selection: IL-4 to downregulate BCL6 and release cells from the GC transcriptional program, and an additional signal to upregulate MBC survival signals. It is likely that the loss of MBCs in response to increased IL-4 observed in our work and that of Duan and colleagues is due to an imbalance in the number of GC B cells that are downregulating BCL6 and

the number of the GC B cells that can receive additional T cell or BCR survival signals[62]. While the additional required signal(s) is still unknown, previous studies have dissected how the strength of T cell-B cell receptor-ligand interactions can dictate whether a GC B cell migrates to the DZ or differentiates into a memory B cell or plasma cell; thus, the amount of IL-4 received may also factor into these fate choices[25,37,38,86].

Interestingly, our results indicated that IL-4 impacts MBC selection, but did not appear to impact plasma cell selection. Similarly, IL-21 has been shown to play an important role in clonal expansion in the DZ as well as in long-lived plasma cell formation, but has not been shown to significantly impact MBC formation[51,53,56,103]. What makes a Tfh cell secrete IL-4 versus IL-21 in response to an interaction with a GC B cell has not been determined; however, it is known that very few Tfh cells can produce both cytokines simultaneously[50]. IL-4 and IL-21 production appear to be relatively segregated to the light zone or dark zone, respectively[7,47,50], suggesting cytokine signals in the GC may be temporally and spatially regulated, and perhaps memory B cell versus plasma cell fate are as well.

The signals underlying GC B cell selection and memory B cell exit have remained elusive, in part due to the complex nature of cellular interactions in the GC. The finding that IL-4 can promote GC entry early in an immune response as well as initiate selection and exit later in the GC illuminates a significant role for cytokines in tuning BCL6, which may go beyond the GC. How GC B cells integrate IL-4 with other cytokine or receptor-ligand signals remains to be determined, yet the ability to modulate IL-4 throughout an immune response may on its own allow for the manipulation of MBC affinity in vaccine settings.

3. Characterization of protein nanoparticles as a vaccine tool

3.1 Introduction

Protein nanoparticles have emerged as a versatile and promising platform in the field of nanotechnology, offering great potential for various applications ranging from drug delivery to vaccine design. These nanoparticles are intricately engineered structures composed of multiple protein subunits that self-assemble into well-defined architectures. They exhibit unique properties such as high stability, controllable size, and tunable surface characteristics, making them highly attractive for a wide range of biomedical applications. The design and fabrication of protein nanoparticles have been revolutionized by advances in computational modeling and protein engineering techniques. Researchers have employed rational design principles to accurately engineer and predict the self-assembly of multi-component protein nanomaterials. In a seminal study by King et al., the authors demonstrated the successful design of co-assembling protein nanomaterials with precise control over their structure and properties[104]. This work showcased the potential of protein engineering to create highly tailored protein nanoparticles with desired characteristics.

Building upon these advances, Bale et al. extended the design principles to larger protein complexes, specifically focusing on the assembly of megadalton-scale two-component icosahedral protein complexes[105]. The step forward highlighted the potential for designing intricate protein architectures at a massive scale, opening up possibilities for creating novel protein nanoparticles with unprecedented complexity and functionality, including as an innovative vaccine platform. This was demonstrated by a study in which immunization with protein nanoparticles displaying the prefusion respiratory syncytial virus (RSV) F protein (preF) successfully induced potent neutralizing anti-preF antibody responses in both mice and non-

human primates[106]. This study exemplifies the potential of protein nanoparticles as a vaccine platform, as it harnesses their ability to present antigens in a highly organized and immunogenic manner.

However, despite the success of these and other nanoparticle designs, the interplay between the immunogenicity of the nanoparticle components and the displayed antigen is not well understood. Specifically, while anti-scaffold antibody responses remained low and did not seem to interfere with the antibody response to the displayed antigen in nanoparticle vaccines for RSV, influenza, or *Plasmodium*[106–109], a study of HIV-1 Env-ferritin nanoparticles did appear to show that anti-ferritin antibody interfered with the formation of anti-Env antibodies[110]. Thus, it is important to understand the immunodominance of the nanoparticle components and displayed antigen, as well as whether 'scaffold masking' by glycan shielding can help to focus B cell responses to the displayed antigen of interest. Here, we demonstrate that glycan shielding does not alter the immune response to the nanoparticle scaffold or displayed antigen when the displayed antigen is immunodominant.

Additionally, as with all vaccine candidates, the platform must be tested for each immunogen of interest. When the SARS-CoV-2 pandemic began in early 2020, the King and Veesler labs were able to rapidly mobilize their nanoparticle design platforms to create potential nanoparticle vaccines that displayed the viral spike receptor-binding domain. One key question was whether these RBD nanoparticles could successfully elicit a robust RBD-specific GC B cell response that would form long-lived memory. In these studies, we first characterize the antibody response to SARS-CoV-2 infection and show that natural infection induces a persistent, neutralizing anti-RBD antibody response. We then analyze the magnitude and quality of the GC

in response to immunization with RBD nanoparticles, and demonstrate that they do induce an RBD-specific, class-switched GC B cell population.

3.2 Results

3.2.1 Displayed antigen is immunodominant to nanoparticle scaffolds

The King lab designed three versions of the I53_dn5 nanoparticle displaying HA (HA-I53_dn5) with different types of scaffold masking by adding *1)* 10 glycans (HA-I53_dn5_Agly), *2)* 1 linear PEG chains (HA-I53_dn5_2Cys2kPEG) to the pentamer, or *3)* 5 unsaturated polypeptides rich in proline, alanine, and serine (PASylation; HA-I53_dn5_PAS)[111,112]. They immunized mice intramuscularly with these nanoparticles or with unmasked HA-I53_dn5 or a non-assembling scaffold control (HA-1naOC3_int2 + dn5A). On day 15 post-immunization, we analyzed the popliteal lymph nodes for HA-specific and scaffold-specific B cells using tetramers for HA as well as the scaffold components dn5A and dn5B (**Figure 3.1A**).

Regardless of masking status, the HA-I53_dn5 nanoparticles elicited similarly large proportions of HA-specific GC B cells, all higher than the unassembled control (**Figure 3.1B**). GC responses to both the dn5A or dn5B scaffold components were quite low across all groups, suggesting that the immunodominance of HA to the scaffold is not enhanced or diminished by scaffold masking (**Figure 3.1C and 3.1D**). We next assessed the level of class-switched antigen-specific B cells in all groups to determine the quality of B cell responses raised to both HA and the nanoparticle scaffold. Immunizing with any of the assembled nanoparticles resulted in ~20-40% of HA-specific B cells switching from $IgD^{+}IgM^{+/-}$ to $IgD^{-}IgM^{+}$, and ~20% of HA-specific B cells becoming $IgD^{-}IgM^{-}$, or class-switched ($swIg^{+}$), whereas the B cells responding to the unassembled control primarily remained IgD^{+}, consistent with the small GC response to HA

(**Figure 3.1E**). Interestingly, a higher proportion of dn5A- and dn5B-specific B cells were $swIg^+$, even in response to the unassembled control protein (**Figure 3.1F and 3.1G**). The lack of GC response to these antigens suggests that these $swIg^+$ cells may be cross-reactive memory B cells; however, further analysis would need to be performed to confirm this. These findings are consistent with other glycan masking studies in which the masking was performed within the antigen instead of on the nanoparticle domains, which demonstrated an increased proportion, but not increased numbers, of antigen-specific B cells[113,114]. Overall, these data demonstrate that scaffold masking does not further focus the B cell response to the displayed antigen when the displayed antigen is immunodominant, and thus immune responses to the nanoparticle itself need only be taken into consideration when the displayed antigen is subdominant, such as in the case of HIV Env-1[110,112].

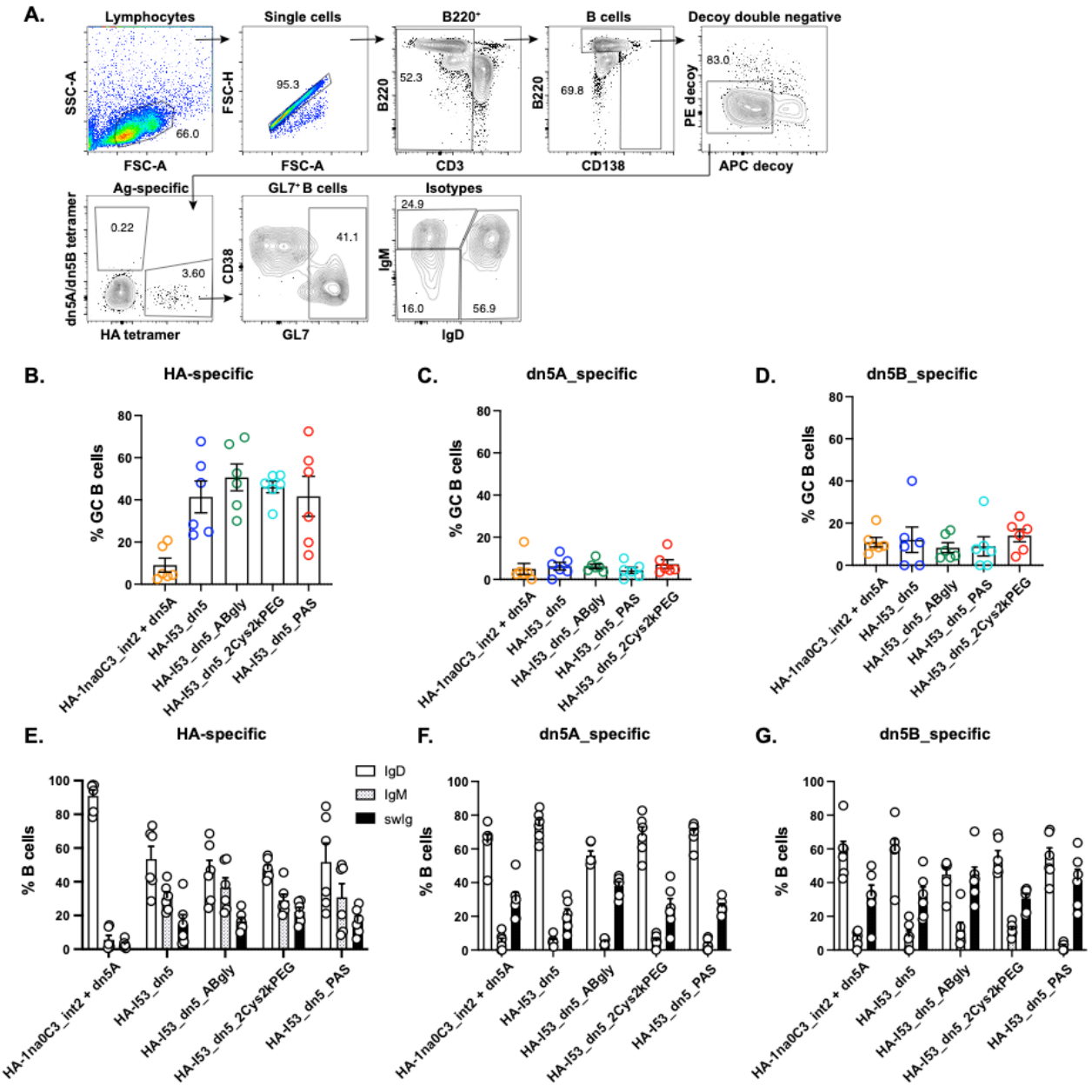

Figure 3.1. B cells responses to nanoparticle scaffolds and displayed antigens. (**A**) Gating strategy for analyzing dn5A, dn5B, or HA-specific B cell responses. Frequency of (**B-D**) GC B cells and (**E-G**) isotype switched B cells in mice immunized with either unassembled protein, an unmasked nanoparticle, or three versions of a masked nanoparticle.

3.2.2 Mild COVID-19 induces persistent, neutralizing anti-SARS-CoV-2 IgG antibody

The SARS-CoV-2 pandemic that began in early 2020 provided an opportunity to study a novel immune response in real time, as well as to take advantage of adaptable vaccine platforms such as protein nanoparticles that can be rapidly mobilized for new pathogens. To first understand the memory response formed in response to infection as a baseline for correlates of protection we would want from a vaccine, we analyzed the antibody responses in 15 SARS-COV-2 qPCR$^+$ individuals who experienced mild COVID-19, as well as 17 healthy controls over the course of three months (**Figure 3.2A-C**; **Figure 3.3A**).

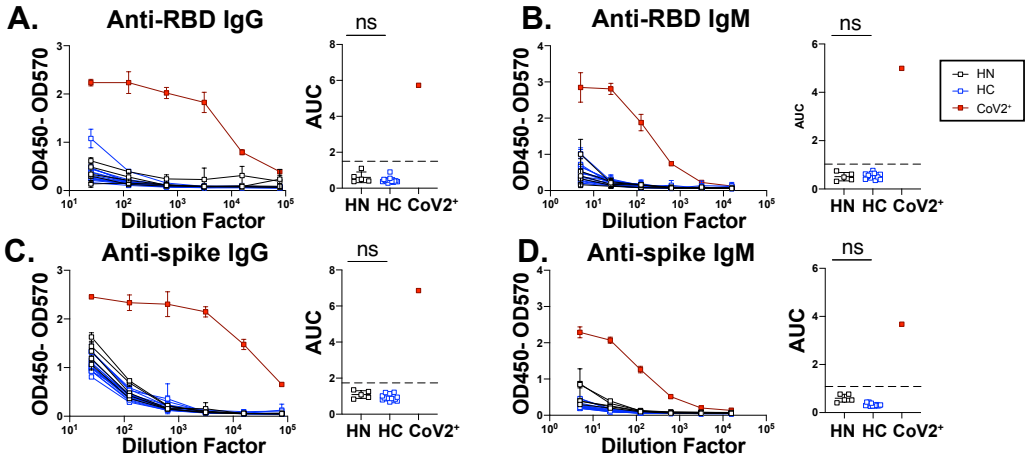

Figure 3.2. Healthy controls do not have SARS-CoV-2 RBD or spike-specific antibodies. ELISA dilution curves and area under the curve (AUC) for anti-RBD and anti-spike (**A, C**) IgG and (**B, D**) IgM in plasma collected from individuals prior to 2020 and the SARS-CoV-2 pandemic (historical negatives, HN, black), from healthy controls (HC, at Visit 2), and from individuals that tested PCR+ for SARS-CoV-2 (COV2$^+$, at Visit 1). Dashed lines indicate mean + 3 SD of HN AUC values.

The presence of anti-RBD and spike antibodies in the 15 qPCR$^+$ individuals was determined by ELISA from plasma samples collected at a median of 35 (Visit 1) and 83 (Visit 2) days following the onset of symptoms, to represent early and late memory timepoints, respectively. At Visit 1, 100% of qPCR+ individuals had anti-RBD IgG AUCs greater than 3 standard deviations above the mean of the uninfected controls, compared to 93% with anti-RBD IgM and 73% with anti-RBD IgA above the negative threshold, indicating the presence of SARS-CoV-2 plasmablasts or early-emerging long-lived plasma cells (LLPCs) (**Figure 3.3B and 3.3C**). A greater percentage of individuals possessed IgG, IgM, and IgA antibodies that could bind to the full spike protein at this timepoint, although antibody responses to the two proteins were highly correlated (**Figure 3.4A and 3.4B**). Anti-RBD IgM and IgA antibodies were found to have decreased by the late timepoint, with 71% of individuals testing positive for IgM and 35% for IgA (**Figure 3.3B and 3.3C**). However, all qPCR$^+$ individuals still tested positive for anti-RBD IgG at the second timepoint, consistent with the emergence of predominantly IgG$^+$ LLPCs observed in other infections.

As RBD is a key domain of the spike protein that is required for viral entry into the cell, antibodies that target the RBD can be potent inhibitors of infection[115,116]. To determine whether CoV2$^+$ individuals form and maintain neutralizing antibodies, we tested plasma antibody neutralization indirectly using a cell-free assay of RBD-ACE2 binding inhibition (surrogate virus neutralization assay, sVNT)[117]. Cov2$^+$ plasma inhibited RBD-ACE2 binding significantly more than HC plasma did, and this inhibition correlated strongly with anti-RBD IgG levels at both Visit 1 and Visit 2 (**Figure 3.3D and 3.3E**). Additionally, this RBD inhibition was maintained from Visit 1 to Visit 2, suggesting LLPC antibody maintains virus neutralizing potential (**Figure**

3.3F). Together, these data indicate that there is a lasting humoral immunity formed in response to SARS-CoV-2 infection, and that RBD could serve as a good target for vaccine responses.

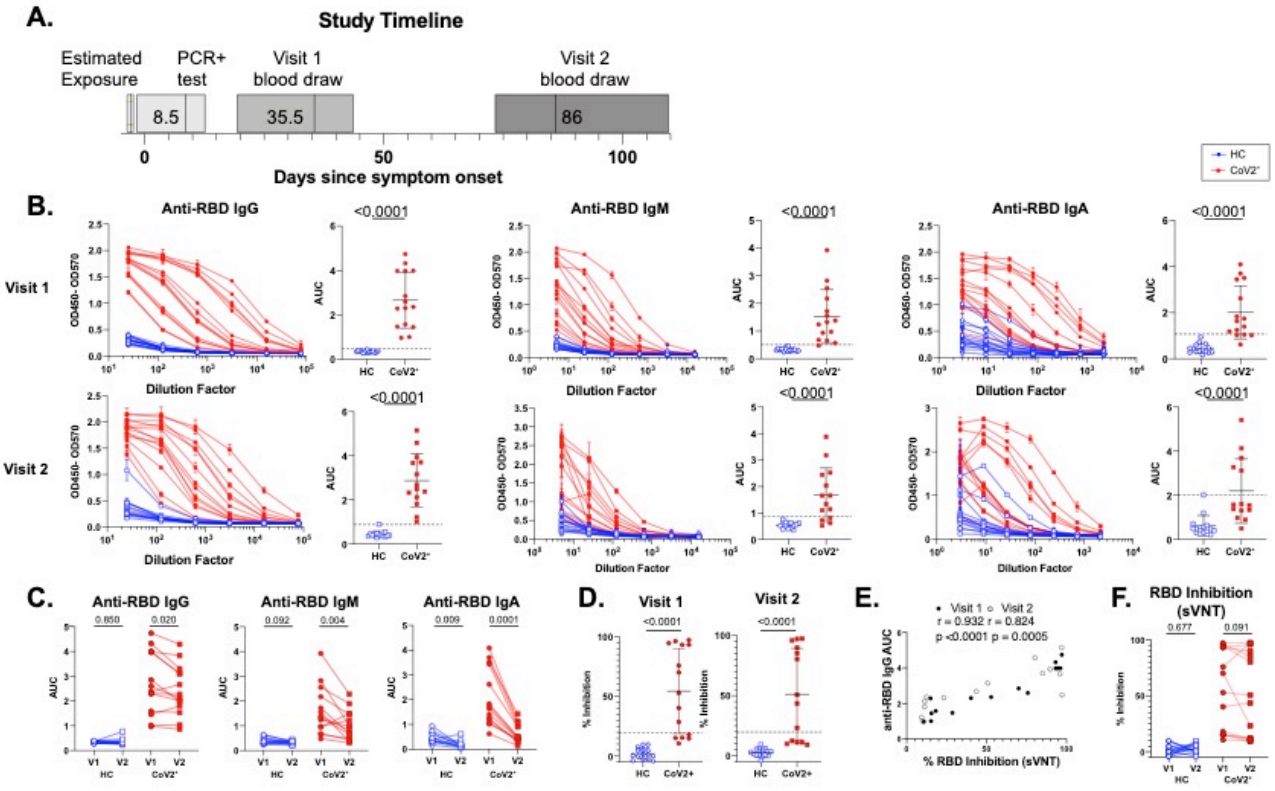

Figure 3.3. Mild COVID-19 induces persistent, neutralizing IgG antibodies. (**A**) Study timeline indicating range and median of each visit. (**B**) ELISA dilution curves and AUC for anti-RBD IgG (left), IgM (middle), and IgA (right) at Visit 1 (top) and Visit 2 (bottom). Dashed line indicates mean + 3D of the HC AUC values. (**C**) Paired Visit 1 and Visit 2 AUC of each isotype for HC and CoV2^{+} individuals. Visit 2 samples were normalized to Visit 1 samples run alongisde Visit 2 samples. (**D**) Percent inhibition of RBD binding to ACE2 by sVNT at a 1:2 plasma dilution. (**E**) Spearman correlation between RBD inhibition by sVNT and anti-RBD IgG at both visits. (**F**) Paired Visit 1 and Visit 2 percent RBD inhibition at a 1:2 plasma dilution.

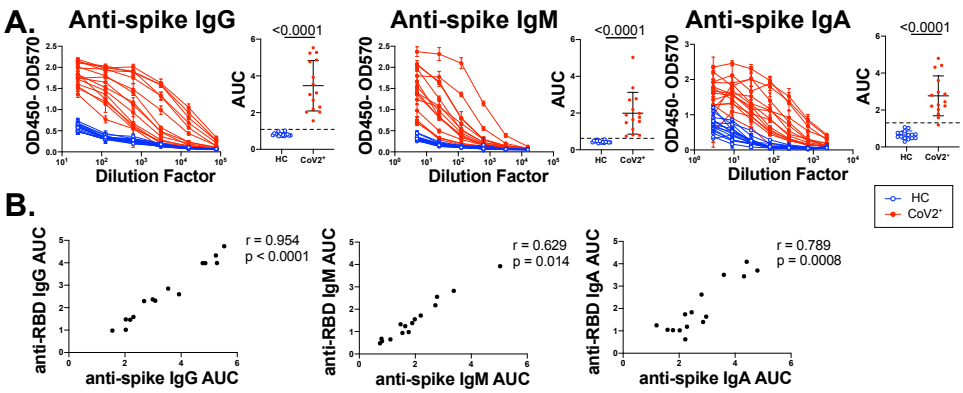

Figure 3.4. Anti-spike antibodies highly correlate with anti-RBD antibodies. (**A**) ELISA dilution curves and AUC for anti-spike IgG (left), IgM (middle) and IgA (right) at Visit 1. (**B**) Spearman correlation of Visit 1 anti-RBD and anti-spike IgG (left), IgM (middle), and IgA (right).

3.2.3 RBD nanoparticle vaccines elicit a robust B cell response

To test whether nanoparticles could be used to elicit an effective immune response against RBD, the King and Veesler labs collaborated to create several versions of the two-component protein nanoparticle I53-50 that displayed RBD in a multivalent manner[105,118]. Specifically, they fused the RBD to I53-50A linkers with either 8, 12, or 16 glycine and serine residues (RBD-8GS-, RBD-12GS-, and RBD-16GS-I53-50A, respectively), to allow for a range of flexible presentation of the RBD off of the nanoparticle surface. Each RBD-I53-50A component was then mixed with pentameric I53-50B to form the full nanoparticles, referred to as RBD-8GS, RBD-12GS, and RBD-16GS. To determine whether these nanoparticles could lead to the formation of class-switched memory B cells and long-lived plasma cells, they immunized mice with monomeric RBD, a prefusion stabilized SARS-CoV-2 S-2P trimer, or the RBD-8GS, RBD-12GS, and RBD-16GS nanoparticles. At 11 days post-immunization, we analyzed the RBD-specific response to

determine whether the immunization had led to the formation of GC precursors and B cells as well as class-switched RBD-specific B cells (**Figure 3.5A**). Immunization with RBD nanoparticles led to an expansion of both RBD-specific B cells as well as RBD-specific $GL7^+$ B cells (**Figure 3.5B-D**). Immunization with the S-2P trimer led to a detectable but modest B cell response, whereas immunization with the RBD monomer did not cause a noticeable expansion of RBD-specific B cells. In keeping with these observations, the majority of $GL7^+$ B cells in mice immunized with the S-2P trimer or RBD nanoparticles were class-switched, suggesting ongoing affinity maturation in a GC (**Figure 3.5E**). This was especially striking when compared to higher proportion of IgD^+ $GL7^+$ B cells in RBD monomer-immunized mice. Lastly, to evaluate the longevity of the humoral response, we measured the number of S-2P-specific antibody-secreting cells in the bone marrow by ELISpot at 20 weeks post-S-2P trimer or -RBD-16GS immunization. There were ~3 fold more S-2P LLPCs in mice immunized with RBD-16GS compared to S-2P trimer, indicating that RBD nanoparticle vaccines do successfully generate a robust, long-lived B cell response (**Figure 3.5F**).

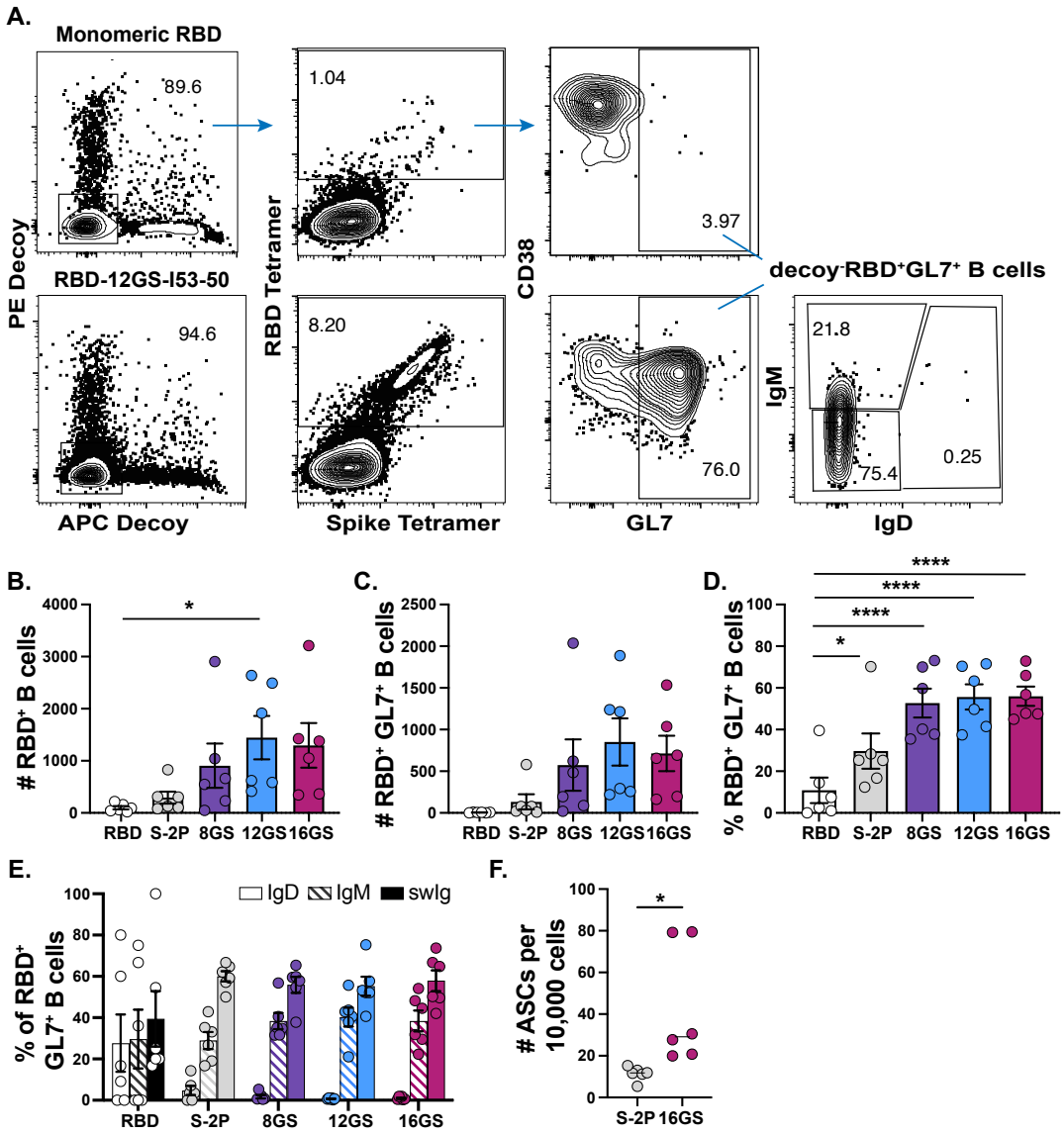

Figure 3.5. RBD nanoparticles elicit a robust B cell response. (**A**) Representative gating strategy for mice immunized with RBD monomer (top) or RBD nanoparticles (bottom) and analyzed 11 days post-immunization. Number of RBD-specific (**B**) total B cells and (**C**) GL7$^+$ B cells across each immunization group. Frequency of RBD-specific (**D**) GL7$^+$ B cells and (**E**) isotype of GL7$^+$ B cells across each immunization group. (**F**) Number of S-2P-specific antibody-secreting cells at 20 weeks post-immunization.

3.3 Discussion

The collaboration with the King and Veesler labs allowed us to investigate the immunogenicity and memory response of protein nanoparticles displaying viral antigens. In all cases, the designed protein nanoparticles elicited robust antigen-specific germinal center B cell responses, indicating their effectiveness in inducing a strong immune response, consistent with previous studies performed using similar nanoparticle scaffolds[106,119]. Importantly, the scaffold itself does not appear to be very immunogenic, and when displaying an immunodominant antigen such as influenza HA, the B cell response generated in response to the nanoparticle cage components is quite minimal. However, responses to the cage components should remain a consideration when designing nanoparticle vaccines with subdominant display antigens.

We additionally helped to demonstrate that nanoparticles displaying the SARS-CoV-2 RBD are able to elicit a robust antigen-specific B cell response that involves the formation of a functional germinal center. One of these candidates has now been tested in several clinical trials, and was recently approved for use in South Korea. This is an especially exciting development, as nanoparticle vaccines provide additional benefits in safety, immunogenicity, and stability, similar to other subunit vaccines. Overall, these studies provide valuable insights into the immunogenicity and memory response induced by protein nanoparticles displaying viral antigens. The findings support the potential use of protein nanoparticles as effective vaccine platforms for eliciting strong and durable immune responses, particularly in the context of infectious diseases such as SARS-CoV-2.

4. Concluding Remarks

Recent advances in our ability to track antigen-specific responses to infection and their contribution to recall responses has spurred an increased appreciation for and interest in the germinal center process. It is through the GC that the bulk of class-switched memory B cells, as well as long-lived plasma cells, are derived, both of which provide significant protection to subsequent exposures[74,120]. The specific molecular mechanisms underlying the selection of high affinity B cells for exit into either of these populations have only begun to be uncovered in recent years. In the case of MBCs, the bulk of discoveries have centered around the identification of memory precursors within the GC, an important first step in then being able to interrogate how they are formed and how they exit into long-lived memory cells[29,34]. Additional work has demonstrated various survival signals that must be expressed for successful memory B cell persistence, such as BCL2, SKI, NFKB, and KLF2[33,36].

In the studies discussed in chapter 2, we show that IL-4 downregulates BCL6 in GC B cells to promote GC B cell exit. To the best of our knowledge, this is the first signaling pathway that has been demonstrated to specifically target GC memory precursors for GC exit. Specifically, we show that IL-4 promotes BCL6 and GC formation in naive B cells, but its continued promotion of BCL6 within the $BCL6^{hi}$ GC B cell population triggers the negative autoregulation of BCL6, such that those B cells are primed for GC exit. Importantly, our findings also illustrate the oversight at play within the GC: while IL-4 provides the critical downregulation of BCL6, it is not sufficient to promote the upregulation of signals required for MBC survival and persistence. The need for integration of several signals for successful B cell differentiation is consistent with the requirements for immune cell activation which prevents expansion of self-reactive cells[121].

Recent findings from Hai Qi's group have provided compelling evidence for a role of IL-9 in inducing the expression of Zbtb18, which is involved in promoting MBC quiescence and survival[31,46]. This latter finding is especially interesting, as the authors demonstrate that Zbtb18 is also capable of directly binding to and repressing S1PR2 to allow B cells to exit the GC. Our work on IL-4 in the GC showed that GC-derived MBCs can still form in the absence of IL-4 signaling in GC B cells, suggesting that other signals can still promote MBC exit from GCs. It is therefore possible that IL-9 is one such compensatory signal.

Although our work was primarily done using a *Plasmodium* model, we believe that the mechanism we uncovered is important in any immune response that involves a germinal center. This is supported by the similar findings regarding the detrimental impact on MBC formation and affinity in the presence of increased bioavailability of IL-4, which were performed in an NP-KLH immunization model[62]. Additionally, studies on anti-opioid vaccines using IL-4 blockade resulted in a similar expansion of GCs as we observed using genetic deletion of IL-4 signaling[122,123]. Lastly, we performed the same regimen of IL4C treatment on days 12 and 14 in influenza-infected mice, and observed the same loss of BCL6 expression in GC B and GC transit cells (**Figure 4.1**).

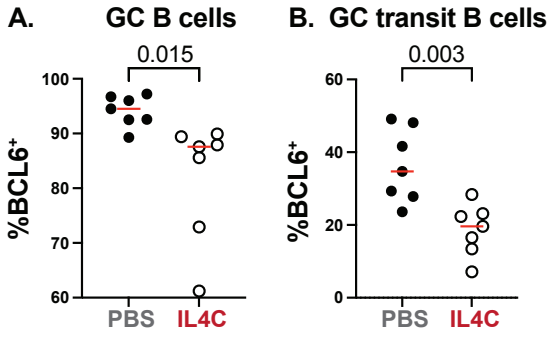

Figure 4.1. IL-4 downregulates BCL6 in type 1 immune responses. BCL6 expression in (**A**) GC B cells and (**B**) GC transit B cells in mice treated with IL4C on days 12 and 14 and analyzed

15 days post-PR8 infection. Data are combined from two independent experiments with 7 mice per group.

It is also worthwhile to consider the potential implications of our finding in a type 2 setting, as IL-4 is responsible for coordinating much of this immune response. Studies have shown that Tfh cells do produce IL-4 in response to helminth infection[50,101]. Interestingly, 4-7 days post-*Heligmosomoides polygrus* infection, IL-4 was found to be produced by Tfh cells exclusively in the B cell follicles or in close proximity to it, but not within the T zone itself, suggesting early IL-4 is more important in governing B cell responses than in directing Th2 differentiation[101]. Recent work has demonstrated that the vast majority of class-switching occurs prior to GC entry, and that GC B cells downregulate APE1, an endonuclease that is required for class-switching[124]. It is therefore possible that this early follicular-restricted IL-4 in a type 2 response is important for promoting BCR class-switching to IgG1 prior to GC formation. However, we do not expect that the role for IL-4 within the GC would be distinct between type 1 and type 2 responses, as the kinetics of MBC and LLPC formation are unchanged between the two.

Within the type 2 context, we are specifically interested in the clinical use of the anti-IL4Rα blocking antibody, dupilumab, which has been prescribed for several indications of aberrant type 2 immunity, including atopic dermatitis, asthma, and nasal polyps[125–127]. Studies thus far have indicated that dupilumab treatment does not impact serum antibody titers formed in response to vaccination[128]. This is consistent with our findings in conditional and global IL4Rα knockout mice. However, considering the lower affinity MBCs formed in the absence of IL-4 signaling, we believe recall responses of dupilumab patients should be evaluated to ensure they are still forming high affinity MBCs in response to vaccination. This could be determined by

restimulating memory B cells isolated from peripheral blood mononuclear cells (PBMCs), and would be important in determining whether dupilumab patients should stop treatment during vaccination windows.

Another setting of interest to consider is the role of IL-4 within Peyer's patches (PPs). PPs are lymphoid follicles within the small intestine that are continuously exposed to microbiome- and food-derived antigens, thus resulting in chronic GCs. The organization of these PP GCs are highly similar to those found in lymph nodes and the spleen, and antigen-driven positive selection does lead to the formation of higher affinity MBCs and LLPCs[130]. However, work from the Victora lab has demonstrated that 5-10% of gut-associated GCs contain a dominant "winner" clone, likely because they benefit stable host-microbiome interactions[19]. However, there is also an increased presence of low affinity PP-derived MBCs and LLPCs, which has led some to hypothesize that the continuous presence of antigen in PPs allows for more low affinity BCR-Ag interactions, supporting the survival of low affinity B cells that would typically die off in classical GC settings[132]. It is possible, then, that bystander IL-4 in PPs would cause less cell death than we observed in splenic GCs in our *Plasmodium* model, if low affinity GC B cells were able to upregulate an MBC survival signal through repeated but limited antigen or Tfh contacts that are not often available in non-PP GCs. Lastly, as the majority of B cells in PP GCs are IgA or IgG2b, it is unlikely that IL-4 is involved in class-switching in this setting, especially in light of evidence that switching to IgA occurs at the $GL7^{int}$ GC precursor stage and that there is very little class-switching within PP GCs themselves[19,124,134].

Two additional outstanding questions that we are particularly interested in are 1) what signals in the GC can promote BCL2 expression and 2) how cytokine signals within the GC are regulated. To begin answering the first question, we have performed preliminary in vitro

experiments that indicate CD40 signaling may be sufficient to upregulate BCL2 (**Figure 4.2**). Pilot experiments in collaboration with the King and Baker labs using nanoparticles displaying an anti-CD40 antibody have also shown promise in promoting B cell survival (data not shown).

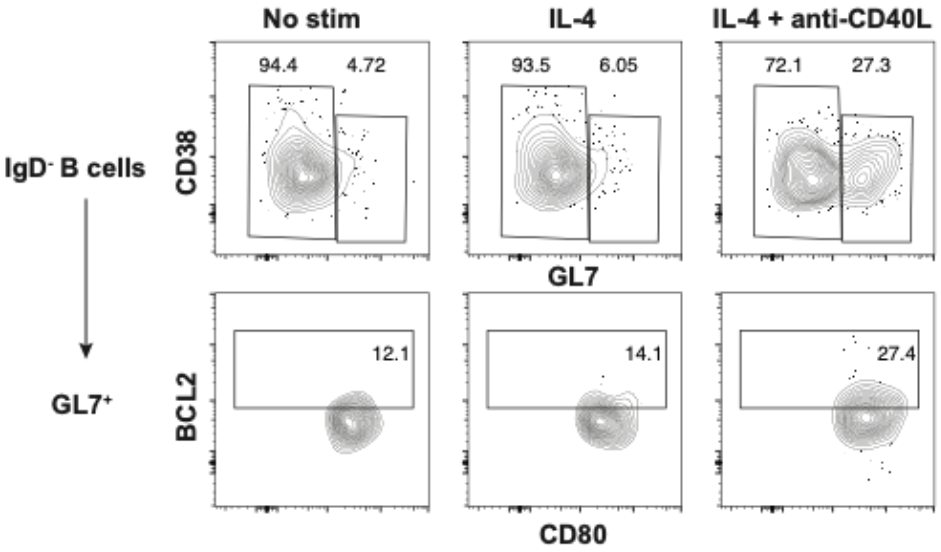

Figure 4.2. CD40:CD40L signaling may promote BCL2 expression. Splenic B cells were cultured with 10 ng/mL IL-4 or 1 ug/mL of agonistic anti-CD40L antibody for 48 hours. Representative flow cytometry plots demonstrating gating on $GL7^+$ B cells (top) for BCL2 expression (bottom).

As discussed briefly in chapter 2, both IL-4 and IL-21 are produced in the GC and GC B cells have shown to express high levels of both receptors at both times. While they appear to have distinct roles in governing MBC and LLPC formation, respectively, it is unclear how their production or receipt is regulated such that only the appropriate cells respond to either cytokine. Of note, Tfh cells have been shown to primarily produce only IL-4 or IL-21, but very few produce both[50]. Very recent work from Chen et al. has suggested a potential mechanism by which GC B cells may be desensitized to IL-21 signaling despite expressing the receptor[129].

Specifically, they demonstrate that GC B cells downregulate N-deacetylase and N-sulfotransferase 1 (Ndst1) which are required for the proper sulfation of heparin sulfate (HS) to mediate IL-21 binding. Interestingly, LLPC precursors re-upregulate Ndst1 to better receive IL-21 signal and complete their differentiation into LLPCs, but what controls Ndst1 expression is still unknown. Although the authors did not find a similar role for HS in mediating IL-4 binding, this study raises the possibility of other biochemical changes that could underlie GC B cell responsiveness to IL-4. Considering the promise that our findings show for the use of IL-4 to modulate MBC selection within the GC, furthering our understanding of how GC B cells perceive IL-4 would only improve the potential for IL-4 in vaccine strategies.

Lastly, in chapter 3 we explored the immune response to protein nanoparticle vaccines in the backdrop of the ongoing SARS-CoV-2 pandemic. Both our findings that the nanoparticle cage components do not generate a significant B cell response as well as that RBD nanoparticles can induce the formation of a robust GC B cell response were exciting and reassuring evidence for the potential of these nanoparticles as vaccines. One of these RBD nanoparticle vaccine candidates has since been successful in phase I/II and phase III clinical trials, and was shown to generate superior neutralizing antibodies compared to a control vaccine as well as provide effective viral clearance in rhesus macaques[131,133]. These studies demonstrate the potential of vaccines that focus on the formation of durable B cell memory for viral protection.

Together, the data presented here not only emphasize the importance of generating high affinity MBCs for lasting humoral immunity, but shifts the paradigm of our understanding of how IL-4 is involved in that process. These findings advance our understanding of GC dynamics and selection, and have potential for use in vaccine settings or autoimmune therapies.

5. Materials and Methods

Mice

C57BL/6, BALB/C, CD45.1^{+} (B6.SJL-*Ptprc^{a} Pepc^{b}/BoyJ*), and STAT6KO (B6.129S2(C)-*Stat6^{tm1Gru}*/J)[135] mice were purchased from Jackson Laboratories. S1PR2creERT2$^{+/-}$TdTomato^{flox} (Tg(S1PR2-cre/ERT2)) mice were provided by Dr. Tomohiro Kurosaki[25]. This strain was crossed to IL4Ra^{flox} (IL4ra^{tm2Fbb}) mice[136], provided by Dr. Jakob von Moltke, to generate S1PR2creERT2$^{+/-}$ TdTomato^{flox}IL4Ra^{flox} mice. IL4RαKO (IL-4Rα$^{-/-}$) mice were provided by Dr. Frank Brombacher and were bred and maintained in our laboratory[137]. KN2$^{+/+}$ mice were provided by Dr. Markus Mohrs[138]. This strain was crossed to C56BL/6 mice to generate KN2$^{+/-}$ mice. ΔBPS1 mice were provided by Dr. Jinyong Choi[71]. BCL2-Tg (B6.Cg-Tg(BCL2)22Wehi/J) mice were provided by Dr. Chris Allen[139]. All mice were bred and housed under specific-pathogen free conditions at the University of Washington. All experiments were performed in accordance with the University of Washington Institutional Care and Use Committee guidelines.

Infections and parasitemia analysis

Plasmodium chabaudi chabaudi (AS) parasites and *Plasmodium yoelii 17XNL-GP66* parasites were maintained as frozen blood stocks and passaged through donor mice. Primary mouse infections were initiated by intraperitoneal (i.p.) injection of 10^6 infected red blood cells (iRBCs) from donor mice. Re-challenge experiments were performed by injecting mice with 10^7 iRBCs i.p. 60 days after primary injection. Parasitemia was measured by flow cytometry by fixing a drop of blood with 0.025% glutaraldehyde, then staining with CD45 APC (Clone 30-F11, BD Biosciences), Ter119 FITC (BD Biosciences), CD71 PE (Clone R17217, Invitrogen), and Hoechst33342. For ΔBPS1 in vitro experiments, mice were infected with 2x10^5 PFU LCMV$_{arm}$

i.p. For influenza experiments, mice were injected intranasally with 2 pfu of Influenza A virus (strain A/Puerto Rico/8/1934 H1N1) (PR8).

Immunizations

For nanoparticle scaffold masking experiments, BALB/C mice were inoculated with 0.9 μg HA and/or 0.6 μg I53_dn5 scaffold (1.2 μg I53_dn5 scaffold for the HA-I53_dn5_ABgly group due to 50% HA valency). Prior to inoculation, immunogen suspensions were gently mixed 1:1 (vol/vol) with AddaVax adjuvant (Invivogen, San Diego, CA). Mice were injected intramuscularly into the gastrocnemius muscle of each hind leg using a 27-gauge needle with 50 μL per injection site (100 μL total) of immunogen under isoflurane anesthesia. For RBD nanoparticle experiments, 6-week old female BALB/c mice, three per dosing group, were immunized intramuscularly with 50 mL per injection site of vaccine formulations containing 5 mg of SARS-CoV-2 antigen (either S-2P trimer or RBD, but not including mass from the I53-50 nanoparticle) mixed 1:1 vol/vol with AddaVax adjuvant on day 0. All experimental mice were euthanized for harvesting of inguinal and popliteal lymph nodes on day 11. Both experiments were repeated two times. Popliteal and inguinal lymph nodes were collected and pooled for individual mice.

Tetramers

The $GP66_{-77}$:I-A^b-APC tetramer (I-A^b/LCMV.GP66.DIYKGVYQFKSV) used for isolating GP66-specific T cells was obtained from the National Institutes of Health Tetramer Core. For *P.ch* MSP1-specific B cell isolation, recombinant His-tagged C-terminal MSP1 protein (amino acids 4960 to 5301) from *P.ch* was produced by *Pichia pastoris* and purified using a Ni-NTA agarose column as previously described[140]. For *P.y*-GP66 MSP1-specific B cell isolation, a plasmid

containing His-tagged 14 kD truncated carboxy terminus of *P.y* MSP1 protein (amino acids 1662-1757) was transfected into HEK293F cells and purified using a Ni-NTA agarose column as described previously[141].

Purified recombinant *P.ch* MSP1, *P.y* MSP1, I53_dn5A pentamer, I53_dn5B trimer, H1 MI15 hemagglutinin trimer, SARS-CoV-2 trimeric spike, and SARS-CoV-2 RBD protein were biotinylated using the EZ-Link Sulfo-NHS-LC Biotinylation Kit (ThermoFisher) and tetramerized with streptavidin-PE (Agilent) or streptavidin-APC (Agilent) as previously described[74,142].

The PE decoy reagent to gate out non-MSP1-specific B cells was generated by conjugating SA-PE to AF647 using an AF647 antibody labeling kit (ThermoFisher Scientific), washing and removing any unbound AF647, and incubating with an excess of irrelevant biotinylated HIS-tagged protein. The APC decoy reagent was generated in the same manner, by conjugating SA-APC to Dylight 755 using a DyLight 755 antibody labeling kit (ThermoFisher Scientific).

Injections

For the administration of complexed IL-4 (IL4C), 5 ug of recombinant mouse IL-4 (BioLegend) was incubated with 25 ug of anti-mouse IL-4 antibody (11B11; BioXCell) for 2 minutes at room temperature (RT). The IL4C was then diluted to 150 uL with sterile PBS and administered intravenously (i.v.). For the administration of non-complexed IL-4, 5 ug of recombinant mouse IL-4 (BioLegend) was diluted to 150 uL with sterile PBS and administered i.v. Emricasan (Sigma-Aldrich) was resuspended to 2mg/mL in DMSO, prepared at 2.5 mg/kg in pre-warmed sterile PBS, and injected i.p.

Mouse cell enrichment and flow cytometry

Splenic cell suspensions were prepared and filtered through 100 uM Nitex mesh (Amazon). For B cell enrichment, cells were resuspended in 200 uL PBS containing 2% FBS and Fc block (2.4G2) and incubated with decoy tetramer at a concentration of 10 nM for 10 min at RT. MSP1-PE or -APC tetramer was added at a concentration of 10 nM and cells were incubated for 20 min on ice. Cells were washed, incubated with anti-PE or anti-APC magnetic beads (Miltenyi) for 30 min on ice, and passed over magnetized LS columns (Miltenyi) to elute the bound cells as previously described[142]. For T cell enrichment, cells were resuspended in 200 uL PBS containing 2% FBS and incubated with 10 nM GP66-77:I-A^b-APC tetramer for 1 hour at RT. Cells were washed, incubated with anti-APC magnetic beads, and passed over magnetized LS columns. All bound cells were stained with surface antibodies followed by fixation and intracellular antibody staining when needed (**Table 5.1**). Cell counts were determined using Accucheck cell counting beads. Cells were analyzed on the Cytek Aurora and analyzed using FlowJo 10 software (Treestar).

In vitro splenocyte cultures

Splenic cell suspensions were prepared and filtered through 100 uM Nitex mesh. For negative selection of naive B cells, splenocytes were resuspended in 200 uL PBS containing 2% FBS and Fc block and incubated with biotin anti-mouse F4/80 (Clone BM8, BioLegend), CD3 (Clone 500A2, BD Biosciences), CD4 (Clone RM4-5, eBioscience), CD8 (Clone 53-6.7, eBioscience), CD11b (Clone M1/70, eBioscience), CD11c (Clone N418, eBioscience), CD43 (Clone eBioR2/60, Invitrogen), Ly6G (Clone RP6-8C5, eBioscience), Ter119 (Clone TER-119, eBioscience), and CD138 (Clone 281-2, BD Biosciences) for 20 min on ice. For negative selection of $GL7^+$ B cells, cells were additionally incubated with biotin anti-mouse CD38 (Clone 90/CD38, BD Biosciences),

IgD (Clone 11-26c, Invitrogen), and CD49b (Clone DX5, BD Biosciences). In both cases, cells were washed, incubated with anti-biotin magnetic beads (Miltenyi) for 30 min on ice, and passed over magnetized LS columns. Flow through was collected and an aliquot of cells were checked for purity prior to culture. 1 million B cells/well were added to 12-well plates in 1 mL DMEM (Gibco) supplemented with 10% FBS (R&D Systems), 1% penicillin/streptomycin (ThermoFisher Scientific), 15 mM Hepes (Gibco), and 55 uM β-mercaptoethanol (Gibco). 1 ug/mL of agonistic anti-CD40 antibody (Clone FGK4.5, BioXCell) diluted in PBS was added to all wells, and 10 ng/mL of recombinant mouse IL-4 (BioLegend) diluted in PBS was added to wells cultured with the cytokine. Plates were incubated at 37°C in a 5% CO2 incubator for 24h, then cells were harvested and washed with PBS containing 2% FBS and stained for flow cytometry as described above.

Adoptive cell transfers

Single cell suspensions from ΔBPS1 spleens were prepared and filtered through 100uM Nitex mesh. Red blood cells were lysed with ACK buffer (ThermoFisher Scientific). Naive B cells were isolated by negative magnetic activated cell sorting using the EasySep™ Mouse B cell Isolation Kit (StemCell Technologies). 30 million B cells were injected i.p. into CD45.1$^+$ mice.

ELISAs

96-well plates (Corning) were coated with 2 ug/mL of recombinant *P.ch* MSP1, *P.y* MSP1, SARS-CoV-2 trimeric spike, or SARS-CoV-2 RBD diluted in PBS and incubated at 4°C overnight. Plates were washed with PBS containing 0.05% Tween-20 (PBS-T) and incubated with blocking buffer (PBS-T and 3% milk) for 1 hour at RT. Serum was serially diluted in dilution buffer (PBS-T and

1% milk), added to plates, and incubated at RT for 2 hours. For murine ELISAs, plates were washed and incubated with biotin anti-mouse IgG (BioLegend) for 1 hour at RT, followed by Streptavidin-HRP (BD) for 30 min at RT. For human ELISAs, plates were washed and incubated with anti-human IgG-HRP (Jackson ImmunoResearch), anti-human IgM-HRP (Southern Biotech), or anti-human IgA-HRP (Southern Biotech) and incubated for 1 hour at RT. In both cases, bound antibodies were detected with 1X TMB (Invitrogen) and quenched with 1M HCl. Sample optical density (OD) was measured at 450 nM and 570 nM using an iMark Microplate Reader (Bio-Rad).

Receptor-binding inhibition assay (sVNT)

sVNT assays were performed as previously described[117]. Briefly, high-binding 96-well plates (Corning) were coated with 5 ug/mL of recombinant human ACE2-Fc diluted in 100mM carbonate-bicarbonate buffer (pH 9.6) and incubated at 4C over-night. Plates were washed with PBS-T and incubated with blocking buffer (3% milk in PBS-T) for 1 hour at RT. Plasma or monoclonal antibody supernatants were serially diluted in triplicate in dilution buffer (1% milk in PBS-T) and incubated with 18 ng of recombinant SARS-CoV-2 RBD-HRP (conjugated using Abcam HRP conjugation kit) for 1 hour at 37°C. Blocked plates were washed and incubated with the pre-incubated plasma/antibody and RBD-HRP for 1 hour at RT, then detected with TMB and 1M HCl. OD was measured by a spectrophotometer at 450nm and 570nm. RBD-HRP alone and plasma with no RBD-HRP incubation were used as controls. The percent inhibition was calculated as (1 – Sample OD value/Average Negative Control OD value) x 100.

ELISpots

96-well ELISpot plates (Millipore) were coated with 20 ug/mL of recombinant *P.y* MSP1 or SARS-CoV-2 RBD diluted in PBS and incubated at 4°C overnight. Plates were washed with PBS-T and blocked with 1% BSA and 5% sucrose in PBS for 2h at RT. Single cell suspensions of murine bone marrow were prepared and passed over 100 uM Nitex mesh. Following red blood cell lysis, cells were plated onto coated ELIspot plates and incubated at 37°C for 5h. Cells were washed off and antibody secreting cells were detected using IgG biotin (BioLegend) followed by streptavidin-alkalkine phosphatase (R&D Systems). Spots were developed using BCIP/NBT (Mabtech) and were counted and analyzed using the CTL ELIspot reader and Immunospot analysis software (Cellular Technology Limited). Non-specific and background spots were determined by wells containing no cells. The number of spots detected per well was used to calculate the spot frequency per 10,000 cells.

B cell sorting and BCR sequencing

Cells were processed and stained as described above, and sorted on a FACS Aria II cell sorter (BD) into SMART-Seq lysis buffer (Takara). cDNA was generated for each sample using the SMART-Seq v4 kit (Takara). Samples were end-repaired, A-tailed, and ligated with custom UMI adapters (IDT) (**Table 5.2**) at 2 uM according to NEBNext Ultra II instructions (NEB). Libraries were prepped following NEBNext Immune Sequencing Kit's protocol (NEB), and qPCR was used to determine cycling conditions prior to plateau. Samples were pooled at equimolar concentration and ran on a MiSeq (Illumina) with a MiSeq Reagent Kit v3 (600-cycle) (Illumina).

BCR sequence processing

All samples were processed with an in-house pipeline using pRESTO, BBDuk, and custom python scripts[143,144]. Sequences were filtered for Q20 average quality and the TSO sequence. Consensus sequences were made using the UMI, and leader sequences were removed. Paired ends were assembled and sequences with bases below Q30 were removed. Sequences were collapsed to remove duplicates and all sequences filtered for at least 2 reads. Resulting fastq files were submitted to IMGT for alignment. Clones were identified using Shazam and Change-O with a clustering threshold of 0.04[145]. Sequences were analyzed further in R (4.0.4) using tidyverse (1.3.0)[146].

Histology and image analysis

Spleens were isolated from infected mice and immediately submerged in BD Cytofix diluted 1:3 with PBS for 24h at 4°C. Spleens were then washed with PBS and dehydrated in 30% sucrose for 24h at 4°C before being embedded in OCT freezing medium. 18 uM sections were cut on a cryostat and stained with anti-mouse IgD ef450 (Clone 11-26c, Invitrogen), CD3 AF488 (Clone 17A2, BioLegend), BCL6 AF647 (Clone K112-91, BD Biosciences), and CD35 biotin (Clone 8C12, BD Biosciences), followed by Streptavidin Cy3 (Jackson ImmunoResearch). Slides were cover-slipped with Fluoromount G mounting media (SouthernBiotech) and images were acquired on a Nikon Eclipse 90i with NIS-Elements software. Imaris (Bitplane) was used for image analysis. GC diameter and circumference were measured as the area around or across the $BCL6^+$ cells using Imaris, with each measurement taken three times and averaged.

Statistical analysis

All statistical analyses were performed in GraphPad Prism 9 (GraphPad Software). Unpaired, two-tailed Student's t tests were applied to determine the differences between two individual groups. Paired, two-tailed Student's t tests were applied to determine the differences between two groups in adoptive transfer experiments. In the event of three or four groups, a one-way ANOVA followed by Tukey's multiple comparisons test was performed. The statistical details of each experiment are indicated in the figure legends.

Surface molecule	Fluorochrome	Clone	Manufacturer
B220	BV510	RA3-6B2	BD Biosciences
B220	BUV737	RA3-6B2	BD Biosciences
B220	PE-CF594	RA3-6B2	BD Biosciences
BCL2	AF488	BCL/10C4	BioLegend
BCL6	AF647	K112-91	BD Biosciences
BCL6	PE-CF594	K112-91	BD Biosciences
BLIMP1	PE-CF594	6D3	BD Biosciences
CD3	APC-ef780	145-2C11	Invitrogen
CD3	PerCP-Cy5.5	145-2C11	BD Biosciences
CD4	BUV805	GK1.5	BD Biosciences
CD4	BV711	RM4-5	BioLegend
CD8	BV510	53-6.7	BD Biosciences
CD11b	PE-CF594	M1/70	BD Biosciences
CD11c	PE-CF594	HL3	BD Biosciences
CD23	BV711	B3B4	BD Biosciences
CD38	AF700	90	Invitrogen
CD44	AF700	IM7	BD Biosciences
CD45.1	FITC	A20	eBioscience
CD45.2	APC-ef780	104	Invitrogen
CD62L	BV786	MEL-14	BD Biosciences
CD73	PE-Cy7	TY/11.8	Invitrogen
CD80	BV605	16-10A1	BD Biosciences
CD86	BV605	GL-1	BioLegend
CD138	BB515	281-2	BD Biosciences
CD138	BV650	281-2	BD Biosciences
c-myc	FITC	Y69	abcam
CXCR4	BV711	L276F12	BioLegend
CXCR5	PE	2G8	BD Biosciences
GL7	ef450	GL-7	Invitrogen
huCD2	Biotin	RPA-2.10	Invitrogen
IgM	BV786	II/41	BD Biosciences
IgD	BUV395	11-26c.2a	BD Biosciences
IL4Rα	Biotin	mIL4R-M1	BD Biosciences
IRF4	FITC	3E4	Invitrogen
PD-1	ef450	J43	Invitrogen
PD-1	PE-Cy7	29F.1A12	BioLegend
Streptavidin	BV605	---	BD Biosciences
Streptavidin	BV711	---	BD Biosciences
Streptavidin	BUV661	---	BD Biosciences

Table 5.1. Antibodies used for flow cytometry.

Adapter	Sequence
1 Top	5'-GTGACTGGAGTTCAGACGTGTGCTCTTCCGATCTNNNNNN NNNNNNNNNNACACTACTCG*T-3'
1 Bottom	5'-/5Phos/CGAGTAGTGT-3'
2 Top	5'-GTGACTGGAGTTCAGACGTGTGCTCTTCCGATCTNNNNNN NNNNNNNNNNTGTGCGGCTC*T-3'
2 Bottom	5'-/5Phos/GAGCCGCACA-3'

Table 5.2. UMI adapters for BCR sequencing.

6. References

1. Janeway, C.A. (1989). Approaching the Asymptote? Evolution and Revolution in Immunology. Cold Spring Harb Symp Quant Biol *54*, 1–13. 10.1101/SQB.1989.054.01.003.
2. Tonegawa, S. (1983). Somatic generation of antibody diversity. Nature 1983 302:5909 *302*, 575–581. 10.1038/302575a0.
3. Fairfax, K.A., Kallies, A., Nutt, S.L., and Tarlinton, D.M. (2008). Plasma cell development: From B-cell subsets to long-term survival niches. Semin Immunol *20*, 49–58. 10.1016/J.SMIM.2007.12.002.
4. Nutt, S.L., Hodgkin, P.D., Tarlinton, D.M., and Corcoran, L.M. (2015). The generation of antibody-secreting plasma cells. Nature Reviews Immunology 2015 15:3 *15*, 160–171. 10.1038/nri3795.
5. Mesin, L., Ersching, J., and Victora, G.D. (2016). Germinal Center B Cell Dynamics. Immunity *45*, 471–482. 10.1016/j.immuni.2016.09.001.
6. Gaya, M., Barral, P., Burbage, M., Aggarwal, S., Montaner, B., Warren Navia, A., Aid, M., Tsui, C., Maldonado, P., Nair, U., et al. (2018). Initiation of Antiviral B Cell Immunity Relies on Innate Signals from Spatially Positioned NKT Cells. Cell *172*, 517-533.e20. 10.1016/J.CELL.2017.11.036.
7. Reinhardt, R.L., Liang, H.-E., and Locksley, R.M. (2009). Cytokine-secreting follicular T cells shape the antibody repertoire. Nat Immunol *10*, 385–393. 10.1038/ni.1715.
8. MacLennan, I.C.M., Toellner, K.M., Cunningham, A.F., Serre, K., Sze, D.M.Y., Zúñiga, E., Cook, M.C., and Vinuesa, C.G. (2003). Extrafollicular antibody responses. Immunol Rev *194*, 8–18. 10.1034/J.1600-065X.2003.00058.X.
9. Victora, G.D., and Nussenzweig, M.C. (2012). Germinal centers. Annu Rev Immunol *30*, 429–457. 10.1146/ANNUREV-IMMUNOL-020711-075032.
10. Victora, G.D., and Nussenzweig, M.C. (2022). Germinal Centers. https://doi.org/10.1146/annurev-immunol-120419-022408 *40*, 413–442. 10.1146/ANNUREV-IMMUNOL-120419-022408.
11. Allen, C.D.C., Okada, T., and Cyster, J.G. (2007). Germinal-Center Organization and Cellular Dynamics. Immunity *27*, 190–202. 10.1016/J.IMMUNI.2007.07.009.
12. De Silva, N.S., and Klein, U. (2015). Dynamics of B cells in germinal centres. Nat Rev Immunol *15*, 137. 10.1038/NRI3804.
13. Ranuncolo, S.M., Polo, J.M., Dierov, J., Singer, M., Kuo, T., Greally, J., Green, R., Carroll, M., and Melnick, A. (2007). Bcl-6 mediates the germinal center B cell phenotype and lymphomagenesis through transcriptional repression of the DNA-damage sensor ATR. Nat Immunol *8*, 705–714. 10.1038/ni1478.
14. Shulman, Z., Gitlin, A.D., Weinstein, J.S., Lainez, B., Esplugues, E., Flavell, R.A., Craft, J.E., and Nussenzweig, M.C. (2014). Dynamic signaling by T follicular helper cells during germinal center B cell selection. Science *345*, 1058. 10.1126/SCIENCE.1257861.
15. McHeyzer-Williams, M., Okitsu, S., Wang, N., and McHeyzer-Williams, L. (2011). Molecular programming of B cell memory. Nature Reviews Immunology 2011 12:1 *12*, 24–34. 10.1038/NRI3128.
16. Victora, G.D., Schwickert, T.A., Fooksman, D.R., Kamphorst, A.O., Meyer-Hermann, M., Dustin, M.L., and Nussenzweig, M.C. (2010). Germinal center dynamics revealed by

multiphoton microscopy with a photoactivatable fluorescent reporter. Cell *143*, 592–605. 10.1016/j.cell.2010.10.032.
17. Meyer-Hermann, M., Mohr, E., Pelletier, N., Zhang, Y., Victora, G.D., and Toellner, K.M. (2012). A theory of germinal center b cell selection, division, and exit. Cell Rep *2*, 162–174. 10.1016/j.celrep.2012.05.010.
18. Tas, J.M.J., Mesin, L., Pasqual, G., Targ, S., Jacobsen, J.T., Mano, Y.M., Chen, C.S., Weill, J.C., Reynaud, C.A., Browne, E.P., et al. (2016). Visualizing antibody affinity maturation in germinal centers. Science (1979) *351*, 1048–1054. 10.1126/SCIENCE.AAD3439/SUPPL_FILE/TAS-SM.PDF.
19. Nowosad, C.R., Mesin, L., Castro, T.B.R., Wichmann, C., Donaldson, G.P., Araki, T., Schiepers, A., Lockhart, A.A.K., Bilate, A.M., Mucida, D., et al. (2020). Tunable dynamics of B cell selection in gut germinal centres. Nature 2020 588:7837 *588*, 321–326. 10.1038/s41586-020-2865-9.
20. Gitlin, A.D., Shulman, Z., and Nussenzweig, M.C. (2014). Clonal selection in the germinal center by regulated proliferation and hypermutation. Nature *509*, 637. 10.1038/NATURE13300.
21. Mcheyzer-Williams, L.J., Milpied, P.J., Okitsu, S.L., and Mcheyzer-Williams, M.G. (2015). Switched-memory B cells remodel B cell receptors within secondary germinal centers. Nat Immunol *16*, 296. 10.1038/NI.3095.
22. Shokat, K.M., and Goodnow, C.C. (1995). Antigen-induced B-cell death and elimination during germinal-centre immune responses. Nature 1995 375:6529 *375*, 334–338. 10.1038/375334a0.
23. Pulendran, B., Kannourakis, G., Nouri, S., Smith, K.G.C., and Nossal, G.J.V. (1995). Soluble antigen can cause enhanced apoptosis of germinal-centre B cells. Nature 1995 375:6529 *375*, 331–334. 10.1038/375331a0.
24. Nakagawa, R., Toboso-Navasa, A., Schips, M., Young, G., Bhaw-Rosun, L., Llorian-Sopena, M., Chakravarty, P., Sesay, A.K., Kassiotis, G., Meyer-Hermann, M., et al. (2021). Permissive selection followed by affinity-based proliferation of GC light zone B cells dictates cell fate and ensures clonal breadth. Proceedings of the National Academy of Sciences *118*. 10.1073/PNAS.2016425118.
25. Shinnakasu, R., Inoue, T., Kometani, K., Moriyama, S., Adachi, Y., Nakayama, M., Takahashi, Y., Fukuyama, H., Okada, T., and Kurosaki, T. (2016). Regulated selection of germinal-center cells into the memory B cell compartment. Nat Immunol *17*, 861–869. 10.1038/ni.3460.
26. Dominguez-Sola, D., Victora, G.D., Ying, C.Y., Phan, R.T., Saito, M., Nussenzweig, M.C., and Dalla-Favera, R. (2012). The proto-oncogene MYC is required for selection in the germinal center and cyclic reentry. Nat Immunol *13*, 1083–1091. 10.1038/ni.2428.
27. Polo, J.M., Ci, W., Licht, J.D., and Melnick, A. (2008). Reversible disruption of BCL6 repression complexes by CD40 signaling in normal and malignant B cells. Blood *112*, 644–651. 10.1182/blood-2008-01-131813.
28. Weisel, F.J., Zuccarino-Catania, G.V., Chikina, M., and Shlomchik, M.J. (2016). A Temporal Switch in the Germinal Center Determines Differential Output of Memory B and Plasma Cells. Immunity *44*, 116–130. 10.1016/J.IMMUNI.2015.12.004.
29. Laidlaw, B.J., Schmidt, T.H., Green, J.A., Allen, C.D.C., Okada, T., and Cyster, J.G. (2017). The Eph-related tyrosine kinase ligand Ephrin-B1 marks germinal center and memory precursor B cells. J Exp Med *214*, 639–649. 10.1084/jem.20161461.

30. Gitlin, A.D., von Boehmer, L., Gazumyan, A., Shulman, Z., Oliveira, T.Y., and Nussenzweig, M.C. (2016). Independent Roles of Switching and Hypermutation in the Development and Persistence of B Lymphocyte Memory. Immunity *44*, 769–781. 10.1016/j.immuni.2016.01.011.
31. Wang, Y., Shi, J., Yan, J., Xiao, Z., Hou, X., Lu, P., Hou, S., Mao, T., Liu, W., Ma, Y., et al. (2017). Germinal-center development of memory B cells driven by IL-9 from follicular helper T cells. Nat Immunol *18*, 921–930. 10.1038/ni.3788.
32. Inoue, T., Shinnakasu, R., Kawai, C., Ise, W., Kawakami, E., Sax, N., Oki, T., Kitamura, T., Yamashita, K., Fukuyama, H., et al. (2021). Exit from germinal center to become quiescent memory B cells depends on metabolic reprograming and provision of a survival signal. J Exp Med *218*. 10.1084/jem.20200866.
33. Bhattacharya, D., Cheah, M.T., Franco, C.B., Hosen, N., Pin, C.L., Sha, W.C., and Weissman, I.L. (2007). Transcriptional Profiling of Antigen-Dependent Murine B Cell Differentiation and Memory Formation. The Journal of Immunology *179*, 6808–6819. 10.4049/jimmunol.179.10.6808.
34. Laidlaw, B.J., and Cyster, J.G. (2021). Transcriptional regulation of memory B cell differentiation. Nat Rev Immunol *21*, 209–220. 10.1038/s41577-020-00446-2.
35. Laidlaw, B.J., Duan, L., Xu, Y., Vazquez, S.E., and Cyster, J.G. (2020). The transcription factor Hhex cooperates with the corepressor Tle3 to promote memory B cell development. Nat Immunol *21*, 1082–1093. 10.1038/s41590-020-0713-6.
36. Smith, K.G.C., Light, A., O'Reilly, L.A., Ang, S.M., Strasser, A., and Tarlinton, D. (2000). bcl-2 Transgene expression inhibits apoptosis in the germinal center and reveals differences in the selection of memory B cells and bone marrow antibody-forming cells. Journal of Experimental Medicine *191*, 475–484. 10.1084/jem.191.3.475.
37. Ise, W., Fujii, K., Shiroguchi, K., Ito, A., Kometani, K., Takeda, K., Kawakami, E., Yamashita, K., Suzuki, K., Okada, T., et al. (2018). T Follicular Helper Cell-Germinal Center B Cell Interaction Strength Regulates Entry into Plasma Cell or Recycling Germinal Center Cell Fate. Immunity *48*, 702-715.e4. 10.1016/J.IMMUNI.2018.03.027.
38. Koike, T., Harada, K., Horiuchi, S., and Kitamura, D. (2019). The quantity of CD40 signaling determines the differentiation of b cells into functionally distinct memory cell subsets. Elife *8*. 10.7554/eLife.44245.001.
39. Good-Jacobson, K.L., Szumilas, C.G., Chen, L., Sharpe, A.H., Tomayko, M.M., and Shlomchik, M.J. (2010). PD-1 regulates germinal center B cell survival and the formation and affinity of long-lived plasma cells. Nat Immunol *11*, 535. 10.1038/NI.1877.
40. Zhong, M.C., Lu, Y., Qian, J., Zhu, Y., Dong, L., Zahn, A., Di Noia, J.M., Karo-Atar, D., King, I.L., and Veillette, A. (2021). SLAM family receptors control pro-survival effectors in germinal center B cells to promote humoral immunity. J Exp Med *218*. 10.1084/jem.20200756.
41. Bélanger, S., and Crotty, S. (2016). Dances with cytokines, featuring TFH cells, IL-21, IL-4 and B cells. Nat Immunol *17*, 1135–1136. 10.1038/ni.3561.
42. Gowthaman, U., Chen, J.S., Zhang, B., Flynn, W.F., Lu, Y., Song, W., Joseph, J., Gertie, J.A., Xu, L., Collet, M.A., et al. (2019). Identification of a T follicular helper cell subset that drives anaphylactic IgE. Science *365*. 10.1126/SCIENCE.AAW6433.
43. Eto, D., Lao, C., DiToro, D., Barnett, B., Escobar, T.C., Kageyama, R., Yusuf, I., and Crotty, S. (2011). IL-21 and IL-6 Are Critical for Different Aspects of B Cell Immunity

and Redundantly Induce Optimal Follicular Helper CD4 T Cell (Tfh) Differentiation. PLoS One *6*, e17739. 10.1371/JOURNAL.PONE.0017739.
44. Rousset, F., Garcia, E., Defrance, T., Peronne, C., Vezzio, N., Hsu, D.H., Kastelein, R., Moore, K.W., and Banchereau, J. (1992). Interleukin 10 is a potent growth and differentiation factor for activated human B lymphocytes. Proc Natl Acad Sci U S A *89*, 1890. 10.1073/PNAS.89.5.1890.
45. Linterman, M.A., Pierson, W., Lee, S.K., Kallies, A., Kawamoto, S., Rayner, T.F., Srivastava, M., Divekar, D.P., Beaton, L., Hogan, J.J., et al. (2011). Foxp3+ follicular regulatory T cells control T follicular helper cells and the germinal center response. Nat Med *17*, 975. 10.1038/NM.2425.
46. Luo, X., Hou, X., Wang, Y., Li, Y., Yu, S., and Qi, H. (2023). An Interleukin 9-Zbtb18 axis promotes germinal center development of memory B cells. bioRxiv, 2023.06.11.544304. 10.1101/2023.06.11.544304.
47. Gonzalez, D.G., Cote, C.M., Patel, J.R., Smith, C.B., Zhang, Y., Nickerson, K.M., Zhang, T., Kerfoot, S.M., and Haberman, A.M. (2018). Nonredundant Roles of IL-21 and IL-4 in the Phased Initiation of Germinal Center B Cells and Subsequent Self-Renewal Transitions. The Journal of Immunology *201*, 3569–3579. 10.4049/JIMMUNOL.1500497.
48. Chevrier, S., Kratina, T., Emslie, D., Tarlinton, D.M., and Corcoran, L.M. (2017). IL4 and IL21 cooperate to induce the high Bcl6 protein level required for germinal center formation. Immunol Cell Biol *95*, 925–932. 10.1038/icb.2017.71.
49. Berglund, L.J., Avery, D.T., Ma, C.S., Moens, L., Deenick, E.K., Bustamante, J., Boisson-Dupuis, S., Wong, M., Adelstein, S., Arkwright, P.D., et al. (2013). IL-21 signalling via STAT3 primes human näive B cells to respond to IL-2 to enhance their differentiation into plasmablasts. Blood *122*, 3940–3950. 10.1182/blood-2013-06-506865.
50. Weinstein, J.S., Herman, E.I., Lainez, B., Licona-Limón, P., Esplugues, E., Flavell, R., and Craft, J. (2016). TFH cells progressively differentiate to regulate the germinal center response. Nat Immunol *17*, 1197–1205. 10.1038/ni.3554.
51. Chou, C., Verbaro, D.J., Tonc, E., Holmgren, M., Cella, M., Colonna, M., Bhattacharya, D., and Egawa, T. (2016). The Transcription Factor AP4 Mediates Resolution of Chronic Viral Infection through Amplification of Germinal Center B Cell Responses. Immunity *45*, 570–582. 10.1016/j.immuni.2016.07.023.
52. Phillips, T.M., Lipsky, P.E., Ettinger, R., Kuchen, S., Robbins, R., Sims, G.P., and Sheng, C. (2020). T Cell-B Cell Collaboration + during CD4 Expansion, and Plasma Cell Generation Essential Role of IL-21 in B Cell Activation. J Immunol References *179*, 5886–5896. 10.4049/jimmunol.179.9.5886.
53. Zotos, D., Coquet, J.M., Zhang, Y., Light, A., D'Costa, K., Kallies, A., Corcoran, L.M., Godfrey, D.I., Toellner, K.-M., Smyth, M.J., et al. (2010). IL-21 regulates germinal center B cell differentiation and proliferation through a B cell-intrinsic mechanism. J Exp Med *207*, 365–378. 10.1084/jem.20091777.
54. Ding, B.B., Bi, E., Chen, H., Yu, J.J., and Ye, B.H. (2013). IL-21 and CD40L synergistically promote plasma cell differentiation through upregulation of Blimp-1 in human B cells. J Immunol *190*, 1827–1836. 10.4049/jimmunol.1201678.
55. Ettinger, R., Sims, G.P., Fairhurst, A.-M., Robbins, R., da Silva, Y.S., Spolski, R., Leonard, W.J., and Lipsky, P.E. (2005). IL-21 induces differentiation of human naive and memory B cells into antibody-secreting plasma cells. J Immunol *175*, 7867–7879. 10.4049/jimmunol.175.12.7867.

56. Iii, H.C.M., Lipsky, P.E., Leonard, W.J., Shaffer, D.J., Akilesh, S., Roopenian, D.C., Kim, H.-P., Wang, G., Qi, C.-F., Ozaki, P.K., et al. (2021). Inducer of Blimp-1 and Bcl-6 Plasma Cell Generation by IL-21, a Novel Regulation of B Cell Differentiation and. J Immunol *173*, 5361–5371. 10.4049/jimmunol.173.9.5361.
57. McKenzie, G.J., Fallon, P.G., Emson, C.L., Grencis, R.K., and McKenzie, A.N.J. (1999). Simultaneous disruption of interleukin (IL)-4 and IL-13 defines individual roles in T helper cell type 2-mediated responses. J Exp Med *189*, 1565–1572. 10.1084/JEM.189.10.1565.
58. Turqueti-Neves, A., Otte, M., da Costa, O.P., Höpken, U.E., Lipp, M., Buch, T., and Voehringer, D. (2014). B-cell-intrinsic STAT6 signaling controls germinal center formation. Eur J Immunol *44*, 2130–2138. 10.1002/eji.201344203.
59. Voehringer, D., Reese, T.A., Huang, X., Shinkai, K., and Locksley, R.M. (2006). Type 2 immunity is controlled by IL-4/IL-13 expression in hematopoietic non-eosinophil cells of the innate immune system. J Exp Med *203*, 1435. 10.1084/JEM.20052448.
60. Yusuf, I., Kageyama, R., Monticelli, L., Johnston, R.J., DiToro, D., Hansen, K., Barnett, B., and Crotty, S. (2010). Germinal Center T Follicular Helper Cell IL-4 Production Is Dependent on Signaling Lymphocytic Activation Molecule Receptor (CD150). The Journal of Immunology *185*, 190–202. 10.4049/jimmunol.0903505.
61. Luzina, I.G., Keegan, A.D., Heller, N.M., Rook, G.A.W., Shea-Donohue, T., and Atamas, S.P. (2012). Regulation of inflammation by interleukin-4: a review of "alternatives." J Leukoc Biol *92*, 753. 10.1189/JLB.0412214.
62. Duan, L., Liu, D., An, J., Laidlaw, B.J., Correspondence, J.G.C., Chen, H., Mintz, M.A., Chou, M.Y., Kotov, D.I., Xu, Y., et al. (2021). Follicular dendritic cells restrict interleukin-4 availability in germinal centers and foster memory B cell generation. Immunity *54*. 10.1016/j.immuni.2021.08.028.
63. Inoue, T., Moran, I., Shinnakasu, R., Phan, T.G., and Kurosaki, T. (2018). Generation of memory B cells and their reactivation. Immunol Rev *283*, 138–149. 10.1111/imr.12640.
64. Haberman, A.M., Gonzalez, D.G., Wong, P., Zhang, T., and Kerfoot, S.M. (2019). Germinal center B cell initiation, GC maturation, and the coevolution of its stromal cell niches. Immunol Rev *288*, 10–27. 10.1111/imr.12731.
65. Ochiai, K., Maienschein-Cline, M., Simonetti, G., Chen, J., Rosenthal, R., Brink, R., Chong, A.S., Klein, U., Dinner, A.R., Singh, H., et al. (2013). Transcriptional Regulation of Germinal Center B and Plasma Cell Fates by Dynamical Control of IRF4. Immunity *38*, 918–929. 10.1016/j.immuni.2013.04.009.
66. Yeh, C.H., Nojima, T., Kuraoka, M., and Kelsoe, G. (2018). Germinal center entry not selection of B cells is controlled by peptide-MHCII complex density. Nat Commun *9*. 10.1038/S41467-018-03382-X.
67. Jacobsen, J.T., Hu, W., Castro, T.B.R., Solem, S., Galante, A., Lin, Z., Allon, S.J., Mesin, L., Bilate, A.M., Schiepers, A., et al. (2021). Expression of Foxp3 by T follicular helper cells in end-stage germinal centers. Science *373*. 10.1126/SCIENCE.ABE5146.
68. Smith, K.G.C., Weiss, U., Rajewsky, K., Nossal, G.J.V., and Tarlinton, D.M. (1994). Bcl-2 increases memory B cell recruitment but does not perturb selection in germinal centers. Immunity *1*, 803–813. 10.1016/S1074-7613(94)80022-7.
69. Saito, M., Gao, J., Basso, K., Kitagawa, Y., Smith, P.M., Bhagat, G., Pernis, A., Pasqualucci, L., and Dalla-Favera, R. (2007). A Signaling Pathway Mediating

Downregulation of BCL6 in Germinal Center B Cells Is Blocked by BCL6 Gene Alterations in B Cell Lymphoma. Cancer Cell *12*, 280–292. 10.1016/j.ccr.2007.08.011.
70. Kuo, T.C., Shaffer, A.L., Haddad, J., Yong, S.C., Staudt, L.M., and Calame, K. (2007). Repression of BCL-6 is required for the formation of human memory B cells in vitro. J Exp Med *204*, 819. 10.1084/JEM.20062104.
71. Choi, J., Diao, H., Faliti, C.E., Truong, J., Rossi, M., Bélanger, S., Yu, B., Goldrath, A.W., Pipkin, M.E., and Crotty, S. (2020). Bcl-6 is the nexus transcription factor of T follicular helper cells via repressor-of-repressor circuits. Nat Immunol *21*, 777–789. 10.1038/s41590-020-0706-5.
72. Ci, W., Polo, J.M., Cerchietti, L., Shaknovich, R., Wang, L., Shao, N.Y., Ye, K., Farinha, P., Horsman, D.E., Gascoyne, R.D., et al. (2009). The BCL6 transcriptional program features repression of multiple oncogenes in primary B cells and is deregulated in DLBCL. Blood *113*, 5536–5548. 10.1182/BLOOD-2008-12-193037.
73. Kumagai, T., Miki, T., Kikuchi, M., Fukuda, T., Miyasaka, N., Kamiyama, R., and Hirosawa, S. (1999). The proto-oncogene Bcl6 inhibits apoptotic cell death in differentiation-induced mouse myogenic cells. Oncogene *18*, 467–475. 10.1038/sj.onc.1202306.
74. Krishnamurty, A.T., Thouvenel, C.D., Portugal, S., Keitany, G.J., Kim, K.S., Holder, A., Crompton, P.D., Rawlings, D.J., and Pepper, M. (2016). Somatically Hypermutated Plasmodium-Specific IgM(+) Memory B Cells Are Rapid, Plastic, Early Responders upon Malaria Rechallenge. Immunity *45*, 402–414. 10.1016/j.immuni.2016.06.014.
75. Arroyo, E.N., and Pepper, M. (2020). B cells are sufficient to prime the dominant CD4+ Tfh response to Plasmodium infection. Journal of Experimental Medicine *217*. 10.1084/JEM.20190849.
76. Langhorne, J., Gillard, S., Simon, B., Slade, S., and Eichmann, K. (1989). Frequencies of CD4+ T cells reactive with plasmodium chabaudi chabaudi: Distinct response kinetics for cells with Th1 and Th2 characteristics during infection. Int Immunol *1*, 416–424. 10.1093/intimm/1.4.416.
77. Katona, I.M., Maliszewski F D Finkelman, C.R., Madden, K.B., Morris, S.C., and Holmes, J.M. (2021). cytokine-anti-cytokine antibody complexes. cytokines by injection of Prolongation of in vivo effects of exogenous Anti-cytokine antibodies as carrier proteins.
78. Taylor, J.J., Pape, K.A., and Jenkins, M.K. (2012). A germinal center-independent pathway generates unswitched memory B cells early in the primary response. J Exp Med *209*, 597–606. 10.1084/jem.20111696.
79. Kerfoot, S.M., Yaari, G., Patel, J.R., Johnson, K.L., Gonzalez, D.G., Kleinstein, S.H., and Haberman, A.M. (2011). Germinal Center B Cell and T Follicular Helper Cell Development Initiates in the Interfollicular Zone. Immunity *34*, 947–960. 10.1016/j.immuni.2011.03.024.
80. Huang, C., Gonzalez, D.G., Cote, C.M., Jiang, Y., Hatzi, K., Teater, M., Dai, K., Hla, T., Haberman, A.M., and Melnick, A. (2014). The BCL6 RD2 domain governs commitment of activated B cells to form germinal centers. Cell Rep *8*, 1497–1508. 10.1016/J.CELREP.2014.07.059.
81. Niu, H., Cattoretti, G., and Dalla-Favera, R. (2003). BCL6 controls the expression of the B7-1/CD80 costimulatory receptor in germinal center B cells. Journal of Experimental Medicine *198*, 211–221. 10.1084/jem.20021395.

82. Tomayko, M.M., Steinel, N.C., Anderson, S.M., and Shlomchik, M.J. (2010). Cutting Edge: Hierarchy of Maturity of Murine Memory B Cell Subsets. The Journal of Immunology *185*, 7146–7150. 10.4049/JIMMUNOL.1002163.
83. Zuccarino-Catania, G. V., Sadanand, S., Weisel, F.J., Tomayko, M.M., Meng, H., Kleinstein, S.H., Good-Jacobson, K.L., and Shlomchik, M.J. (2014). CD80 and PD-L2 define functionally distinct memory B cell subsets that are independent of antibody isotype. Nature Immunology 2014 15:7 *15*, 631–637. 10.1038/ni.2914.
84. Weisel, F.J., Mullett, S.J., Elsner, R.A., Menk, A. V., Trivedi, N., Luo, W., Wikenheiser, D., Hawse, W.F., Chikina, M., Smita, S., et al. (2020). Germinal center B cells selectively oxidize fatty acids for energy while conducting minimal glycolysis. Nat Immunol *21*, 331. 10.1038/S41590-020-0598-4.
85. Luo, W., Conter, L., Elsner, R.A., Smita, S., Weisel, F., Callahan, D., Wu, S., Chikina, M., and Shlomchik, M. (2023). IL-21R signal reprogramming cooperates with CD40 and BCR signals to select and differentiate germinal center B cells. Sci Immunol *8*. 10.1126/SCIIMMUNOL.ADD1823.
86. Good-Jacobson, K.L., Song, E., Anderson, S., Sharpe, A.H., and Shlomchik, M.J. (2012). CD80 Expression on B Cells Regulates Murine T Follicular Helper Development, Germinal Center B Cell Survival, and Plasma Cell Generation. The Journal of Immunology *188*, 4217–4225. 10.4049/jimmunol.1102885.
87. Baumjohann, D., Preite, S., Reboldi, A., Ronchi, F., Ansel, K.M., Lanzavecchia, A., and Sallusto, F. (2013). Persistent Antigen and Germinal Center B Cells Sustain T Follicular Helper Cell Responses and Phenotype. Immunity *38*, 596–605. 10.1016/J.IMMUNI.2012.11.020.
88. Green, J.A., Suzuki, K., Cho, B., Willison, L.D., Palmer, D., Allen, C.D.C., Schmidt, T.H., Xu, Y., Proia, R.L., Coughlin, S.R., et al. (2011). The sphingosine 1-phosphate receptor S1P2 maintains germinal center B cell homeostasis and promotes niche confinement. Nat Immunol *12*, 672. 10.1038/NI.2047.
89. Perona-Wright, G., Mohrs, K., Mayer, K.D., and Mohrs, M. (2010). Differential regulation of IL-4Ralpha expression by antigen versus cytokine stimulation characterizes Th2 progression in vivo. J Immunol *184*, 615–623. 10.4049/JIMMUNOL.0902408.
90. Pasqualucci, L., Migliazza, A., Basso, K., Houldsworth, J., Chaganti, R.S.K., and Dalla-Favera, R. (2003). Mutations of the BCL6 proto-oncogene disrupt its negative autoregulation in diffuse large B-cell lymphoma. Blood *101*, 2914–2923. 10.1182/blood-2002-11-3387.
91. Mendez, L.M., Polo, J.M., Yu, J.J., Krupski, M., Ding, B.B., Melnick, A., and Ye, B.H. (2008). CtBP Is an Essential Corepressor for BCL6 Autoregulation. Mol Cell Biol *28*, 2175–2186. 10.1128/mcb.01400-07.
92. Schroder, A.J., Pavlidis, P., Arimura, A., Capece, D., and Rothman, P.B. (2002). Cutting Edge: STAT6 Serves as a Positive and Negative Regulator of Gene Expression in IL-4-Stimulated B Lymphocytes. The Journal of Immunology *168*, 996–1000. 10.4049/jimmunol.168.3.996.
93. Wurster, A.L., Withers, D.J., Uchida, T., White, M.F., and Grusby, M.J. (2002). Stat6 and IRS-2 Cooperate in Interleukin 4 (IL-4)-Induced Proliferation and Differentiation but Are Dispensable for IL-4-Dependent Rescue from Apoptosis. Mol Cell Biol *22*, 117. 10.1128/MCB.22.1.117-126.2002.

94. Linterman, M.A., Beaton, L., Yu, D., Ramiscal, R.R., Srivastava, M., Hogan, J.J., Verma, N.K., Smyth, M.J., Rigby, R.J., and Vinuesa, C.G. (2010). IL-21 acts directly on B cells to regulate Bcl-6 expression and germinal center responses. Journal of Experimental Medicine *207*, 353–363. 10.1084/jem.20091738.
95. Tauzin, A., Gong, S.Y., Beaudoin-Bussières, G., Vézina, D., Gasser, R., Nault, L., Marchitto, L., Benlarbi, M., Chatterjee, D., Nayrac, M., et al. (2022). Strong humoral immune responses against SARS-CoV-2 Spike after BNT162b2 mRNA vaccination with a 16-week interval between doses. Cell Host Microbe *30*, 97-109.e5. 10.1016/J.CHOM.2021.12.004/ATTACHMENT/BD4DA173-5A3F-408E-A5A2-9803CC3B4922/MMC1.PDF.
96. Kopr, M., Kobler, G., and Langhorne, J. (1994). Max·Planck·lnstitut fiir Immunbiologie, Freiburg P. chabaudi infection in ll..-4-deficient mice The immune response to Plasmodium chabaudi malaria in interleukin-4-deficient mice*.
97. Pape, K.A., Maul, R.W., Dileepan, T., Paustian, A.S., Gearhart, P.J., and Jenkins, M.K. (2018). Naïve B cells with high-avidity germline-encoded antigen receptors produce persistent IgM+ and transient IgG+ memory B cells. Immunity *48*, 1135. 10.1016/J.IMMUNI.2018.04.019.
98. Chao, G., Lau, W.L., Hackel, B.J., Sazinsky, S.L., Lippow, S.M., and Wittrup, K.D. (2006). Isolating and engineering human antibodies using yeast surface display. Nat Protoc *1*, 755–768. 10.1038/NPROT.2006.94.
99. Paus, D., Tri, G.P., Chan, T.D., Gardam, S., Basten, A., and Brink, R. (2006). Antigen recognition strength regulates the choice between extrafollicular plasma cell and germinal center B cell differentiation. J Exp Med *203*, 1081. 10.1084/JEM.20060087.
100. Garrett Rappazzo, C., Tse, L. V., Kaku, C.I., Wrapp, D., Sakharkar, M., Huang, D., Deveau, L.M., Yockachonis, T.J., Herbert, A.S., Battles, M.B., et al. (2021). Broad and potent activity against SARS-like viruses by an engineered human monoclonal antibody. Science (1979) *371*, 823–829. 10.1126/SCIENCE.ABF4830/SUPPL_FILE/ABF4830_TABLE_S2_GISAID_ACKNOWLEDGMENTS.PDF.
101. King, I.L., and Mohrs, M. (2009). IL-4-producing CD4+ T cells in reactive lymph nodes during helminth infection are T follicular helper cells. Journal of Experimental Medicine *206*, 1001–1007. 10.1084/jem.20090313.
102. Huse, M., Lillemeier, B.F., Kuhns, M.S., Chen, D.S., and Davis, M.M. (2006). T cells use two directionally distinct pathways for cytokine secretion. Nature Immunology 2006 7:3 *7*, 247–255. 10.1038/ni1304.
103. Quast, I., Dvorscek, A.R., Pattaroni, C., Steiner, T.M., McKenzie, C.I., Pitt, C., O'Donnell, K., Ding, Z., Hill, D.L., Brink, R., et al. (2022). Interleukin-21, acting beyond the immunological synapse, independently controls T follicular helper and germinal center B cells. Immunity *0*. 10.1016/J.IMMUNI.2022.06.020.
104. King, N.P., Bale, J.B., Sheffler, W., McNamara, D.E., Gonen, S., Gonen, T., Yeates, T.O., and Baker, D. (2014). Accurate design of coassembling multi-component protein nanomaterials. Nature *510*, 103. 10.1038/NATURE13404.
105. Bale, J.B., Gonen, S., Liu, Y., Sheffler, W., Ellis, D., Thomas, C., Cascio, D., Yeates, T.O., Gonen, T., King, N.P., et al. (2016). Accurate design of megadalton-scale two-component icosahedral protein complexes. Science *353*, 389. 10.1126/SCIENCE.AAF8818.

106. Marcandalli, J., Fiala, B., Ols, S., Perotti, M., de van der Schueren, W., Snijder, J., Hodge, E., Benhaim, M., Ravichandran, R., Carter, L., et al. (2019). Induction of Potent Neutralizing Antibody Responses by a Designed Protein Nanoparticle Vaccine for Respiratory Syncytial Virus. Cell *176*, 1420. 10.1016/J.CELL.2019.01.046.
107. Kanekiyo, M., Wei, C.J., Yassine, H.M., McTamney, P.M., Boyington, J.C., Whittle, J.R.R., Rao, S.S., Kong, W.P., Wang, L., and Nabel, G.J. (2013). Self-assembling influenza nanoparticle vaccines elicit broadly neutralizing H1N1 antibodies. Nature *499*, 102–106. 10.1038/NATURE12202.
108. Gordon, D.M., Mc Govern, T.W., Krzych, U., Cohen, J.C., Schneider, I., La Chance, R., Heppner, D.G., Yuan, G., Hollingdale, M., Slaoui, M., et al. (1995). Safety, immunogenicity, and efficacy of a recombinantly produced Plasmodium falciparum circumsporozoite protein-hepatitis B surface antigen subunit vaccine. J Infect Dis *171*, 1576–1585. 10.1093/INFDIS/171.6.1576.
109. Aide, P., Dobaño, C., Sacarlal, J., Aponte, J.J., Mandomando, I., Guinovart, C., Bassat, Q., Renom, M., Puyol, L., Macete, E., et al. (2011). Four year immunogenicity of the RTS,S/AS02(A) malaria vaccine in Mozambican children during a phase IIb trial. Vaccine *29*, 6059–6067. 10.1016/J.VACCINE.2011.03.041.
110. Sliepen, K., Van Montfort, T., Melchers, M., Isik, G., and Sanders, R.W. (2015). Immunosilencing a highly immunogenic protein trimerization domain. J Biol Chem *290*, 7436–7442. 10.1074/JBC.M114.620534.
111. Schlapschy, M., Binder, U., Börger, C., Theobald, I., Wachinger, K., Kisling, S., Haller, D., and Skerra, A. (2013). PASylation: a biological alternative to PEGylation for extending the plasma half-life of pharmaceutically active proteins. Protein Eng Des Sel *26*, 489–501. 10.1093/PROTEIN/GZT023.
112. Kraft, J.C., Pham, M.N., Shehata, L., Brinkkemper, M., Boyoglu-Barnum, S., Sprouse, K.R., Walls, A.C., Cheng, S., Murphy, M., Pettie, D., et al. (2022). Antigen- and scaffold-specific antibody responses to protein nanoparticle immunogens. Cell Rep Med *3*. 10.1016/J.XCRM.2022.100780.
113. Duan, H., Chen, X., Boyington, J.C., Cheng, C., Zhang, Y., Jafari, A.J., Stephens, T., Tsybovsky, Y., Kalyuzhniy, O., Zhao, P., et al. (2018). Glycan Masking Focuses Immune Responses to the HIV-1 CD4-Binding Site and Enhances Elicitation of VRC01-Class Precursor Antibodies. Immunity *49*, 301-311.e5. 10.1016/J.IMMUNI.2018.07.005.
114. Thornlow, D.N., Macintyre, A.N., Oguin, T.H., Karlsson, A.B., Stover, E.L., Lynch, H.E., Sempowski, G.D., and Schmidt, A.G. (2021). Altering the Immunogenicity of Hemagglutinin Immunogens by Hyperglycosylation and Disulfide Stabilization. Front Immunol *12*. 10.3389/FIMMU.2021.737973.
115. Robbiani, D.F., Gaebler, C., Muecksch, F., Lorenzi, J.C.C., Wang, Z., Cho, A., Agudelo, M., Barnes, C.O., Gazumyan, A., Finkin, S., et al. (2020). Convergent antibody responses to SARS-CoV-2 in convalescent individuals. Nature *584*, 437–442. 10.1038/S41586-020-2456-9.
116. Shi, R., Shan, C., Duan, X., Chen, Z., Liu, P., Song, J., Song, T., Bi, X., Han, C., Wu, L., et al. (2020). A human neutralizing antibody targets the receptor-binding site of SARS-CoV-2. Nature *584*, 120–124. 10.1038/S41586-020-2381-Y.
117. Tan, C.W., Chia, W.N., Qin, X., Liu, P., Chen, M.I.C., Tiu, C., Hu, Z., Chen, V.C.W., Young, B.E., Sia, W.R., et al. (2020). A SARS-CoV-2 surrogate virus neutralization test

based on antibody-mediated blockage of ACE2-spike protein-protein interaction. Nat Biotechnol *38*, 1073–1078. 10.1038/S41587-020-0631-Z.
118. Walls, A.C., Fiala, B., Schäfer, A., Wrenn, S., Pham, M.N., Murphy, M., Tse, L. V., Shehata, L., O'Connor, M.A., Chen, C., et al. (2020). Elicitation of Potent Neutralizing Antibody Responses by Designed Protein Nanoparticle Vaccines for SARS-CoV-2. Cell *183*, 1367-1382.e17. 10.1016/J.CELL.2020.10.043/ATTACHMENT/EA7109DA-6271-4519-979B-323BF3DDA49A/MMC5.XLSX.
119. Walls, A.C., Miranda, M.C., Schäfer, A., Pham, M.N., Greaney, A., Arunachalam, P.S., Navarro, M.J., Tortorici, M.A., Rogers, K., O'Connor, M.A., et al. (2021). Elicitation of broadly protective sarbecovirus immunity by receptor-binding domain nanoparticle vaccines. Cell *184*, 5432. 10.1016/J.CELL.2021.09.015.
120. Pritchard, G.H., Krishnamurty, A.T., Netland, J., Arroyo, E.N., Takehara, K.K., and Pepper, M. (2019). The Development of Optimally Responsive Plasmodium-specific CD73+CD80+ IgM+ Memory B cells Requires Intrinsic BCL6 expression but not CD4+ Tfh cells. bioRxiv, 564351. 10.1101/564351.
121. Charles A Janeway, J., Travers, P., Walport, M., and Shlomchik, M.J. (2001). Immunobiology. Immunobiology, 1–10.
122. Laudenbach, M., Baruffaldi, F., Robinson, C., Carter, P., Seelig, D., Baehr, C., and Pravetoni, M. (2018). Blocking interleukin-4 enhances efficacy of vaccines for treatment of opioid abuse and prevention of opioid overdose. Sci Rep *8*. 10.1038/S41598-018-23777-6.
123. Crouse, B., Baehr, C., Hicks, D., and Pravetoni, M. (2023). IL-4 Predicts the Efficacy of a Candidate Antioxycodone Vaccine and Alters Vaccine-Specific Antibody-Secreting Cell Proliferation in Mice. J Immunol. 10.4049/JIMMUNOL.2200605.
124. Roco, J.A., Mesin, L., Binder, S.C., Nefzger, C., Gonzalez-Figueroa, P., Canete, P.F., Ellyard, J., Shen, Q., Robert, P.A., Cappello, J., et al. (2019). Class-Switch Recombination Occurs Infrequently in Germinal Centers. Immunity *51*, 337-350.e7. 10.1016/J.IMMUNI.2019.07.001.
125. Voorberg, A.N., Kamphuis, E., Christoffers, W.A., and Schuttelaar, M.L.A. (2023). Efficacy and safety of dupilumab in patients with severe chronic hand eczema with inadequate response or intolerance to alitretinoin: a randomized, double-blind, placebo-controlled phase IIb proof-of-concept study. Br J Dermatol. 10.1093/BJD/LJAD156.
126. De Corso, E., Pasquini, E., Trimarchi, M., La Mantia, I., Pagella, F., Ottaviano, G., Garzaro, M., Pipolo, C., Torretta, S., Seccia, V., et al. (2023). Dupilumab in the treatment of severe uncontrolled chronic rhinosinusitis with nasal polyps (CRSwNP): A multicentric observational Phase IV real-life study (DUPIREAL). Allergy. 10.1111/ALL.15772.
127. Pavord, I.D., Bourdin, A., Papi, A., Domingo, C., Corren, J., Altincatal, A., Radwan, A., Pandit-Abid, N., Jacob-Nara, J.A., Deniz, Y., et al. (2023). Dupilumab sustains efficacy in patients with moderate-to-severe type 2 asthma regardless of ICS dose. Allergy. 10.1111/ALL.15792.
128. Blauvelt, A., Simpson, E.L., Tyring, S.K., Purcell, L.A., Shumel, B., Petro, C.D., Akinlade, B., Gadkari, A., Eckert, L., Graham, N.M.H., et al. (2019). Dupilumab does not affect correlates of vaccine-induced immunity: A randomized, placebo-controlled trial in adults with moderate-to-severe atopic dermatitis. J Am Acad Dermatol *80*, 158-167.e1. 10.1016/J.JAAD.2018.07.048.

129. Chen, Z., Cui, Y., Yao, Y., Liu, B., Yunis, J., Gao, X., Wang, N., Cañete, P.F., Tuong, Z.K., Sun, H., et al. (2023). Heparan sulfate regulates IL-21 bioavailability and signal strength that control germinal center B cell selection and differentiation. Sci Immunol *8*. 10.1126/SCIIMMUNOL.ADD1728.
130. Chen, H., Zhang, Y., Ye, A.Y., Du, Z., Xu, M., Lee, C.S., Hwang, J.K., Kyritsis, N., Ba, Z., Neuberg, D., et al. (2020). BCR Selection and Affinity Maturation in Peyer's Patches Germinal Centers. Nature *582*, 421. 10.1038/S41586-020-2262-4.
131. Jacob-Dolan, C., Yu, J., McMahan, K., Giffin, V., Chandrashekar, A., Martinot, A.J., Anioke, T., Powers, O.C., Hall, K., Hope, D., et al. (2023). Immunogenicity and protective efficacy of GBP510/AS03 vaccine against SARS-CoV-2 delta challenge in rhesus macaques. NPJ Vaccines *8*. 10.1038/S41541-023-00622-0.
132. Reboldi, A., and Cyster, J.G. (2016). Peyer's patches: Organizing B cell responses at the intestinal frontier. Immunol Rev *271*, 230. 10.1111/IMR.12400.
133. Song, J.Y., Choi, W.S., Heo, J.Y., Lee, J.S., Jung, D.S., Kim, S.W., Park, K.H., Eom, J.S., Jeong, S.J., Lee, J., et al. (2022). Safety and immunogenicity of a SARS-CoV-2 recombinant protein nanoparticle vaccine (GBP510) adjuvanted with AS03: A randomised, placebo-controlled, observer-blinded phase 1/2 trial. EClinicalMedicine *51*. 10.1016/J.ECLINM.2022.101569.
134. Bergqvist, P., Stensson, A., Lycke, N.Y., and Bemark, M. (2010). T cell-independent IgA class switch recombination is restricted to the GALT and occurs prior to manifest germinal center formation. J Immunol *184*, 3545–3553. 10.4049/JIMMUNOL.0901895.
135. Kaplan, M.H., Schindler, U., Smiley, S.T., and Grusby, M.J. (1996). Stat6 is required for mediating responses to IL-4 and for the development of Th2 cells. Immunity *4*, 313–319. 10.1016/S1074-7613(00)80439-2.
136. Herbert, D.R., Hölscher, C., Mohrs, M., Arendse, B., Schwegmann, A., Radwanska, M., Leeto, M., Kirsch, R., Hall, P., Mossmann, H., et al. (2004). Alternative macrophage activation is essential for survival during schistosomiasis and downmodulates T helper 1 responses and immunopathology. Immunity *20*, 623–635. 10.1016/S1074-7613(04)00107-4.
137. Barner, M., Mohrs, M., Brombacher, F., and Kopf, M. (1998). Differences between IL-4Rα-deficient and IL-4-deficient mice reveal a role for IL-13 in the regulation of Th2 responses. Current Biology *8*, 669–672. 10.1016/s0960-9822(98)70256-8.
138. Mohrs, K., Wakil, A.E., Killeen, N., Locksley, R.M., and Mohrs, M. (2005). A two-step process for cytokine production revealed by IL-4 dual-reporter mice. Immunity *23*, 419–429. 10.1016/j.immuni.2005.09.006.
139. Strasser, A., Whittingham, S., Vaux, D.L., Bath, M.L., Adams, J.M., Cory, S., and Harris, A.W. (1991). Enforced BCL2 expression in B-lymphoid cells prolongs antibody responses and elicits autoimmune disease. Proc Natl Acad Sci U S A *88*, 8661. 10.1073/PNAS.88.19.8661.
140. Ndungu, F.M., Cadman, E.T., Coulcher, J., Nduati, E., Couper, E., MacDonald, D.W., Ng, D., and Langhorne, J. (2009). Functional Memory B Cells and Long-Lived Plasma Cells Are Generated after a Single Plasmodium chabaudi Infection in Mice. PLoS Pathog *5*, e1000690. 10.1371/JOURNAL.PPAT.1000690.
141. Keitany, G.J., Kim, K.S., Krishnamurty, A.T., Hondowicz, B.D., Hahn, W.O., Dambrauskas, N., Sather, D.N., Vaughan, A.M., Kappe, S.H.I., and Pepper, M. (2016).

Blood Stage Malaria Disrupts Humoral Immunity to the Pre-erythrocytic Stage Circumsporozoite Protein. Cell Rep *17*, 3193–3205. 10.1016/j.celrep.2016.11.060.
142. Taylor, J.J., Martinez, R.J., Titcombe, P.J., Barsness, L.O., Thomas, S.R., Zhang, N., Katzman, S.D., Jenkins, M.K., and Mueller, D.L. (2012). Deletion and anergy of polyclonal B cells specific for ubiquitous membrane-bound self-antigen. Journal of Experimental Medicine *209*, 2065–2077. 10.1084/JEM.20112272.
143. vander Heiden, J.A., Yaari, G., Uduman, M., Stern, J.N.H., O'connor, K.C., Hafler, D.A., Vigneault, F., and Kleinstein, S.H. (2014). pRESTO: a toolkit for processing high-throughput sequencing raw reads of lymphocyte receptor repertoires. Bioinformatics *30*, 1930. 10.1093/BIOINFORMATICS/BTU138.
144. BBTools User Guide - DOE Joint Genome Institute https://jgi.doe.gov/data-and-tools/software-tools/bbtools/bb-tools-user-guide/.
145. Gupta, N.T., vander Heiden, J.A., Uduman, M., Gadala-Maria, D., Yaari, G., and Kleinstein, S.H. (2015). Change-O: a toolkit for analyzing large-scale B cell immunoglobulin repertoire sequencing data. Bioinformatics *31*, 3356. 10.1093/BIOINFORMATICS/BTV359.
146. Wickham, H., Averick, M., Bryan, J., Chang, W., D', L., Mcgowan, A., François, R., Grolemund, G., Hayes, A., Henry, L., et al. (2019). Welcome to the Tidyverse. J Open Source Softw *4*, 1686. 10.21105/JOSS.01686.